NASA Contractor Report 201694

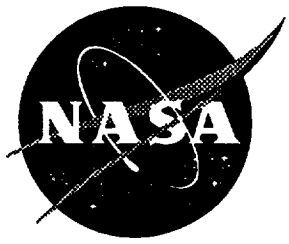

Shock Tunnel Studies of Scramjet Phenomena 1995

Supplement 13

R. G. Morgan, R. J. Stalker, and A. Paull
The University of Queensland, Brisbane, Australia

Grant NAGW-674
April 1997

National Aeronautics and
Space Administration
Langley Research Center
Hampton, Virginia 23681-0001

SHOCK TUNNEL STUDIES OF SCRAMJET PHENOMENA 1995
NASA GRANT NAGW-674 - SUPPLEMENT 13

Following the format of previous reports, this consists of reports on specific projects. After a brief introduction on each project, the project reports follow in the order of the headings in the introduction.

"Program A" corresponds to work funded jointly by NAGW-674 and Australian sources, and "Program B" to that funded by Australian sources alone.

PROGRAM A

(i) Area Change in an Expansion Tube
Boundary-layer Blockage in Expansion Tube Nozzles
(O. Sudnitsin and R.G. Morgan)

The effect of the boundary layer on the flow in a hypersonic nozzle placed at the end of the acceleration tube has been subjected to theoretical analysis, and the technique of analysis has been checked against some GASL experimental results for a diffuser in an expansion tube.

(ii) Skin Friction Measurements in a Shock Tunnel
(C.P. Goyne, R.J. Stalker and A. Paull)

Measurements of skin friction in a turbulent boundary layer formed in a zero pressure gradient rectangular duct have been made in the T4 free piston shock tunnel. Analysis of results is not yet complete, however, they indicate that Van Driest II is suitable for predicting the skin friction, at least at the lowest stagnation enthalpy studied.

Other tests were made involving the measurement of skin friction in a duct in the presence of hydrogen combustion. In one series, hydrogen was injected via a central strut spanning the duct, and it was found that combustion increased the heat transfer to the walls of the duct, but not the skin friction. In a second series, hydrogen was injected from a rear ward facing step, in a film cooling mode. Again, the skin friction did not increase with the heat transfer.

PROGRAM B

(i) Direct Measurement of Thrust/Drag

(a) A Study of Scramjet Scaling
(M.V. Pulsonetti and R.J. Stalker)

This was a study carried out to determine the scaling laws for a simple case of supersonic hydrogen-air combustion. It was expected to provide a criterion for determining when vigorous combustion would take place in a model, and therefore define when the drag would be substantially altered by combustion induced thrust. It was found that two types of combustion occurred, a mixing limited or reaction limited. The latter took place at the lower range of air temperatures at which auto-ignition occurred, and was therefore associated with greater heat release. Both types of combustion scaled by a pressure-length correlation, though at higher pressures the reaction limited exhibited a rate of combustion pressure rise which did not scale according to that correlation.

(b) A Shock Tunnel Investigation of Scramjet Performance with Partially Premixed Combustion
(R.J. Stalker, R.G. Morgan and A. Paull)

The reaction limited combustion revealed by the previous study is investigated in more detail here. Particular attention is given to the location, in the combustion duct, of the explosive pressure rise which accompanies combustion in this case. The distance along the duct from injection to the location of the peak of this pressure rise depended on a parameter involving the flow velocity and the pressure. When the pressure rise occurred downstream of the combustion chamber, thrust production by a thrust nozzle downstream of the combustion duct was inhibited.

(c) Experiments on Cruise Propulsion with a Hydrogen Scramjet
(R.J. Stalker and A. Paull)

The drag of an integrated vehicle-engine model combination with hydrogen scramjet propulsion was measured, and it was found that the cruise condition of zero drag could be obtained at a velocity of 2.45 km s^{-1}. The specific impulse was 835 sec. Comparison with some results from the previous investigation suggested that substantial combustion may be taking place in the thrust nozzle. This may have an important effect on the lift.

(ii) Expansion Tubes

(a) Drag Measurements in Carbon Dioxide Test flows using a Hypervelocity Expansion Tube
(A.L. Smith and D.J. Mee)

The stress wave force balance is theoretically able to measure model drag in a very short time. Here measurements are made up in small expansion tube, with a test flow duration of 50 μsec, on a series of sharp cones, and on two re-entry shield configurations.

(b) A Two-Stage Free-Piston Driver for Expansion Tubes
(C.J. Doolan and R.G. Morgan)

The concept of a two-stage free piston driver has been discussed in previous reports. Here the concept is applied successfully, and the results of tests on this type of driver are presented.

(iii) Mass Spectrometric Measurements
(R.R. Boyce, M. Takahashi and R.J. Stalker)

The mass spectrometer used for previous measurements has been improved, and new measurements have been taken in the shock tunnel T4 of the test gas composition and of driver gas contamination of the test flow

Boundary-layer blockage in expansion-tube nozzles

O. Sudnitsin and R. G. Morgan
University of Queensland
Brisbane, QLD, 4072, AUSTRALIA

Abstract: The results of a first-order perfect gas correction for the effects of the boundary-layer formation within expansion tubes with nozzles are presented. The analytical model developed to describe the boundary-layer formation within the expansion tube and an expansion nozzle located at the end of the acceleration tube is based on the Kármán integral equations. The results of this analytical model are compared with experimental data from an expansion diffuser. The model provides a useful tool for the preliminary design of nozzles for such facilities.

Key words: Boundary layer formation, Boundary layer blockage, Nozzle flow, Expansion tubes, Hypersonic flows, Kármán integral equations

1. Introduction

Scale modeling of hypersonic flows cannot be achieved with complete matching of all non-dimensional scaling parameters. Laboratory testing generally involves only partial similarity and can be justified if the phenomenon of interest is controlled primarily by matchable parameters. For example, the binary scaling parameter allows accurate modeling of binary finite-rate dissociation processes, simultaneously reproducing viscous effects.

However, many processes of interest in hypersonic flow do not follow binary scaling, and exact simulation requires full size models. Combustion, recombination and gas radiation are examples of such processes. The size of the test section, therefore, limits the size of flight vehicle which can be tested in this way. Expansion of laboratory test flows enables larger models to be tested, but the associated drop in pressure limits the range of flight conditions which can be reproduced. Because of their high total-pressure simulation capability, expansion tubes can potentially provide improved performance over other existing facilities.

In the superorbital expansion tube, it is of interest to model rarefied flow phenomena, for which it is necessary to reduce gas density by means of a nozzle.

The limited test size of an expansion tube may be increased by means of an expansion nozzle located at an appropriate section of the tube (Sudnitsin and Morgan 1994). The starting process associated with nozzle flows reduces the steady test time available (Leyva 1994), and may provide additional limitation on model size.

A nozzle was tested successfully by Miller and Jones (1983) on an expansion tube. However, for their purpose, the unmodified expansion tube was found to be better and the use of the nozzle was discontinued.

Despite the reduction of the binary scaling parameter associated with the use of nozzles, direct simulation over a useful range of flight conditions may still be obtained.

However, certain problems need to be addressed if such nozzles are to be used. Firstly, reservoir pressure must be sufficient to reproduce real-flight conditions. A simple ideal-gas analysis (Sudnitsin and Morgan 1994) provides a quick assessment of operational conditions in terms of the important non-dimensional parameters. Using this approach, the characteristics of simulated flow in terms of total pressure, driver-noise attenuation (Paull and Stalker 1992) and test-gas temperature may be found for three different configurations of an expansion tube with the divergent nozzle placed at A — the end of the driver section, B — the end of the shock tube, and C — the end of the acceleration tube. Configurations and conditions which may give superior performance and for which further investigation is justified can thus be easily identified.

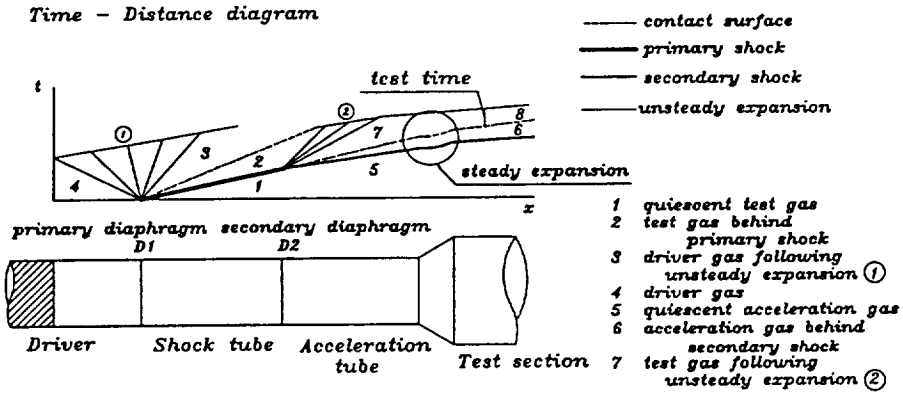

Figure 1. Configuration C

According to the results of the performance comparison in terms of nose-to-tail pressure ratio, configuration C has been chosen for initial investigation (Fig. 1). This configuration is advantageous because it is relatively sim-

ple to modify the existing facility and it can be shown that its performance at some operating conditions is comparable to the configurations A and B (Sudnitsin and Morgan 1994).

One aspect of nozzle design concerns the influence of the boundary layers on the effective test-flow area that is achieved in the core flow. This effect is small for low-Mach-number flows, and is often not corrected for in the design stage, because direct calibration under operating conditions can be used to determine precisely the expanded-flow parameters. However, in superorbital expansion flows, significant boundary-layer blockage may arise, and the nozzle geometric area ratio may be quite different to that seen by the core flow. Consequently, an analysis is presented which couples the boundary-layer displacement thickness to the expansion process, giving an improved indication of the state of the core flow.

The present analysis has been done for a small-scale expansion tube at the University of Queensland (X1), and the nozzle is currently under construction. Experimental data for a diffuser on an expansion tube obtained by General Applied Science Laboratories, Inc (GASL) (Bakos et al. 1992, Bakos 1994) were used to validate the analytical results prior to designing the nozzle for X1 at the University of Queensland.

2. Boundary layer analysis

The present analysis investigates the growth of the boundary layer on the walls of the expansion tube which will reduce the size of the available test core from A to A' (Fig. 3) and change the area ratio of the nozzle, resulting in a decrease in the pressure ratio associated with it. Flow is assumed to be compressible, and the formation process has been divided into two stages, formation within the tube and growth within the divergent nozzle.

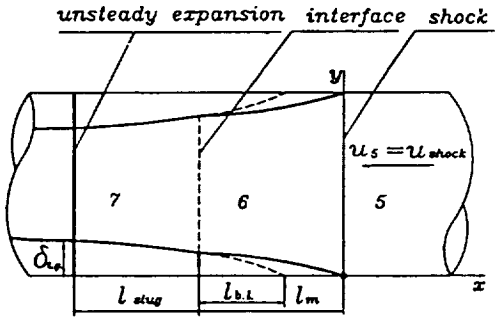

Figure 2. Boundary layer formation in the acceleration tube.

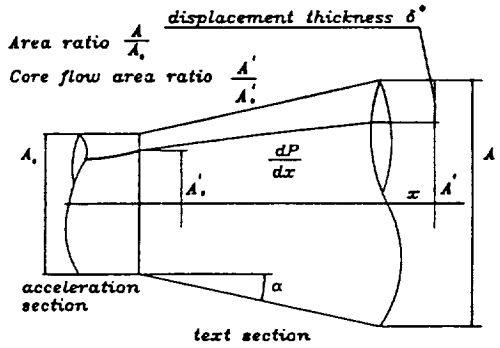

Figure 3. Boundary layer formation in the nozzle.

2.1. Boundary-layer formation within the acceleration tube

A boundary layer grows between the head of the rarefaction wave and the shock. Fig. 2 schematically demonstrates the different stages of the boundary-layer formation and flow for each region.

Boundary layers within the shock tube act as an aerodynamic sink for the acceleration gas in region 6 between the shock and interface (Fig. 2). Test gas is also lost by this process in region 7, behind the interface. The boundary layer at the exit plane of the acceleration tube grows with time. The worst boundary-layer thickness occurs with the arrival of the secondary unsteady-expansion head (Fig. 2). Useful gas flow in this region is completed at this time.

For the present calculations a worst-case approach was adopted, assuming the origin of the test-gas boundary layer coincided with the shock location. Therefore, region 6 (Fig. 3) is considered infinitesimally small and $l_{b.l.} = l_m$, which is a good approximation at high shock speeds. Thus, the test-gas boundary layer develops under the influence of conditions behind the interface (region 7 in Fig. 3).

Table 1. Sample predicted condition for X1, targeting supersonic combustion.

Regions Fig. 1	Pressure, Pa	Temperature, K	Velocity, m/s	Speed of sound, m/s
4	5E+07	2000	0	1827[a]
7	6E+5	3082	3727	1112[b]
8	25E+3	1250	4200	709

Primary shock speed $U_{sh1} = 3000$ m/s, secondary shock speed $U_{sh2} = 4500$ m/s
Speed of sound ratio across the driver gas-test gas interface $a_3/a_2 = 0.7$
[a] driver gas is a mixture of He and Ar with $\gamma = 1.67$ and $\mathcal{R} = 1000$ J/(kg K)
[b] test and acceleration gas is air with $\gamma = 1.4$ and $\mathcal{R} = 287$ J/(kg K)

In the sample calculation for X1 (Table 1), it was assumed that the boundary layer behind the interface in the acceleration tube is turbulent. The characteristic thicknesses δ — the boundary layer thickness, δ^* — the displacement thickness, and θ — the momentum thickness, which define integral deficits, were calculated from Hayes and Probstein (1959) and act as starting conditions for the nozzle boundary-layer calculation.

2.2. Boundary-layer formation within the expansion nozzle

The modeling of the nozzle boundary layer assumed that the surface can be represented by a flat plate with a favorable pressure gradient, that the flow is

compressible, and that the Kármán-based method of Walz (1969) may be used to quantify the development of δ^* and θ with x.

The approach that was used allows the bulk boundary-layer properties to be calculated without solving for the internal profiles. These properties can then be used in a one-dimensional approach to calculate nozzle-exit conditions.

The physical information required to complete the calculations was incorporated into the differential equation for the velocity, density, and area-ratio variations along the nozzle. After the initial values of the variable parameters (Walz 1969) were estimated, final bulk properties of the boundary layer were obtained by solving the system of differential equations. A conical nozzle with an area ratio of 9 was used to generate the axial-pressure distribution that was used for the computations. When the effect of the boundary-layer displacement thickness was added to the contour, the geometric area ratio that was needed to expand the core flow to the correct pressure was found to be 20. This illustrates the importance of boundary-layer blockage for these flow conditions. The increase of displacement thickness is due to the entrainment of new fluid in the nozzle and also to the expansion of the boundary-layer gas. In this example, 66% of the downstream displacement thickness is due to entrainment in the nozzle, illustrating the importance of minimizing nozzle length. The experimental validation of this result is yet to be made.

3. Comparison with experimental data

In order to validate the analysis above, it was applied to data from a diffuser placed at the end of the expansion tube at GASL (Bakos et al. 1992). The 0.85-m-long diffuser with the initial conditions M17 (Bakos 1994) produced a boundary layer with a thickness $\delta_{exit} \approx 6.25$ mm (from an exit Mach number profile from Bakos et al. 1992). The nozzle-starting condition, M17, and the history of the boundary layer were deduced from Bakos at al. (1992) where the boundary-layer thickness was measured to be $\delta_0 \approx 25$ mm at the acceleration-tube exit.

The diffuser was designed to produce an increase in static pressure of 11.9 (perfect gas approximation) relative to the incoming flow. After correction of the contour to account for the displacement thickness, the pressure increase that is expected is 8. The actual experimental pressure ratio (Table 2) (Bakos et al. 1992) was measured to be 8.8. Therefore it can be seen that the inviscid calculation of a diffuser contour somewhat overestimates the pressure ratio, whereas the boundary-layer-corrected contour can predict the pressure ratio much more realistically. The fact that the viscously corrected and experimental pressure ratios are not exactly the same may be partly due to the fact that the boundary-layer thickness is not precisely known from the data that is available.

Further validation will be provided by the planned experiments.

4. Conclusions

The present work indicates the importance of viscous effects in expansion tubes with nozzles. It demonstrates the significant effect of the displacement-thickness correction on the contour and the predicted pressure ratio. As the velocities and Mach numbers of the phenomena of interest increase, it will be important to correct for viscous effects from the early stages of nozzle design, rather than by calibrating for viscous effects after construction. The simple correction technique is provided to assist with this type of problem.

Acknowledgement. This work was partially supported by the NASA Langley Research Center (Grant NAGW 674, contract monitor R.C. Rogers).

References

Bakos R (1994) An investigation of test flow nonequilibruim effects on scramjet combustion. Ph.D. thesis, University of Queensland.

Bakos RJ, Tamago J, Rizkalla O, Pulsonetti MV, Chinitz W, Erdos JI (1992) Hypersonic mixing and combustion studies in the hypulse facility. J Propulsion and Power 8:900–906

Hayes WD, Probstein RF (1959) Hypersonic flow Theory. Academic Press, New York.

Leyva IA (1994) Study of the addition of a divergent nozzle to an expansion tube for increasing test time. Paper No. AIAA 94–2533 In: 18th AIAA Aerospace Ground Testing Conference, Colorado Springs, CO.

Miller CG, Jones JJ (1983) Development and performance of the NASA Langley Research Center expansion tube/tunnel, a hypersonic-hypervelocity real-gas facility. AIAA 14th International Symposium on Shock Tubes and Waves, Sydney, Australia.

Paull A, Stalker R (1992) Test flow disturbances in an expansion tube. J Fluid Mech 245:493–521.

Sudnitsin O, Morgan RG (1994) Expansion tube area change optimisation. In: 4th International Workshop on Shock Tube Technology, Brisbane, Australia.

Walz A (1969) Boundary layers of flow and temperature. The M.I.T. Press.

BLANK

SKIN FRICTION MEASUREMENTS IN A SHOCK TUNNEL

C.P. Goyne, R.J. Stalker and A. Paull

INTRODUCTION

In order to obtain experimental skin friction estimates for both internal and external surfaces of a supersonic combustion ramjet, a series of experiments were conducted in the T4 Shock Tunnel using a new skin friction gauge. In the first experiment, skin friction was measured in laminar, transitional and turbulent boundary layers within a rectangular duct. In the second experiment, skin friction was measured along a rectangular, constant area combustor with central hydrogen injection. Lastly, skin friction was measured within a rectangular, constant area combustor with hydrogen injection behind a wall step. The test section free stream conditions for each experiment are listed in Table 1.

SKIN FRICTION GAUGE

The skin friction gauge is an acceleration compensated piezoceramic sensor. The transducer is similar to that described by Goyne et al. 1995. Some design changes, however, have been incorporated to provide added protection of the sensing piezoceramic from heat transfer and ionisation associated with the free stream flow. Both the measuring and acceleration compensating piezoceramics consists of a 1.5 mm thick, 8 mm diameter PZT block with a 2 mm hole through the centre. The ceramics are located on each side of an aluminium base and 10 mm diameter invar disks are joined to each of the two remaining faces. One of these invar disks forms the skin friction sensing surface while the other, protected from the flow, is used for acceleration compensation. Both ceramics are covered by an acrylic insulator which is then coated with a conductive paint. The coating is earthed and acts as an electrical shield. The sensing ceramic is also wrapped in approximately 8 layers of fine brass mesh. The mesh acts to cool free stream air that enters the cavity formed between the peizoceramic/invar assembly and the gauge housing. The transducer is calibrated for shear, pressure and acceleration forces separately and independently from the shock tunnel flow.

EXPERIMENTS - THE LONG DUCT

In the first experiment in T4, skin friction measurements were obtained at five locations along a 1.5 m long flat plate. The instrumented plate formed one of the inner walls of a rectangular duct, 120 x 60 mm at the inlet. The three remaining walls each had a divergence of 0.5 degrees in order to allow for boundary layer displacement and maintain a nominally constant pressure along the instrumented plate. Thin film heat transfer gauges and PCB pressure transducers were located adjacent to each skin friction gauge tapping.

Table 1. Free stream conditions

	Long Duct	Central Injection	Step Injection
H_0	3-10 MJ/kg	6.6 MJ/kg	8.2 MJ/kg
M	5.5-6.5	4.4	4.3
T	400-1300 K	1360 K	1760 K
P	1-20 kPa	66 kPa	85 kPa
ϕ	-	1.1	0.5-1.6

The heat transfer measurements indicated that transitional and fully turbulent boundary layers were achieved. The skin friction gauges in the transitional regions exhibited fluctuations in skin friction associated with the passing of turbulent spots. Preliminary results indicated that the skin friction measurements obtained within the turbulent region of the boundary layer agreed most with the theory of van Driest II 1956, at least in the low stagnation enthalpy end of the range. These results are shown in Figure 1.

EXPERIMENTS - CENTRAL INJECTION

The second series of skin friction measurements were obtained in a 1320 mm long constant area combustor, 100 x 47 mm in cross section which is shown schematically in Figure 2(a). Four skin friction transducers were located along the centreline of one of the 100 x 1320 mm walls. Thin film heat transfer gauges and PCB pressure transducers were also located along the wall. Hydrogen was injected into the combustor from a central strut that spanned the 100 mm dimension. The strut protruded from the inlet so that the strut bow shock and associated expansion did not enter the duct. A fact acting valve and a Ludwieg tube supplied the fuel to the injector. The arrangement was similar to that used by Jacobs et al. 1991 for pressure measurements.

Pressure and heat transfer measurements, shown in Figure 3, indicated that mixing limited combustion occurred and that the boundary layer was turbulent at the measurement locations. Preliminary skin friction results in Figure 4 indicated that Reynold's analogy did not apply in the wall boundary layer when fuel was injected. The 'fuel on' heat transfer and pressure levels reached a maximum of 1.6 and 2 respectively times the 'fuel off' levels. However, the 'fuel on' skin friction levels only reached a maximum of 1.3 times the 'fuel off' level, at a point separate from the normalised heat transfer and pressure maximums.

Two sets of results are shown in Figure 4, showing measurements taken with the position of the gauges reversed. This was done with the intention of eliminating the influence of factors peculiar to a particular gauge.

EXPERIMENTS - STEP INJECTION

The final experiment in the series involved skin friction measurements in a constant area rectangular combustor with hydrogen injection from a step on the wall. The previously mentioned combustor configuration was modified such that the instrumented plate was placed flush with one of the surfaces of the strut injector as shown schematically in Figure 2(b). The arrangement formed a step at the upstream end of the instrumented plate, from which fuel was injected into the boundary layer at a number of different mass flow rates.

The results indicated that mixing limited combustion occurred. Again, Reynold's analogy was found not to hold when 'fuel on' levels were compared with 'fuel off' levels. The heat transfer results of Figure 5 showed that the fuel significantly cooled the boundary layer immediately downstream of the injector and the heat transfer rose above 'fuel off' levels near the end of the duct. The skin friction levels with 'fuel on', however, were less than the 'fuel off' levels along the entire length of the plate, as may be seen in Figure 6.

REFERENCES

Goyne CP, Paull A, Stalker RJ (1995) A skin friction gauge for impulsive flows. 31st Joint Propulsion Conference, AIAA 95-3152.

Van Driest ER (1956) The problem of aerodynamic heating. Aero Eng Review October.

Jacobs PA, Morgan RG., Rogers RC. Wendt M, Brescianini C, Paull A, Kelly G (1995) Preliminary calibration of a generic scramjet combustor. NASA CR-187539.

Skin friction

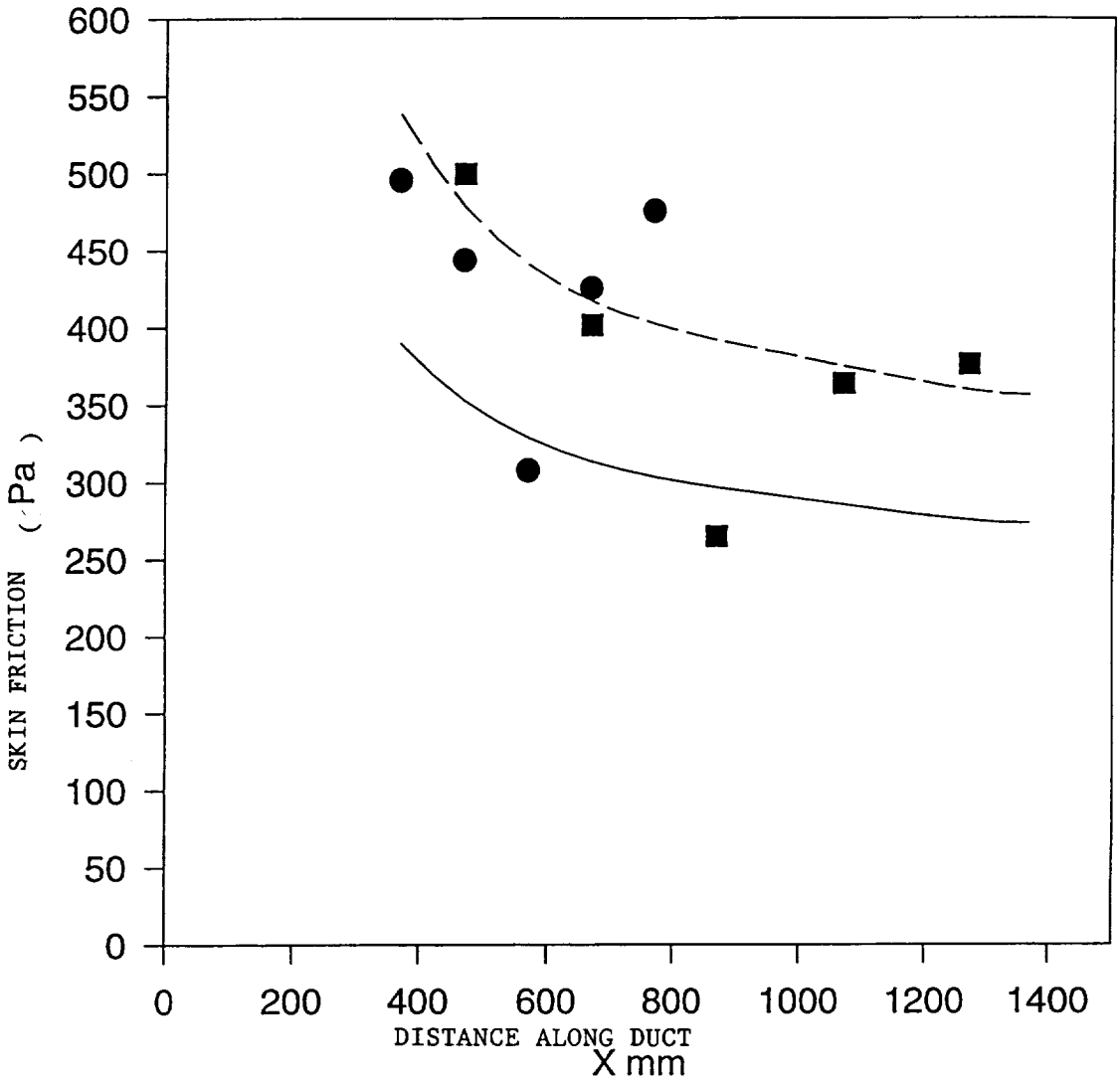

—— Spalding and Chi

--- van Driest II

Ho = 3.6 MJ/kg, M = 6.5, T = 370 K, p = 8.6 kPa, u = 2521 m/s

virtual origin: 270 mm

FIG. 1. SKIN FRICTION IN LONG DUCT

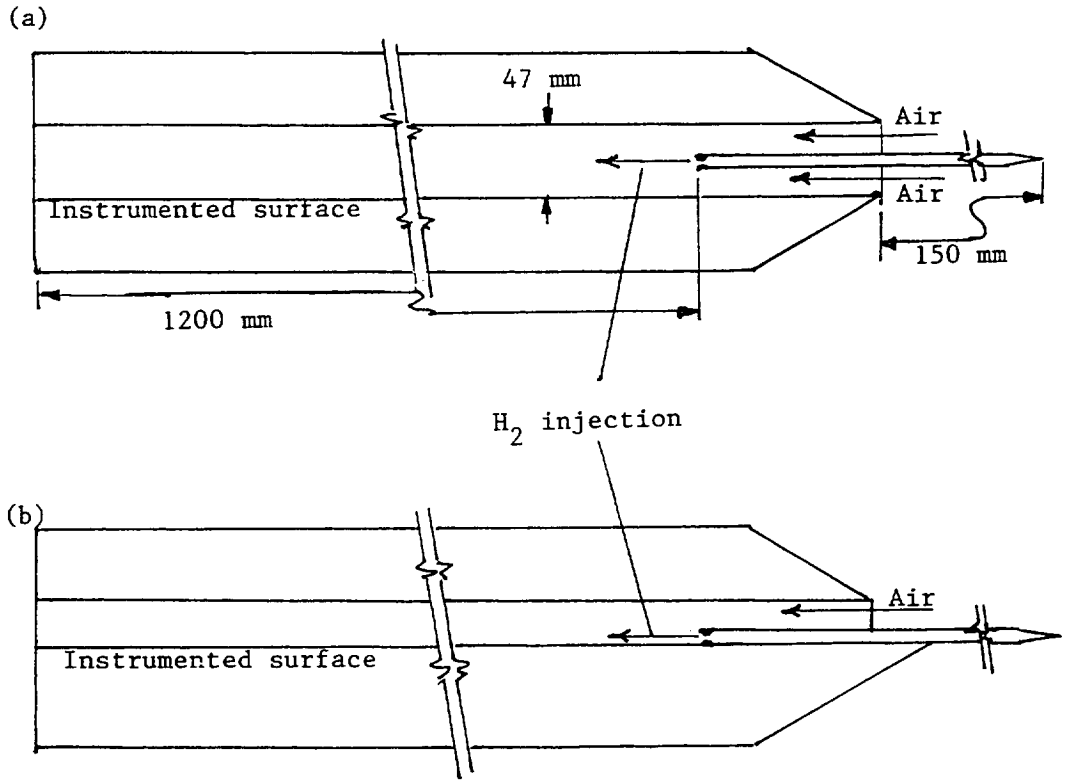

FIG.2. COMBUSTION DUCTS

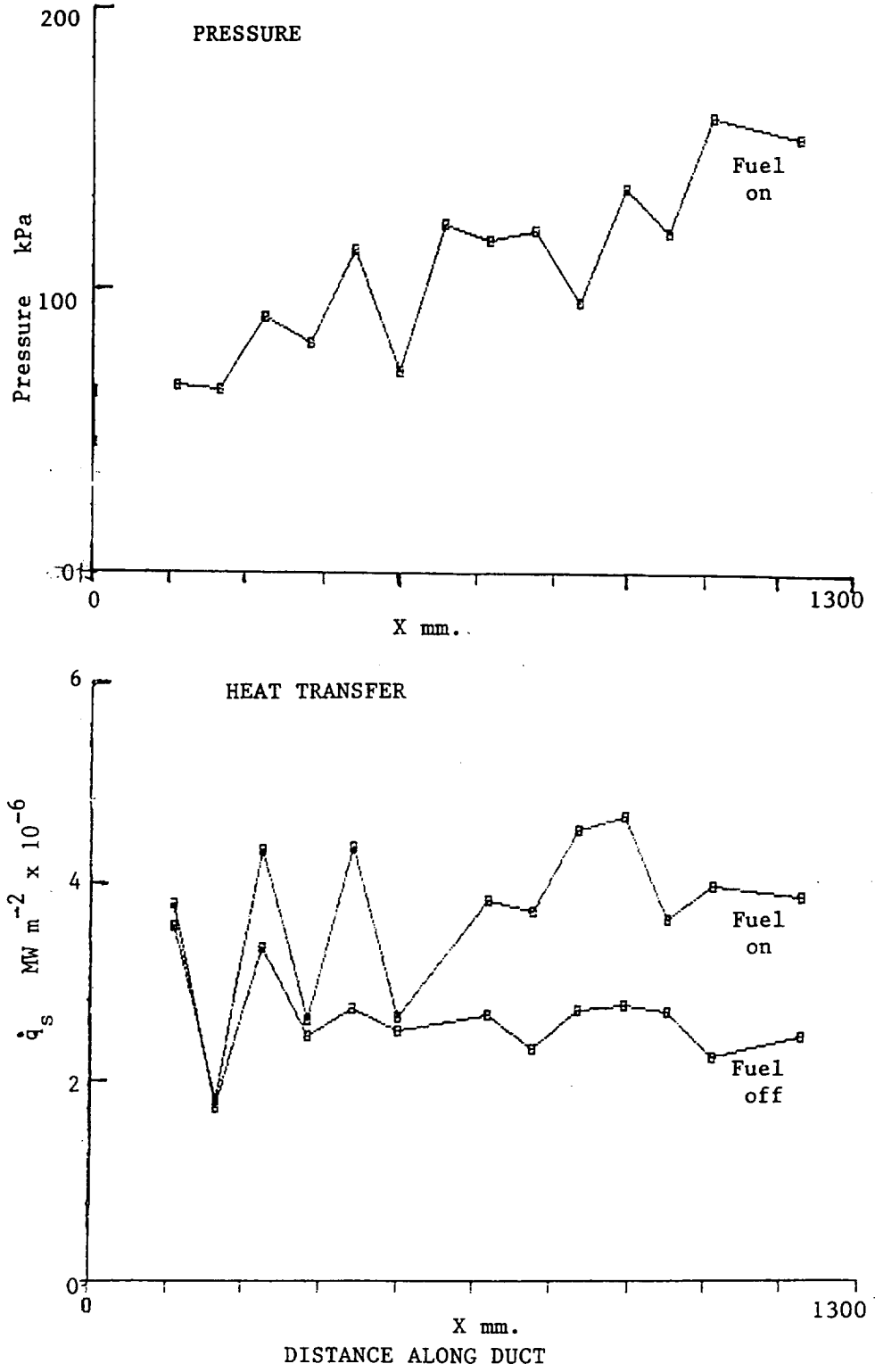

FIG.3. CENTRAL INJECTION - COMBUSTION DUCT. PRESSURE AND HEAT TRANSFER DISTRIBUTIONS

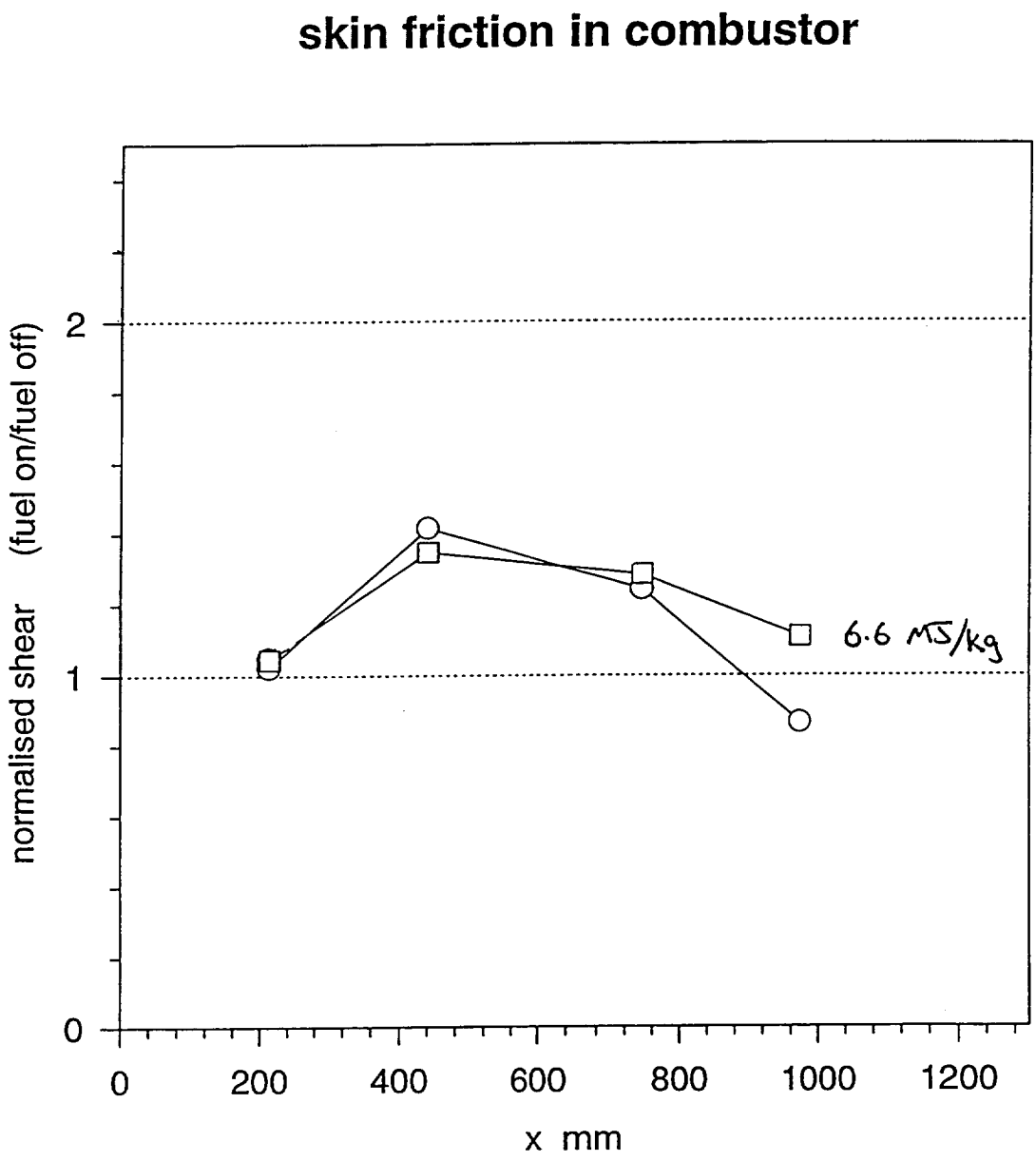

FIG.4. CENTRAL INJECTION - COMBUSTION DUCT. SKIN FRICTION DISTRIBUTION

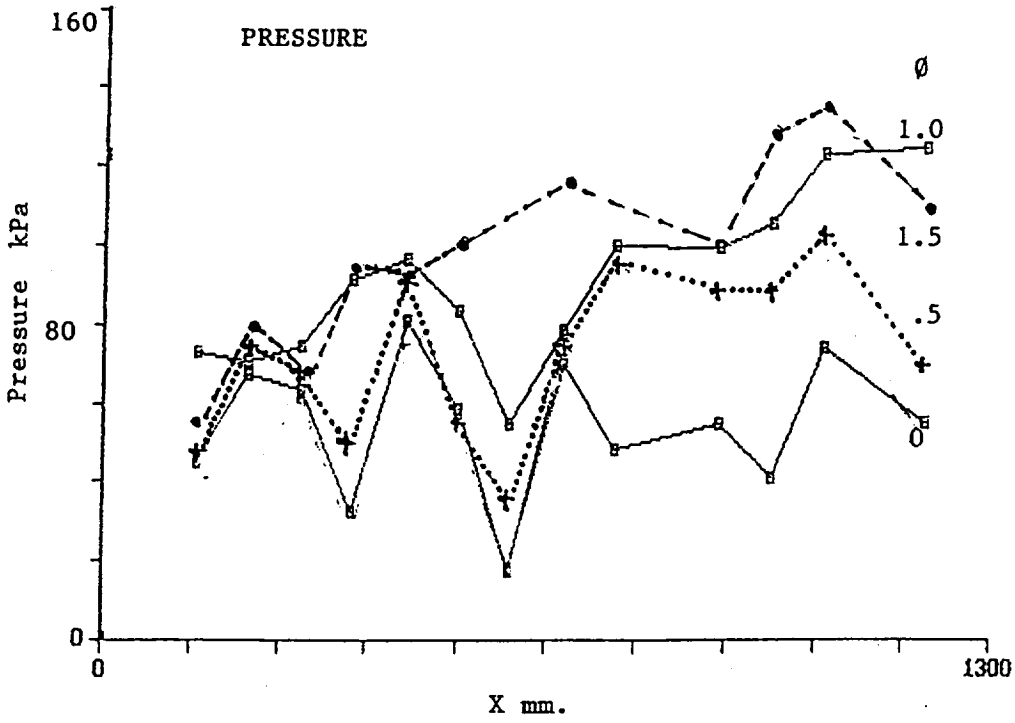

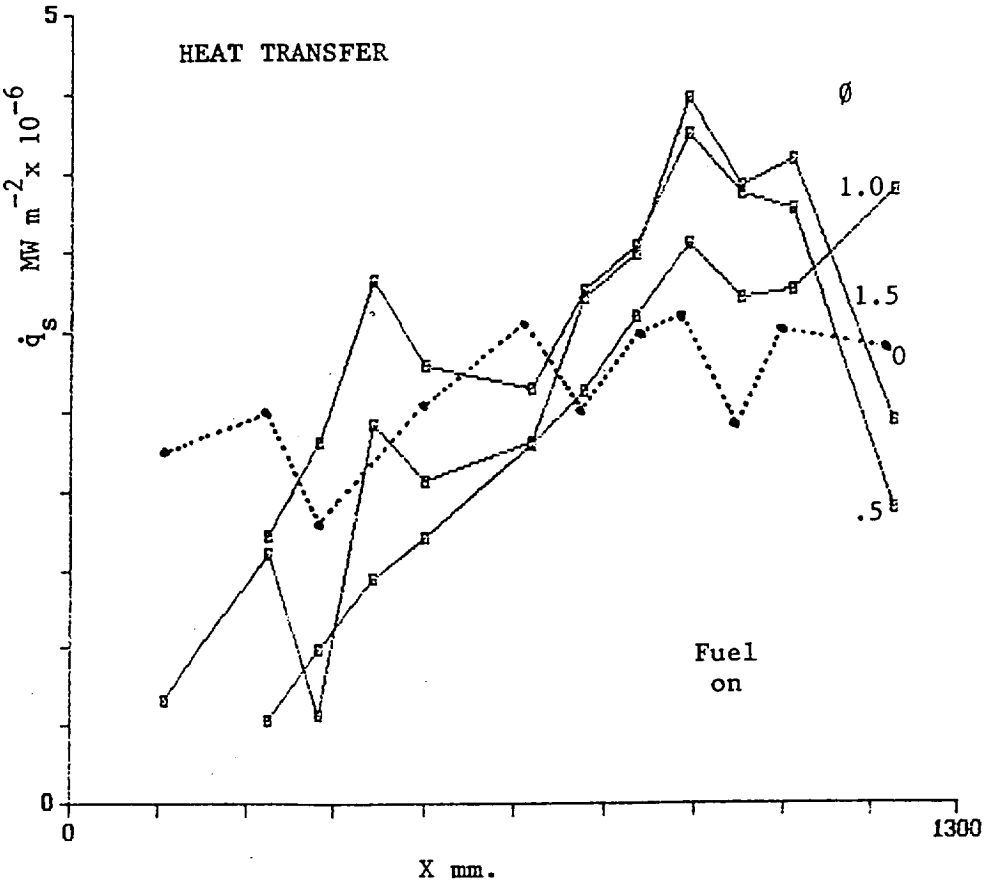

FIG. 5. STEP INJECTION - COMBUSTION DUCT. PRESSURE AND HEAT TRANSFER DISTRIBUTIONS

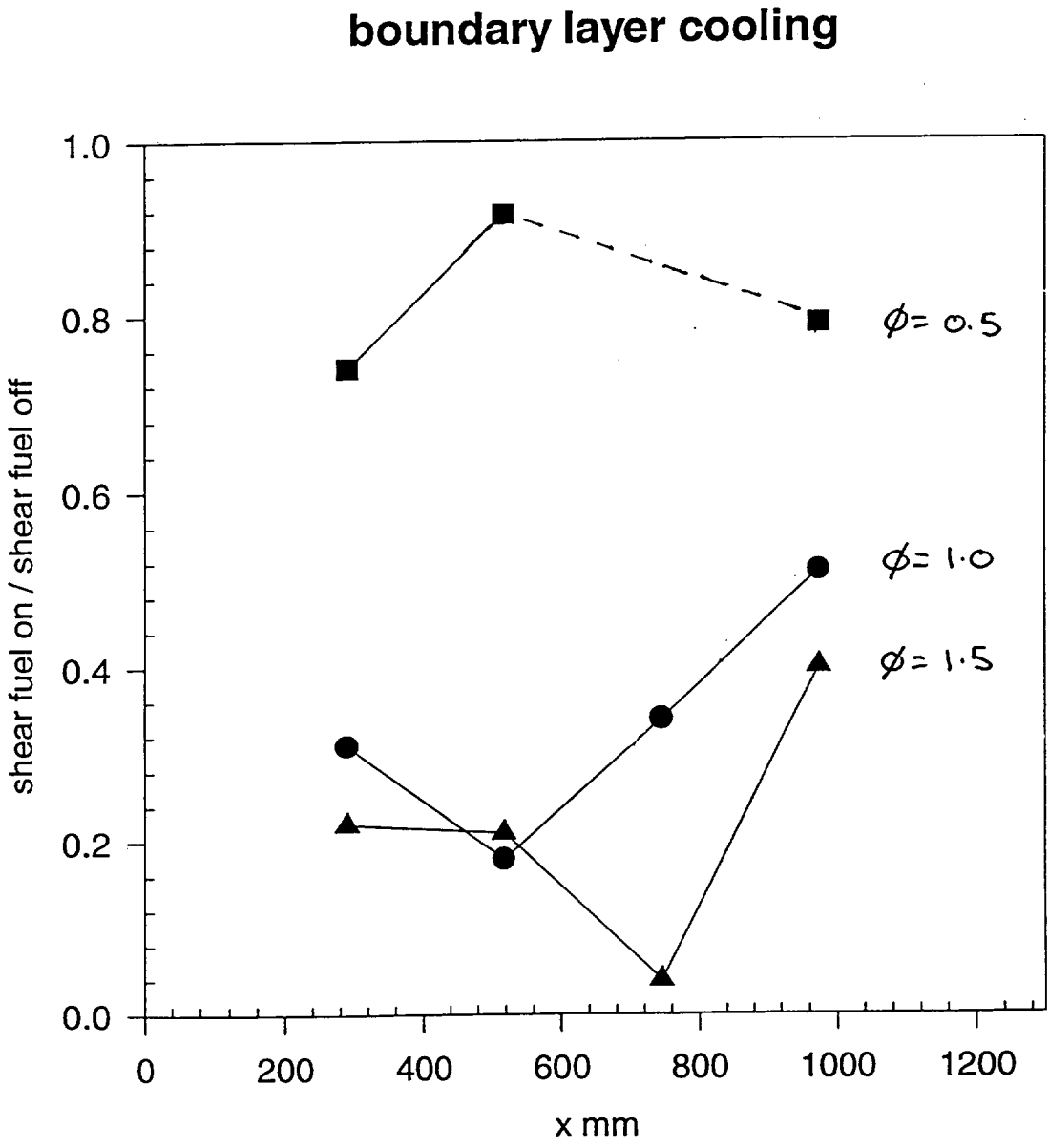

FIG. 6. STEP INJECTION - COMBUSTION DUCT. SKIN FRICTION DISTRIBUTIONS

BLANK

AIAA-96-4533

A STUDY OF SCRAMJET SCALING

by M. V. Pulsonetti* and R. Stalker†

Abstract

A scaling study was performed to determine the scaling laws for the performance of scramjet engines. Experiments were performed on two centrally injected scramjets in the reflected shock tunnel, T4. The scramjets had a 5:1 scale to all their dimensions. The binary scaling (pressure scaling) law was tested on the two scramjets meaning the product of the static pressure in the duct and characteristic length was held constant. A number of test conditions were used to test the scaling law. Five conditions were at approximately the same nozzle stagnation pressure (36.9 MPa) however the stagnation enthalpy was varied from 3.59 to 10.7 MJ/kg. Additionally five conditions were held at approximately the same stagnation enthalpy (5.61 MJ/kg) while the nozzle stagnation pressure was varied from 5.9 to 37.5 MPa. For each of these conditions great care was taken to ensure that the Mach number, temperature and species concentrations were the same as nearly as possible in the two scramjets. The pressure distributions obtained show combustion in the mixing-limited regime and the reaction-limited regime. The ignition time was found to scale well by the pressure-length scaling law. The rate of pressure rise due to combustion was found to be more sudden in the large scramjet for the reaction-limited cases than it was in the small scramjet. The scaled pressure rise due to combustion was slightly larger in the large scramjet than in the small scramjet for all but the highest enthalpy condition. Possible explanations for the above two effects are put forward. The results indicate that the pressure-length scaling law is effective as a first approximation in predicting scramjet performance.

Nomenclature

η_{m_0}	mixing efficiency for tangential injection
$\eta_{m_{90}}$	mixing efficiency for normal injection
f_m	empirical mixing rate constant
ϕ	equivalence ratio
G	effective inviscid duct height
h	height of scramjet duct
k_f	forward reaction rate constant
L	characteristic length
M	third body
P	static pressure
P_{ie}	static pressure at injection station (exp)
P_{it}	static pressure at injection station (theory)
T	static temperature
τ_i	ignition time
x	axial distance from fuel injection
x_{fm}	length for minor constituent to be fully mixed

Introduction

Over the last thirty years much energy has gone into the research and development of scramjet engines. Some of the effort has been devoted to the experimental testing of scramjets while other has taken the form of theoretical analysis of scramjet performance using computational fluid dynamics (CFD) codes. Although these codes are constantly being improved upon they are still unable to accurately predict scramjet performance over the complete range of flight conditions. Thus to facilitate the design of a scramjet powered hypersonic vehicle the researcher must rely upon experimental data to estimate scramjet performance and to calibrate the CFD codes.

The experimental testing of scramjets is currently done in ground based facilities. While blowdown facilities provide some data of scramjet behaviour at the lower mach numbers, testing of scramjet performance at the higher mach number range is done in impulse facilities. Due to the short test times in these impulse facilities only small scramjet models can be tested. Thus scaling laws are needed to relate the abundance of performance data obtained in these small scramjet models to a full sized scramjet. It was the determination of these scaling laws that provided the motivation for this study.

* PhD student, University of Queensland, Lecturer, Queensland University of Technology Member, AIAA

† Emeritus Professor, University of Queensland Associate Fellow, AIAA

In ramjet and gas turbine combustors it was found that as long as similarity of the fuel distribution and heat transfer could be achieved, the pressure-length scaling factor was an effective means of scaling combustor performance[1,2]. Thus if all other properties were held constant, the performance would scale the same for half the length and twice the pressure. To consider if this law would be an appropriate guess at the scaling of performance in a scramjet one must look theoretically at the flow phenomenon occurring in a scramjet combustor.

Theoretical Scaling of Scramjet Ducts

There are a number of physical phenomenon which may affect the scaling of a scramjet combustion chamber. These include the ignition time, complete reaction time, the wall boundary layers, the mixing layer thickness, the mixing efficiency, the heat transfer and the effect of pressure on equilibrium heat release. Although it is acknowledged that these effects are coupled, as a first order estimate of their effects on scaling these phenomena were look at individually to see how each would scale with pressure. The results are presented briefly however they can be found in detail in the thesis by Pulsonetti[3].

Ignition Time

The ignition time is generally thought of as the time for the temperature rise to reach 5 % of the complete reaction temperature rise. Physically this means the time required for sufficient free radicals to be formed which will initiate the reaction system. The ignition reaction which produces these free radicals is a two body reaction and as such should scale by the pressure-length scaling law (equation 1).

$$P\,L = \text{constant} \tag{1}$$

The global model of ignition time given by Pergament[4] shown in equation 2 agrees with this.

$$\tau_i = \frac{8 \times 10^{-9}\, e^{\frac{9600}{T}}}{P} \tag{2}$$

In equation 2 the units of ignition time, static pressure and temperature are microseconds, atmospheres and degrees Kelvin, respectively. Pergament's global model was developed from the results of an eight reaction, six species scheme which in turn was developed to model an expanded chemistry model with many more reactions and species.

Reaction Time

The reaction time is defined as the time required until 95 % of the heat is released due to the formation of water as measured from the point of ignition. The reaction which produces water is a three body reaction and therefore theoretically this reaction should scale by pressure^2-length (equation 3).

$$P^2\,L = \text{constant} \tag{3}$$

It must be pointed out, however, that the above equation was derived by considering only the three body reaction which produces water. In a hydrogen-air system there are many intermediate reaction which will occur before this final reaction, many of which are two body reactions. Therefore it is reasonable that the power on the static pressure in the scaling law be less than two. Additionally, for the case of mixing-limited combustion it is expected that the effect of the scaling of the three body reactions will not play a dominant role in the performance scaling since the rate of reaction depends on the rate of mixing which will be shown to scale by equation 1. For the reaction-limited combustion these effects are also expected to be minimal after the reactions catch up to the mixing, thereby becoming a mixing-limited situation.

Wall Boundary Layer

Another factor which can effect the performance of a scramjet is the growth of the boundary layer on the inside surface of the duct. Examining the simple case of an incompressible turbulent boundary layer on a flat plate Prandtl[5] derived the power law expressions as discussed by White[6]. These showed that the boundary layer thickness, the displacement thickness and the momentum thickness normalized by the axial coordinate were a function of the Reynolds number. Since the Reynolds number can be expressed as a function of the static pressure, the static temperature and the Mach number it is clear that the wall boundary layers should scale by the pressure-length scaling law.

Mixing Efficiency

The term mixing efficiency stands for a one-dimensional, empirical measure of the completeness of mixing. Anderson[7] correlated numerous results of hydrogen-air mixing data to arrive at the empirical correlation for the length for the minor constituent to be fully mixed and the mixing rate. His relations for mixing efficiency as a function of the axial coordinate are specified for parallel injection and normal injection in equations 4 and 5, respectively.

$$\eta_{m_0} = \frac{x}{x_{fm}} \quad (4)$$

$$\eta_{m_{90}} = 1.01 + 0.176 \ln\left(\frac{x}{x_{fm}}\right) \quad (5)$$

In these equations the length for the minor constituent to be fully mixed is given by equation 6.

$$x_{fm} = f_m G \begin{pmatrix} 0.179e^{1.72\phi} & \phi \le 1 \\ 3.333e^{-1.204\phi} & \phi > 1 \end{pmatrix} \quad (6)$$

From these relations it can be shown that for either normal or tangential fuel injection the pressure-length scaling law will scale the mixing efficiency.

Effect of Pressure on Equilibrium Heat Release

Another factor which may affect the scaling results is the impact of the static pressure level on the amount of heat released due to combustion. Since it is clear that as the static pressure of a gas including atomic and molecular species increases the gas is forced into a more molecular form. It is thus expected that performing combustion experiments at higher static pressures will cause more products to take the form of molecular species rather than atomic or free radical species. If the molecular species formed consist primarily of water the energy released due to combustion will be a larger value than that at lower static pressure.

To quantify this effect a quasi one-dimensional code called NTRAIN[8] was used to study the effect on combustion of a factor of 5 variation on inlet static pressure. The code considers a scramjet flowfield of two streams, an air stream and a fuel/mixing stream, each of which has its own properties and composition, however, at any axial location the static pressure of the two streams is constant. An entrainment rate for the air into the fuel/mixing stream is specified in the code and reactions are allowed to occur with equilibrium chemistry.

Three test conditions were chosen to examine the effect of inlet static pressure on equilibrium heat release. One (condition B) was at a relatively high stagnation pressure and low stagnation enthalpy, another (condition E) was at a relatively high stagnation pressure and stagnation enthalpy and the last (condition H) was at a relatively low stagnation pressure and enthalpy (see table 1).

The results indicate that for 100 % mixing of the minor constituent, the percent difference in the maximum pressure rise normalized by the inlet pressure in the duct was less than 6.1 %, with the maximum difference occuring at the highest enthalpy condition (condition E). For lower values of mixing efficiency, about 30 %, the difference becomes negligible. Even at the 100 % mixing efficiency, however, this difference is within the experimental uncertainty of the data. Thus the effect of pressure on equilibrium heat release will not severely change the outcome of this thesis.

The Facility

The experiments were performed in the free piston driven reflected shock tunnel, T4, at the University of Queensland in Brisbane, Australia shown in figure 1. The facility's compression tube is 26 m long and 229 mm in diameter. It was filled with either helium at the higher enthalpies or a mixture of helium and argon at the lower enthalpies. The shock tube is 10 m long and 75 mm in diameter. It contained either nitrogen test gas for the mixing runs or air for the combustion or tare runs. Two nozzles[9] were used in the study, one designed to produce a test section mach number of 4 and one to provide a mach number in the test section of 8.

The Scramjet Models

The experimental scramjet models used for this study are shown in figure 2. The length of the large scramjet was 1.320 m with a width and height of the combustion duct being 100 mm and 47.14 mm, respectively. The central fuel injector which supplied gaseous hydrogen to the test gas was 10 mm thick and had a throat height of 1.60 mm. The model was instrumented with recess mounted piezo electric pressure transducers and thin film hest flux gauges, manufactured in house, spaced 40 mm apart.

The small scramjet was 300 mm long with a combustor width and height of 20 mm and 9.43 mm respectively. The central fuel injector was 2.016 mm thick and had a throat height of 0.323 mm.

The Test Conditions

The aim of the experiment was to test the pressure-length scaling factor. Therefore since the large scramjet was a factor of 5 greater than the small scramjet it was desired that the static pressure in the large scramjet be one fifth of that in the small scramjet. At the same time it was desired that the other properties such as the static temperature, the mach number and the species concentrations remain the same. One might think this could be achieved by decreasing both the fill

pressure in the shock tube and the burst pressure of the primary diaphragms while keeping the pressure ratio the same. However, this was not an acceptable procedure since the lowering of the pressure in the shock tube reservoir while the temperature remains constant will cause an entropy increase. A report by Harris and Warren[10] and Harris[11] showed that the gas composition in the nozzle exit flow is strongly correlated with the entropy of the shock tube reservoir. Thus it was felt that a factor of 5 change in the pressure would change the free radical concentrations too drastically in the shock tube reservoir and in the scramjet model since freezing of the species in the nozzle was expected to occur. Since ignition in the scramjet is highly dependent on the amount of free radicals present this method was discarded.

The method chosen to produce the test flow was to run the facility at the same conditions but in the large scramjet instead of expanding the flow to Mach 4.5 the flow would be over expanded in a different nozzle to mach 8. The flow was then processed by a set of 15 degree opposing compression wedges and a slight internal expansion at the start of the model to achieve a Mach number of 4.5. It was assumed that the flow would remain chemically frozen as it passed through the wedges since the entropy rise across the oblique shocks would be far less than across a normal shock.

The test conditions were chosen to maximize the amount of information that could be obtained. Since the two properties that could be varied in the reflected shock tunnel were the stagnation enthalpy and the stagnation pressure, it was decided to hold each property constant while varying the other. As can be in figure 3 of the nine test conditions chosen, five (conditions A, B, C, D and E) were at approximately the same nozzle stagnation pressure (38.7 MPa) while the stagnation enthalpy was varied from 3.6 MJ/kg to 10.7 MJ/kg. Likewise, five conditions (B, F, G, H and I) were at approximately the stagnation enthalpy (5.6 MJ/kg) while the nozzle stagnation pressure was varied from 37.5 MPa to 5.9 MPa. The test conditions are presented in table 1. The percent error in the nozzle stagnation pressure between the two scramjets ranged from 0.0 % to 8.3 % with an average value of 2.8 %. For the stagnation enthalpy the percent error between the two models ranged from 1.2 % to 7.4 % with an average value of 3.9 %.

The technique of data reduction[3] began with finding the time, in a shock aligned time frame, at which the pitot pressure at the model inlet, the static pressure at the start of the duct and the static pressure at the end of the duct attained a constant value when normalized by the nozzle stagnation pressure using an appropriate time delay such that the test slug is followed. In doing this it is assured that the flow is established throughout the scramjet duct before the test slug arrives. Using the shock speed as a guess at the flow velocity in the test section the stagnation pressure and pitot pressure for the test slug was determined form the normalized values and the time delays. The ESTC[12] code uses the experimentally determined shock speed to calculate the conditions in the nozzle reservoir for the test slug of gas using equilibrium chemistry. The NENZF[13] program is then used to calculate the flow through the Mach 4 and Mach 8 nozzle in the small and large scramjets, respectively, to obtain the nozzle exit conditions using finite rate chemistry. For the large scramjet the flow conditions are then calculated, assuming frozen chemistry, as the flow is processed by the opposing shocks off the opposing wedges, the shock and expansion fan off the fuel injector tip and the internal expansions at the start of the scramjet duct. For the small scramjet, in order to more effectively match the conditions in the large scramjet, the flow is processed by a slight internal expansion through which frozen chemistry is assumed.

The gaseous hydrogen fuel was injected at approximately Mach 2.65 with a static temperature and velocity of 120 K and 2200 m/s, respectively. The discharge coefficients for the fuel injectors in large and small scramjets were 0.69 and 0.48, respectively. Thus the effective throat height in the small scramjet was less than the scaled value. This required that the total pressure of the fuel in the small scramjet be greater than the scaled value in order to achieve the desired equivalence ratio. The ratio of the total pressures in the two scramjets therefore had an average value of 6.63.

The theoretical Mach number, static temperature, velocity, equivalence ratio, and theoretical and experimental values of the test gas static pressure at the fuel injector exit plane in the two models are given in table 2. Based on these values the scaled pressure between the two scramjets varied from 4.59 to 5.90 with an average value of 5.03. The average percent error between the two scramjets for the Mach number, static temperature, velocity and equivalence ratio was 2.2 %, 5.4 %, 2.9 % and 10 %.

The Pressure Distributions

Tare (air test gas, no fuel injection), mixing (nitrogen test gas, hydrogen fuel) and combustion runs (air test gas, hydrogen fuel) were obtained in the both scramjets at the conditions mentioned above. The exception to this is condition I where in the large scramjet no runs were obtained. Additionally, condition A in the small scramjet produced flow which was thermally choked, therefore, it will be eliminated from the following discussions.

Figure 4 shows the pressure distributions obtained in the small scramjet for condition C. The graph is plotted as a function of the distance from the fuel injector exit normalized by the scramjet duct height. Additionally, the static pressure is plotted as the ratio of the static pressure at any point in the duct to the pressure of the test gas just prior to fuel injection in order to remove any small differences in the static pressure due to slight run to run variations in the test gas intake pressure.

The pressure distributions for the combustion runs at this condition show the gradual rise in pressure characteristic of mixing limited combustion in the scramjet duct. This type of result was also obtained at conditions D and E in both scramjets as well as condition C in the large scramjet. This type of result occurs at the higher enthalpy conditions as the reaction lengths are much shorter at the higher temperatures. Also evident in figure 4 is the good repeatability obtained in the tare, mixing and combustion runs.

Figure 5 shows the pressure distributions obtained in the large scramjet for condition B. The combustion run pressure distributions for this condition show the sudden pressure rise characteristic of a reaction limited combustion situation. This was also observed for conditions F, G and H in both scramjets as well as condition B in the small scramjet. This result is expected at the lower stagnation enthalpies due to longer reaction times at the lower static temperatures. After the reactions catch up to the mixing process it is observed at each of these conditions that the reaction proceeds in a mixing limited manner.

Scaling of the Ignition Time

As was previously mentioned, the ignition times should scale be correctly scaled by the pressure length scaling factor which was tested in the experiments. Thus the ratio of the air static pressures in the small scramjet to that in the large scramjet at the point of fuel injection should equal the ratio of the ignition time in the large scramjet to that in the small scramjet. These two ratios are plotted as a function of stagnation enthalpy in figure 6. The ignition lengths are measured from the fuel injector exit to the midpoint of the two transducers where the deviation from the mixing run pressure rise is observed. Since it is unknown where between these two transducers that the combustion started, half the distance between the transducers can be used as maximums and minimums on the ignition length. From these values maximum and minimum ignition time ratios can be obtain by the quotient of the maximum and minium ignition lengths in the two scramjets. Specifically, the lower limit on the ignition time ratios is obtained by dividing the minimum value of the large scramjet ignition length by the maximum value of the small scramjet ignition length. The upper and lower limit of the ignition time ratios are also plotted in figure 6.

From this figure it is observed that for conditions B, D and E the ignition time scales well with the pressure-length scaling factor while for condition C the pressure ratio was a bit lower than the ignition time ratio. Also derived from the plots is that the pressure-length scaling law for the ignition time does not seem to be a function of stagnation enthalpy. Hence it is concluded that the at the high pressure conditions the pressure-length scaling law is a good predictor of the ignition time.

The pressure ratios and ignition time ratios, along with the upper and lower limits, are also plotted as a function of nozzle stagnation pressure in figure 7. The results indicate good agreement of the ignition time with the pressure-length scaling law for the higher pressure conditions (B and F). For the lower pressures (G and H), however, the pressure ratio is somewhat larger than the ignition time ratio. This may in part be due to the fact that the pressures in the large scramjet measured experimentally were a bit higher than those determined theoretically, as shown in table 2. Raising the pressure value for the large scramjet will lower the pressure ratio bringing it closer to the ignition time ratio. Figure 8 shows the experimental pressure ratios and ignition time ratios based on the calculated value of test gas velocity at the experimental static pressure. As can be seen, the experimental pressure ratios lie significantly closer to the ignition time ratios at the lower pressure conditions (G and H) showing more strongly the validity of the pressure-length scaling law for the ignition phenomenon.

Thus it can be concluded that the pressure-length scaling law does reasonably well at predicting the ignition times in hydrogen-air systems.

Scaling of the Combustion Pressure Rise

Possibly the most important property which determines the performance of a scramjet engine is the final pressure achieved prior to the nozzle expansion since this determines the thrust achieved from the engine. Thus this is the property which it is of the most interest to be able to understand the scaling of. The final pressures in the scramjet duct was determined by averaging the pressure level measured by the last few transducers in the duct. These pressures ratioed to the air pressure at the point of fuel injection should match the value in the scaled scramjet at the same scaled distance if it obeys the pressure-length scaling law. For

mixing-limited combustion it is expected that the pressure-length scaling law will effectively predict the pressure levels achieved in the scaled ducts. For the reaction-limited combustion cases, however, the pressure rise is not expected to rigorously hold to this scaling law since the reaction time was shown to scale by a power of pressure multiplied by the characteristic length given theoretically by equation 3.

Figure 9 shows the scaling of the combustion run pressure distributions in the large and small scramjets for test conditions B, C, D, E, F, G and H. The normalized pressure on the y-axis is the pressure divided by the experimental air pressure at the point of fuel injection which should remove any run to run variations.

By examining conditions B, C, D and E in order one can see the effect on the scaled pressure distributions of increasing the stagnation enthalpy while the nozzle stagnation pressure is held constant. The results indicate that the mixing-limited combustion cases (conditions C, D and E) show good agreement with the rate of pressure rise between the two scaled scramjets. For the reaction-limited case, condition B, the pressure rise in the large scramjet was more sudden than in the small scramjet. It is also evident from the graphs that for conditions B, C and D the normalized pressure level attained by the end of duct was slightly larger in the large scramjet that in the small scramjet. For condition E the normalized pressure level attained in both scramjet was the same.

The effect on the scaled pressure distributions of varying the nozzle stagnation pressure while the stagnation enthalpy is held constant can by shown by considering conditions B, F, G and H in figure 9. All four cases show the sudden pressure rise indicative of reaction limited combustion. The results also clearly show that again the pressure rise in the large scramjet is more sudden. Also evident again is the higher normalized pressure level achieved in the large scramjet than in the smaller one. The average value of the normalized pressure rise in the small scramjet to that in the large scramjet is 0.82.

One explanation for the difference in the rate of pressure rises for the reaction-limited cases in the large and small scramjets has to do with the ignition chemistry. Three important reactions which govern the ignition in a hydrogen/air combustion system at the pressures and temperatures for the nine test conditions (in the region of the second explosion limit) are given in equations 7, 8 and 9.

$$H + O_2 + M \xrightarrow{k_f} HO_2 + M \qquad (7)$$

$$H + O_2 \xrightarrow{k_f} OH + O \qquad (8)$$

$$O + H_2 \xrightarrow{k_f} OH + H \qquad (9)$$

Equation 7 is a three body chain breaking reaction which depletes the system of free radicals. Equations 8 and 9 are two body chain branching reactions which supply the system with free radicals. As discussed previously, the reaction rate for a two body reaction is proportional to the static pressure while the reaction rate for a three body reaction is proportional to the square of the static pressure. This means that as the pressure of the system increases, the frequency of the three body collisions increases relative to the frequency of the binary or two body collisions. Thus equation 7 has a more dominant role at higher pressures, such as the conditions in the small scramjet, stifling the production of the free radicals necessary to initiate the combustion process. This is one possible explanation for the differences in the reaction rates between the two scramjets for the reaction-limited combustion cases.

As mentioned previously, for all conditions except the highest enthalpy condition the normalized pressure level attained in the large scramjet was slightly higher than that in the small scramjet. One possible explanation for this is that since that pressure rise at the higher enthalpies was fairly small the accuracy of the ratio for this condition may be somewhat less than for the lower enthalpy conditions. This could also partially be due to the effect of the pressure on the dissociated species. As was mentioned briefly, an theoretical analysis on the effect of pressure on the equilibrium heat release was conducted. The results indicated that the pressure rise at the higher pressure level (small scramjet) would be slightly larger than that at the lower pressure level (large scramjet). This was due to the effect of the larger static pressure forcing the species into a more molecular form, forcing the dissociated species into water. The effect of was greatest at the highest enthalpy condition (E) because at the higher enthalpies there is a greater amount of free radicals present which may be affected. This could have aided in increasing the normalized pressure rise in the small scramjet relative to the large scramjet.

While considering the small variations in scaled pressure levels attained in the two scramjets it should be pointed out that the deviations from the pressure-length scaling law are relatively minor. It should therefore be considered a second order effect. The important point is that the pressure rise does not scale by the pressure^2-length scaling law as was initially guessed at prior to this study.

Conclusions

It has been show that the ignition time scales reasonably well by the pressure-length scaling law as was expected from study of the chemical reactions involved in the ignition process and the semi-empirical model of Pergament[4]. The pressure rise attained and the rate of pressure, however, showed second order deviations from the binary scaling law. The rate of pressure rise in the large scramjet at the reaction-limited conditions was found to be more sudden than in the small scramjet. This may be due to the effect of the higher pressure in the small scramjet enhancing the three body reactions which deplete the supply of free radicals. The normalized pressure levels attained due to combustion in the large scramjet were found to be somewhat higher than in the small scramjet at all but the highest enthalpy condition (E). The reason that condition E did not follow the same trend may have to do with the lower accuracy's at the higher enthalpies or possibly due to the effect of the higher pressure in the small scramjet forcing the dissociated species into water.

The above effects, however, are considered minor to the fact that the pressure-length scaling law seems to provide, with reasonable accuracy, a relation for predicting the fundamental phenomena occurring in a scramjet combustor. Thus, while there are second order effects, the pressure-length scaling law is effective as a first order approximation for scaling scramjet performance.

Acknowledgements

The authors wish to acknowledge the work of Dr. Peter Jacobs for the initial design and preliminary testing of the large scramjet. The authors are additionally pleased to acknowledge the support received through NASA grant NAGW-674, and through the Australian Research Council.

Bibliography

1. Stewart, D.G. (1951) "Similarity and Scale Effects in Combustion Chambers," National Gas Turbine Establishment, Memorandum M129, October.

2. Stewart, D.G. (1956) "Scaling of Gas Turbine Combustion Systems," *Selected Combustion Problems II*, Advisory Group for Aeronautical Research and Development, Butterworths Scientific Publications, London, pp. 384-413.

3. Pulsonetti, M.V. (1996), "Scaling Laws for Scramjets," Ph.D. Thesis, Department of Mechanical Engineering, University of Queensland, Australia.

4. Pergament, H.S. (1963), "A Theoretical Analysis of Non-Equilibrium Hydrogen-Air Reactions in Flow Systems," [Preprint] 63113, American Institute of Aeronautics and Astronautics, April.

5. Prandtl, L. (1927), *Ergeb. AVA Goett.*, ser. III, pp. 1-5.

6. White, F.M. (1974), *Viscous Fluid Flow*, McGraw Hill Book Company.

7. Anderson, G.Y. (1974), "An Examination of Injector/Combustor Design Effects on Scramjet Performance," *Proceedings of the Second International Symposium on Air Breathing Engines*, Sheffield, England, March 1974

8. Morgan, R.G., Bakos, R.J., Tamagno, J. (1990), "Bulk Parameter Analysis of Hypersonic Combustion Experiments," GASL TR 321, August.

9. Jacobs, P.A. and Stalker, R.J. (1991), "Mach 4 and Mach 8 Axisymmetric Nozzles for a High-Enthalpy Shock Tunnel," *The Aeronautical Journal of the Royal Aeronautical Society*, Vol. 95, No. 949, November 1991.

10. Harris, C.J., Warren, W.R. (1964), "Correlation of Nonequilibrium Chemical Properties of Expanding Air Flows," General Electric Document R64SD92, December.

11. Harris, C.J. (1966), "Comment on 'Nonequilibrium Effects on High-Enthalpy Expansion of Air'," AIAA Journal, Vol. 4, No. 6, June, p.1148.

12. McIntosh, M.K. (1968), "Computer Program for the Numerical Calculation of Frozen and Equilibrium Conditions in Shock Tunnels," Dept. of Physics, School of General Studies, Australian National University, Canberra.

13. Lordi, J.A., Mates, R.E., and Moselle, J.R. (1966), "Computer Program For the Numerical Solution of Nonequilibrium Expansion of Reacting Gas Mixtures," NASA CR-472.

TABLE 1 Nozzle Stagnation Pressures and Stagnation Enthalpies for the Nine Test Conditions

Test Condition	Nozzle Stagnation Pressure (MPa)			Stagnation Enthalpy (MJ/kg)		
	LS	SS	Average Value	LS	SS	Average Value
A	45.8	45.8	45.8	3.65	3.53	3.59
B	37.5	37.5	37.5	5.68	5.61	5.65
C	40.0	40.0	40.0	7.64	7.17	7.41
D	33.9	33.9	33.9	8.47	8.06	8.27
E	36.1	36.1	36.1	10.65	10.75	10.70
F	32.2	32.2	32.2	5.90	5.48	5.69
G	19.2	20.8	20.0	5.36	5.49	5.43
H	13.1	15.1	14.1	5.52	5.79	5.66
I	-	5.9	5.9	-	5.37	5.37

TABLE 2 Air Properties and Equivalence Ratios at Fuel Injection

Test Condition		Mach Number	Pressure (kPa)	Temperature (K)	Velocity (m/s)	Equivalence Ratio	Measured Pressure (kPa)
A	LS	4.52	18.6	710.	2420.	1.33	47.6
	SS	4.56	88.3	690.	2380.	1.11	116.
B	LS	4.42	17.0	1100.	2940.	1.23	16.6
	SS	4.46	78.0	1110.	2910.	1.33	75.3
C	LS	4.36	18.6	1520.	3380.	1.36	18.5
	SS	4.30	91.2	1500.	3230.	1.27	85.0
D	LS	4.38	14.0	1640.	3540.	1.26	18.3
	SS	4.17	82.7	1740.	3380.	1.60	89.2
E	LS	4.26	20.9	2080.	3870.	1.32	25.3
	SS	3.96	99.7	2390.	3760.	1.33	101.
F	LS	4.45	13.3	1130.	3000.	1.29	15.4
	SS	4.47	66.8	1080.	2870.	1.30	73.6
G	LS	4.47	7.8	1010.	2840.	1.59	11.0
	SS	4.47	42.9	1080.	2870.	1.31	48.4
H	LS	4.38	6.6	1060.	2860.	1.23	10.4
	SS	4.44	31.9	1150.	2940.	1.16	31.9
I	SS	4.47	12.2	1030.	2810.	1.44	12.5

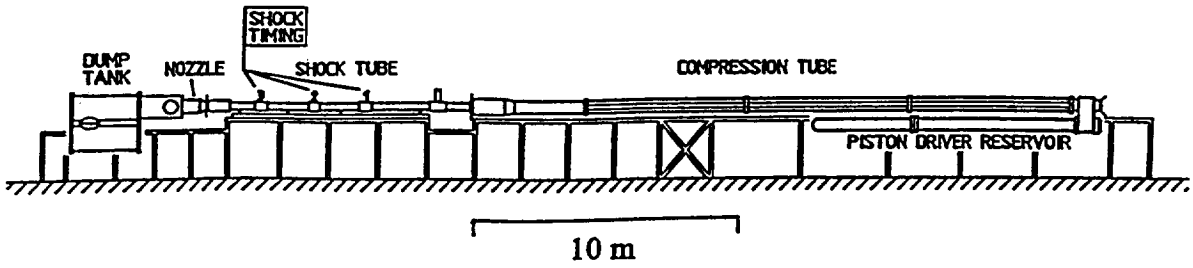

Figure 1 The Free Piston Driven Reflected Shock Tunnel, T4

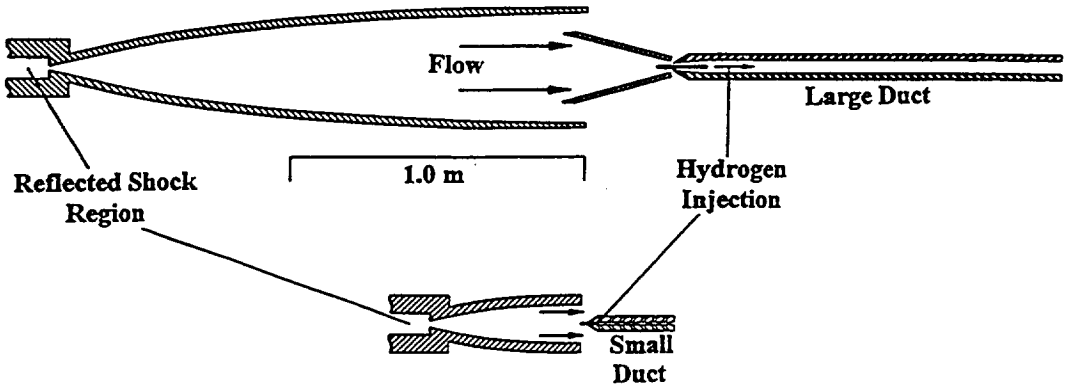

Figure 2 Test Configurations of the Large and Small Scramjets

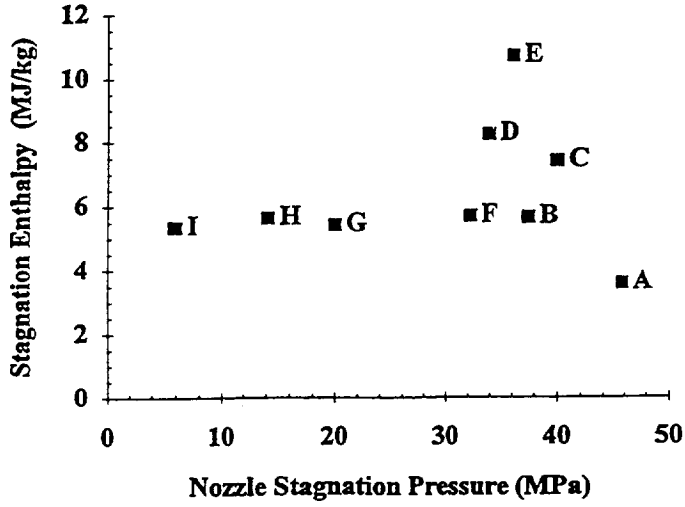

Figure 3 Test Conditions as a Function of Nozzle Stagnation Pressure and Stagnation Enthalpy

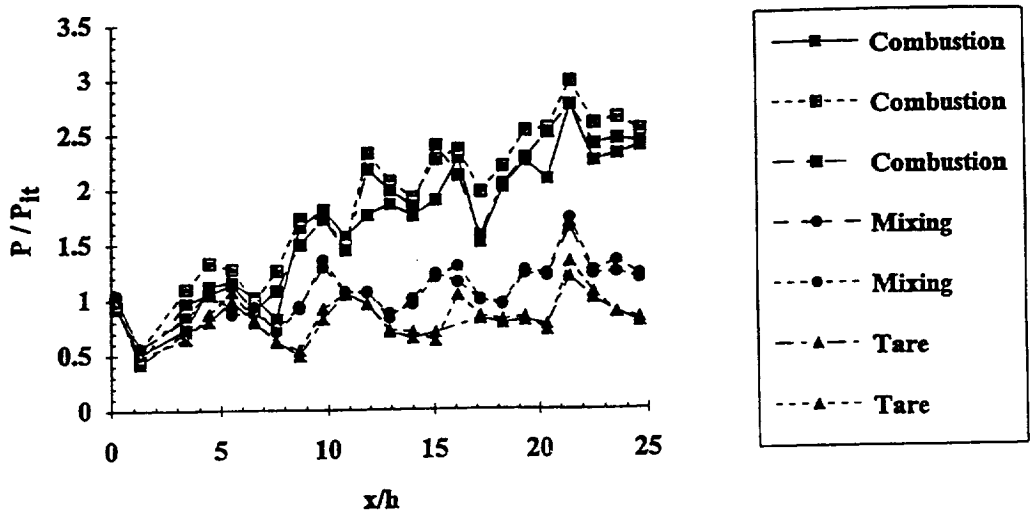

Figure 4 Pressure Distributions Obtained at Condition C in the Small Scramjet

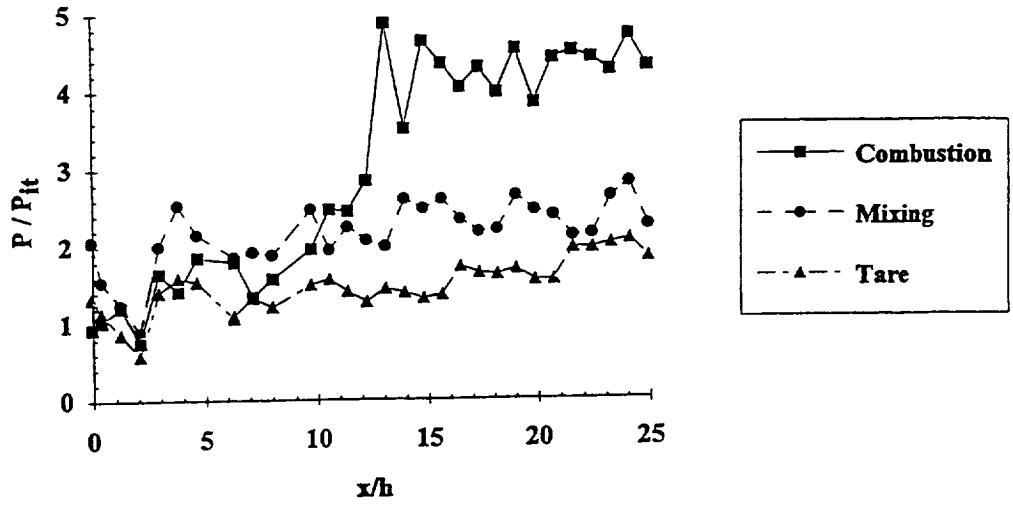

Figure 5 Pressure Distributions Obtained at Condition B in the Large Scramjet

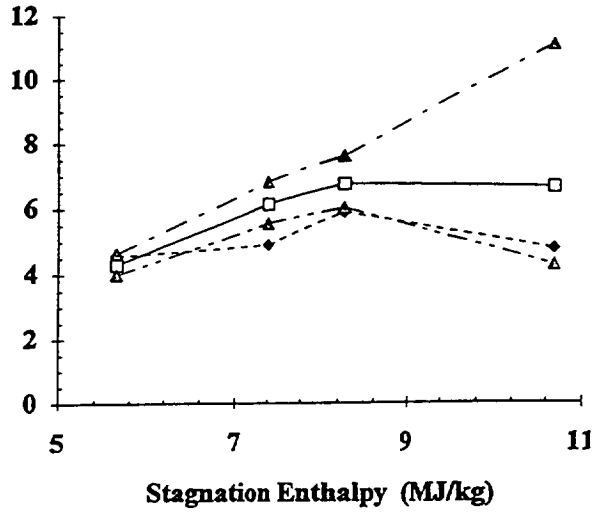

ure 6 Variation of Ignition Scaling with Stagnation Enthalpy

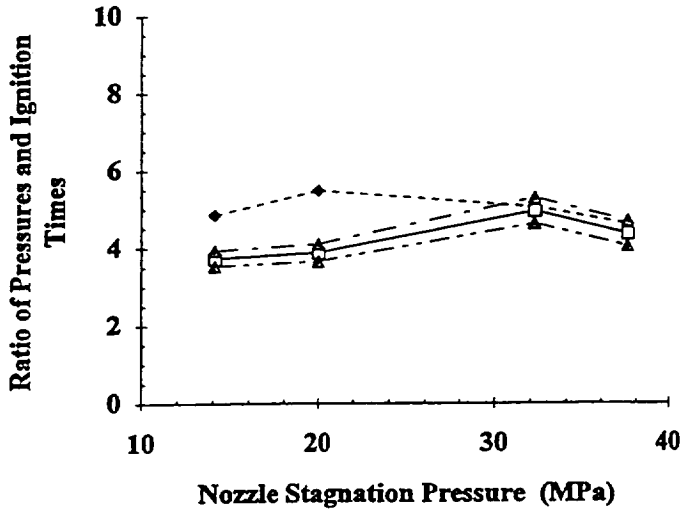

Figure 7 Variation of Ignition Scaling with Nozzle Stagnation Pressure

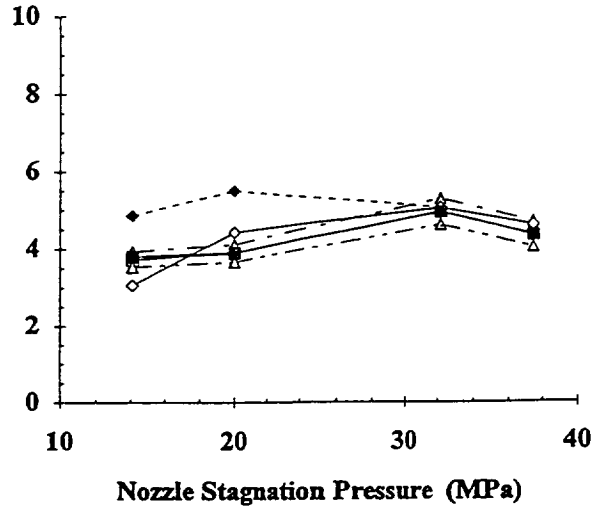

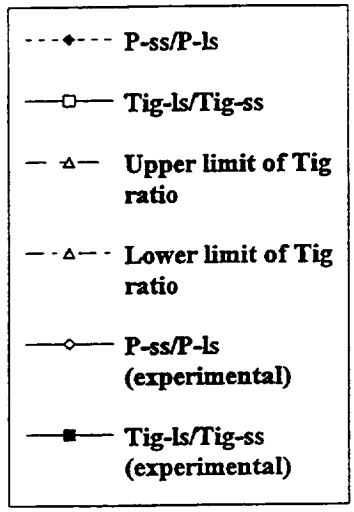

igure 8 Variation of Ignition Scaling with Nozzle Stagnation Pressure using the Experimental Values of Static Pressure in the Duct

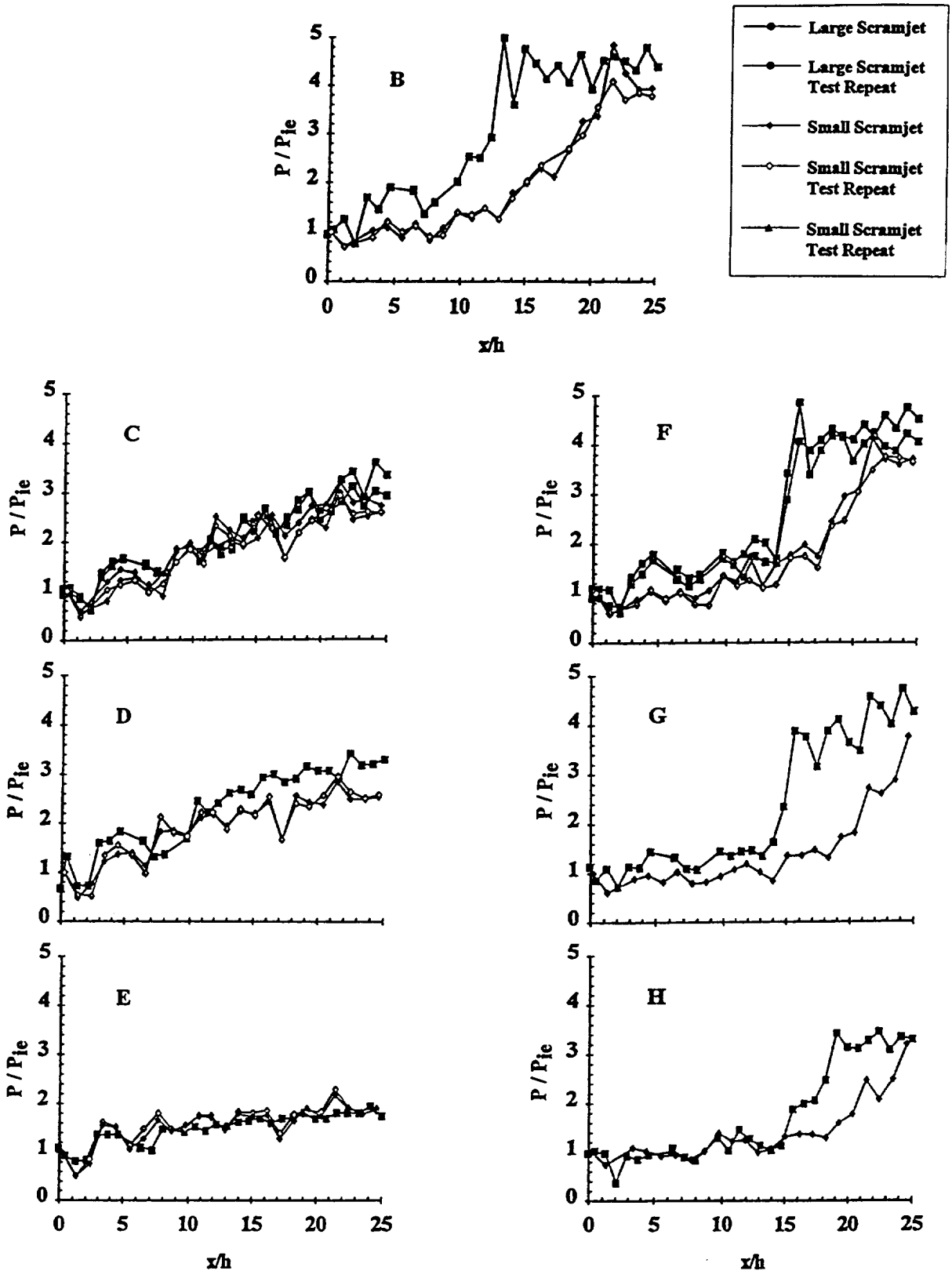

Figure 9 Scaling of the Combustion Run Pressure Distributions

AIAA 96-4534

A SHOCK TUNNEL INVESTIGATION OF SCRAMJET PERFORMANCE WITH PARTIALLY PREMIXED COMBUSTION

by

R.J. Stalker, R.G. Morgan & A. Paull
Department of Mechanical Engineering
The University of Queensland
Brisbane, Australia

A SHOCK TUNNEL INVESTIGATION OF SCRAMJET PERFORMANCE WITH PARTIALLY PREMIXED COMBUSTION

R.J. Stalker*, R.G. Morgan†, & A. Paull‡
The University of Queensland, Brisbane Queensland 4072, Australia.

ABSTRACT

The effect of allowing partial premixing of fuel and air before combustion heat release takes place is investigated for supersonic combustion of hydrogen in air. This premixing leads to a sharp, explosive, pressure rise at combustion. Attention is focussed on the thrust generated with a simple combustion chamber-thrust nozzle combination at approximate pre-combustion temperatures of 1100 K. The occurrence of the explosive pressure rise in the combustion chamber depends on a parameter involving the flow velocity and the pressure, as well as the length of the combustion chamber. Thrust production is inhibited when the value of this parameter is too low to allow the explosive pressure rise to develop in the combustion chamber.

NOMENCLATURE

Symbols

- D - effective combustion chamber length
- h - duct height
- ΔI_{sp} - incremented specific impulse
- M - Mach number
- p - pressure
- r - distance downstream of expansion corner
- U - velocity
- x - distance downstream of injection station
- x_c - distance from injection station to pressure peak
- ρ - density
- ϕ - equivalence ratio

Subscripts

- $_i$ - pre-combustion
- $_o$ - adjacent to injector strut

---

* Emeritus Professor of Space Engineering, Associate Fellow, AIAA.
† Reader in Mechanical Engineering, Member, AIAA
‡ Research Fellow

---

1. INTRODUCTION

Because of the difficulty and expense associated with flight tests, experimental development of scramjets will be forced to rely on ground facilities for the foreseeable future. Shock tunnels are part of the family of ground facilities which are able to achieve high test section velocities at static pressure levels suitable for supersonic combustion, and may therefore be expected to play an important role in scramjet development.

In a shock tunnel study of hydrogen-air combustion scaling at a Mach number of 4.4, Pulsonetti[1] considered two constant area ducts of rectangular cross section which differed in size by a factor of 5, and investigated the pressure distributions along the ducts associated with combustion. Two types of combustion were evident. At pre-combustion temperatures of 1400 K and above, the pressure distributions were typical of mixing limited combustion, exhibiting a nearly constant positive gradient along the ducts. However, at temperatures of 1100 K, a very different pressure distribution occurred, with a sharp combustion pressure rise at some distance downstream of the fuel injection station. This phenomenon is apparently controlled by combustion kinetics and, until it is better understood, it may conveniently be referred to as an explosive pressure rise.

The present study concerns the influence that this effect may have on the generation of thrust in a simple combustor-thrust nozzle combination. As shown in fig.2, the model was such as to produce approximately two-dimensional flow, with a constant area combustion chamber, and one wall deflected to make a simple thrust nozzle. Choice of such a configuration was made to simplify interpretation of the results, rather than to yield high thrust performance. As Pulsonetti's work showed that the location of the explosive pressure rise depended on the pressure, the experiments were used to explore the influence of the length and the pressure level of the combustion chamber on the generation of thrust.

The paper begins with a description of the experimental apparatus, followed by a discussion of the features of the explosive pressure rise in the combustion chamber. Next the flow mechanisms which lead to thrust production in the nozzle are considered. The results of the experiments are then presented, and their implications are discussed before concluding.

2. EXPERIMENTAL APPARATUS

(a) The Shock Tunnel

The experiments were done in the free piston shock tunnel T3 at the Australian National University, Canberra. This is described in some detail in ref 2, and is shown in fig.1. It employs a shock tube 76 mm in diameter and 6 m long, and the driver gas is heated by compression with a free piston in a tube 300 mm in diameter and 6 m long. A contoured nozzle with a 25 mm diameter throat and a 92 mm exit diameter was located at the downstream end of the shock tube. The tunnel was operated in the shock reflection mode, with the reflected shock rupturing a thin mylar diaphragm at the throat of the nozzle. This allowed the shock heated test gas to expand through the nozzle, and after completion of the nozzle flow starting process, to establish a steady free jet flow in the test section.

The nozzle reservoir conditions were obtained by using measurements of the shock speed and the initial pressure in the shock tube to give the conditions after shock reflection, and then assuming isentropic expansion to the measured value of the pressure near to the end of the shock tube. Helium and Argon were used as driver gas and, by mixing these in various ratios, it was possible to control the decay in the nozzle reservoir conditions during the test time. The flow conditions in the test section were calculated by assuming one-dimensional equilibrium nozzle flow. Non-equilibrium flow computations indicate that the assumption of equilibrium is reasonable for the low area ratio nozzle employed. Calculated conditions at the nozzle exit are presented in Table 1 for selected values of the stagnation enthalpy and a reservoir pressure of 10 MPa.

Table 1 Tunnel Test Section Conditions

Stag. Enthalpy ($MJkg^{-1}$)	Static pressure Reservoir Pressure (10^{-2})	Mach Number	Static Temp (K)	Velocity ($km\ s^{-1}$)
2.5	0.94	3.55	690	1.90
4.0	1.02	3.45	1180	2.40
5.5	1.11	3.35	1790	2.75
7.0	1.20	3.20	2270	3.10

Assumed reservoir pressure - 10 MPa

(b) The Model

The model is shown in fig.2(a). It was essentially two-dimensional, with an internal width throughout of 50 mm, and consisted of a duct of constant height 25 mm, followed by a thrust nozzle in which the upper surface was fixed and parallel to the tunnel axis, while the lower surface was set at a divergence angle of 15°. The lower surface therefore became the sole thrust surface, and was instrumented with Pcb Piezotronic quartz piezoelectric pressure transducers.

The fuel injector strut was located midway between the upper and lower surfaces of the constant area channel, and fully spanned its width. A pressure transducer was located in each of the 50 mm walls of the duct adjacent to the injector to monitor the pressure there. Hydrogen was injected through a two dimensional supersonic nozzle, with a 1.6 mm throat, which spanned the full width of the blunt trailing edge of the injection strut. The hydrogen was supplied from a room temperature reservoir, and the mass flow rate was determined, from precalibration of the injector, by monitoring the reservoir pressure. The leading edge of the strut was a symmetric wedge of 20° included angle, and was located sufficiently far upstream of the inlet that the leading edge wave system did not interfere with the inlet airflow.

The experiments were conducted with two combustion chamber lengths, as shown schematically in fig.2(b). For the shorter one, the expansion corner was located 25 mm downstream of the fuel injection station. If the combustion zone is regarded as terminated by the expansion from this corner then, noting that the leading edge of the fan will intersect the midplane of the duct approximately 40 mm downstream of the corner at a Mach number of 3.5, the effective combustion chamber length, D, is 65 mm. It should be noted that, although this is a somewhat arbitrary estimate, it does attempt to approximate the effective length of the combustion zone. The longer combustion chamber involved a 150 mm insert to lengthen the constant area section, so that the corner was then 175 mm downstream of the injection station, and the effective combustion chamber length became 215 mm.

In order to increase the pre-combustion pressure, provision was made for compression of the inlet flow by attaching an intake consisting of two opposing simple wedges, as shown in fig.2(a). This was designed to produce a flow pattern with the two opposing shocks reflecting on the centreline, and spilling out of a gap ahead of the inlet, thus ensuring uniform inlet flow. The wedges were enclosed by side plates, set 50 mm apart and, when they were set at an angle of 5°, raised the pressure and temperature by factors of 2.3 and 1.27 respectively, and lowered

the Mach number and velocity by factors of 0.84 and 0.94 respectively.

(c) Thrust Measurement

The thrust was obtained by integrating the measured pressures over the thrust surface, and taking account of the surface slope to convert the integrals to a thrust. The data processing arrangement allowed the thrust to be calculated at intervals of 16 μsec during the test time to produce an effectively continuous thrust record. This was then normalised by the reservoir pressure, the period for which the resultant record was steady was taken as the period of steady flow, and the thrust was measured during that time. Typical records are shown in fig.3, obtained both with a decaying and a nearly steady reservoir pressure. It can be seen that, in both cases, the normalised thrust reaches an essentially steady value, through the approach to a steady value is slower with the long duct than with the short duct.

At a duct air velocity of 2 km^{-1}, the time for the airflow to pass from the injector to the last pressure transducer on the thrust surface was 140 μsec for the short duct, and 210 μsec for the long duct. Thus, a normalised thrust steady period of 0.5 milliseconds represents 3.5 flow transit times for the short combustion chamber model and 2.3 for the long one.

The fuel supply pressure was constant during each test, and therefore the fuel equivalence ratio increased during the tests in which the reservoir pressure decayed. A constant normalised thrust therefore implied that increasing the fuel equivalence ratio did not increase the relative degree of mixing or the heat release. The slow approach to a steady value sometimes observed with decaying pressure with the long duct may be an indication that the increase in fuel equivalence ratio has a residual effect, as may be seen for the constant area duct in fig.5(d).

3. COMBUSTION PROCESSES

The combustion reaction of hydrogen with air is characterised by an ignition phase, during which a supply of free radicals is produced, followed by a phase during which heat release takes place. If these processes take place rapidly with respect to the time scale for mixing between the hydrogen and air, then mixing controlled combustion occurs, as shown in fig.4(b). However if the ignition phase is slow compared with the mixing time scale, then an unburnt combustible mixture forms in the mixing wake downstream of hydrogen injection. Now, it is well known that a hydrogen-air mixture, upon completion of the ignition phase, will react very rapidly (e.g. ref.3). Therefore the formation of a combustible mixture may reasonably be expected to lead, at a sufficient distance downstream of injection, to an explosive type heat release, as shown in fig.4(b).

Whereas the mixing controlled combustion shown in fig.4(a) causes continual heat release as mixing progresses, with an associated gradual pressure rise along the duct, the situation in fig.4(b) is different. Here the mixing takes place without heat release for some distance, and then heat release occurs in a short streamwise distance as the mixture burns energetically. If the heat release is sufficient, the associated temperature rise causes an increase in the reaction rates which allows subsequent mixing and combustion to proceed as a mixing controlled process. The rapid temperature rise also causes a correspondingly rapid increase in the displacement thickness of the wake, and this gives rise to the oblique shock waves shown in the figure. These are closely followed by expansion waves as the streamwise rate of growth of displacement thickness reduces with the completion of the process of rapid heat release. These overtake the shock waves, so that they cease to be in evidence after one or two reflections at the wall of the duct. Thus the overall effect of the rapid heat release is to cause a sharp rise in pressure at the wall, which is seen as an explosive pressure rise.

This mechanism has been used in offering an explanation for results obtained in Pulsonetti's study [1] of scaling of supersonic combustion. Pressure distributions along two rectangular, constant area, ducts were measured, one of 100 mm x 47 mm cross section, and the other 20 mm x 9.4 mm. At pre-combustion temperatures of 1400 K and above, the gradual pressure rise along the duct, as in fig.5(a), which is associated with mixing controlled combustion was experienced. However, at temperatures slightly in excess of 1100 k, the explosive rise in pressure seen in figs.5(b) and 5(c) occurred. This also occurred with the constant area duct in the present tests, at a temperature of 1200 K, as shown in fig.5(d).

It might be noted that the approach of the flow to a steady state in pulse combustors of this nature has been treated numerically in refs.4 & 5. The analysis done there indicates that the pressure distributions in fig.5 represent a steady state and, in the case of

fig.5(b) and 5(c), this was confirmed by observing the time dependence of the pressure distributions. In the case of fig.5(d), the pressure distributions are presented, for an equivalence ratio of 0.6, over a time period of 192 μsec. This represents 1.3 times the time take for the mainstream flow to pass from the injector to the last downstream pressure orifice, and 5.3 times the time to the point where the explosive pressure rise peaks. The pressure distributions exhibit only minor variations over this period, confirming that they represent steady flow.

The streamwise distance from injection to the point at which the explosive pressure rise ceases is denoted as x_c, and the parameter $p_i x_c/U_i$ is plotted against the pre-combustion pressure, p_i in fig.6. Here U_i is the pre-combustion air velocity and p_i is calculated as 0.75 P_0 where P_0 is the measured wall pressure adjacent to the injector strut, and the factor of 0.75 accounts for isentropic expansion of the airflow to the full duct area. Experiments are also reported in ref.1 in which the pre-combustion pressure was varied, while the pre-combustion temperature was maintained within the range 1060 K to 1140 K, and the results of these are incorporated in the figure. It can be seen that $p_i x_c/U_i$ is fairly insensitive to the pressure level, varying only by a factor of 2.6 as p_i varies by a factor of 30. A tentative explanation for the variation, based on the possible effect of three body reactions is offered in ref.1 but, for the present purpose, it is sufficient to regard fig.6 simply as affording an empirical basis for locating the position of the pressure rise.

It will be observed that the explosive pressure rise in fig.5(d) is considerably less, as a proportion of the pre-combustion pressure, than that in figs.5(b) or 5(c). This is consistent with the flow model set forth above. The magnitude of the pressure rise will depend on the ratio of the duct height to the increase in displacement thickness due to rapid heat release, and the increase in displacement thickness will depend on the amount of fuel which has mixed with air to form a combustible mixture. Now, the growth of a wake in incompressible flow is independent of the pressure[6], and if it assumed that the same applies to a compressible wake with mixing, then the increase in the fraction of fuel-air mixture along the wake will also be independent of the pressure. The correlation of fig.6 then implies that, with a given wake in a given duct, increasing the pressure reduces the distance over which the combustible mixture forms, and therefore, by reducing the proportion of combustible mixture at rapid heat release, also reduces the explosive pressure rise. The scaling rule of ref.1. indicates that the duct of fig.5(d) will experience the same explosive pressure rise as seen in figs.5(b) and 5(c) if $P_0 \approx 35\,kPa$. Thus the high value of P_0 noted on the figure leads to a smaller proportional pressure rise than figs.5(b) and 5(c).

It might be noted, as a corollary of this, that further increases of pressure in the same duct would, by leading to even small explosive pressure rises, tend to produce pressure distributions typical of mixing controlled combustion, as in the downstream part of fig.5(d).

It can be seen in fig.5(d) that increasing the amount of fuel injected does not change the magnitude of the explosive pressure rise, indicating that it does not affect the amount of fuel mixed, at least until the rapid heat release has taken place. It also does not change the location of the explosive pressure rise, and observation which is consistent with a dependence on the kinetics of the combustion process.

4. THE THRUST NOZZLE

The thrust delivered by the combustion chamber-thrust nozzle combination depends not only on the combustion process, but also on the flow in the thrust nozzle. Considering first the case where a uniform flow issues from the combustion chamber then, by assuming isentropic flow of a calorically perfect gas, the flow patterns shown in fig.7(a) are obtained. With a pre-combustion Mach number of 3.5, the nozzle entrance Mach number of 3 and ratio of specific heats, γ, of 1.4 of fig.7(a)(i) would be an example of small heat addition, with a pressure rise in the combustion chamber of only 33% of the pre-combustion pressure. The Mach number of 2.0 and $\gamma = 1.2$ of fig.7(a)(ii) would correspond to substantial heat addition, with a pressure rise of 175% and a nozzle flow of hot combustion products. Mach lines in the two flows are shown, tracing the waves generated by the 15° expansion corner. It can be seen that at a Mach number of 3, the reflected wave intersects the thrust surface just upstream of the trailing edge, and therefore does not significantly influence the thrust. At a Mach number of 2, the reflected waves will have more influence.

It is possible to compare the thrust generated by this nozzle with that which would be generated if the

surface were to be contoured to cancel the reflected waves, and produce a uniform flow at the nozzle exit. As shown schematically in fig.7(b), this produces a conventional supersonic nozzle and the thrust therefore can be obtained from one dimensional theory [7]. For the same nozzle area ratio, the thrust is 70% of that for the contoured nozzle for the case of fig.7(a)(i), and 106% for the case of fig.7(a)(ii). This indicates that, for uniform flow from the combustor, the thrust in this study is approximately determined by the nozzle area ratio.

When the combustion chamber is too short to produce a uniform flow, then the fuel and the heat release tend to be concentrated in the wake close to the injection strut, as shown in fig.7(c). The combustion induced increment of thrust is then produced by two types of waves[8] impinging on the thrust surface. The first is the compression waves which arise from the combustion induced increase of the wake displacement thickness, and the second is the waves which arise from the interaction of the wake with the expansion fan. These expansion interaction waves are generated when the expansion fan crosses the wake, and again when the reflected expansion crosses the wake. However, in the experiments, the wave resulting from the second crossing passes downstream of the trailing edge of the thrust surface, and so the thrust from this wave is not recovered.

5. RESULTS AND DISCUSSION

Results of thrust measurement with the short combustion duct are shown in fig.8. The flow representative of these measurements is shown in fig.7(c). It was intended that the expansion corner would be sufficiently close to the fuel injection station to ensure that all compression waves generated by the combustion wake would impinge on the thrust surface, but the lower Mach number achieved with the 5° wedges was such that this was not quite realised.

Tests were conducted both with and without introduction of the hydrogen fuel. The thrust obtained with no fuel flow was subtracted from the thrust with fuel on, and the result was divided by the hydrogen mass flow and the acceleration due to gravity to yield the increment of specific impulse due to introduction of the fuel.

The variation of this incremental specific impulse with pre-combustion temperature is shown in fig.8(a) for three values of the pre-combustion pressure. The results at 2.8 atm and 0.6 atm. were obtained with the intake wedges in place. The fuel equivalence ratio varied from 0.7 to 1.1 in these tests, and advantage was taken of the decaying reservoir pressure and the constancy of normalised thrust, outlined in section 2(c), to obtain a value for an equivalence ratio of unity. This value is plotted in the figure. The incremental specific impulse shows no significant effect as p_i is reduced from 2.8 atm to 1.1 atm, but with further reduction to 0.6 atm, it is seen to fall off dramatically. At this pre-combustion pressure the normalised thrust remained steady only for periods of 200 to 300 μsec. Note that the short length of the combustion zone implies limited mixing of hydrogen with air, and therefore only modest values of the incremental specific impulse are obtained.

Thrust surface pressure distributions corresponding to each of the three pre-combustion pressures are shown in fig.8(b). At $p_i = 2.8$ atm, the correlation for the location of the explosive pressure peak represented by the cross hatching in fig.6 indicates that the peak of the pressure rise will occur at $x_c \approx 40\,mm$ from the injector, and the pressure rise therefore will be reduced in strength below that evident in fig.5(d), but the associated compression wave will be incident on the thrust surface. This is consistent with the pressure distribution which shows a sharp, though relatively weak pressure rise with a location, at the peak of the distribution, which is approximately correct. At $p_i = 1.1$ atm, $x_c \approx 90\,mm$, and it will be expected that the Prandtl-Meyer expansion from the corner will cause the peak of the explosive pressure rise to be suppressed. However, the rising pressure which precedes the peak will still occur, and the observed pressure distribution is consistent with that[7] At $p_i = 0.6$ atm, $x_c \approx 150\,mm$, and only a little of the pressure rise preceding the peak will occur before combustion is terminated by the falling pressure of the expansion. Thus the pressure on the thrust surface is reduced, and so is the thrust. It may be noted that in this case two pressure distributions are shown, 100 μsec apart. These demonstrate that, although the flow is unsteady at this condition, the main features of the pressure distribution do not change.

The incremental specific impulse associated with the long combustion duct is plotted in fig.9(a), again for three values of the pre-combustion pressure. The fuel equivalence ratio varied from 0.6 to 1.2 in these tests and, as before, the specific impulse appropriate to an equivalence ratio of unity is plotted. In this case, the

intake wedges were used only at the highest of the three pressures. It can be seen that incremental specific impulse values approximately twice those with the short duct were obtained. As before, reducing ρ_i from 2.5 atm to 1.0 atm has no significant effect, whereas further reduction to 0.5 atm causes the specific impulse to be substantially reduced.

Pressure distributions on the thrust surface are shown in fig.9(b). Two pressure transducers were also located in the constant area section, respectively 102 mm and 171 mm downstream of the injection station, and the pressures recorded there are also displayed. With $p_i = 2.5$ atm, fig.6 indicates that $x_c \approx 50\,mm$, and so the flow in the combustion duct will essentially be mixing limited following a small explosive pressure rise. The thrust surface pressure distribution therefore does not exhibit the rapid rise to a peak which is evident in fig..8(b), but is qualitatively consistent with a Prandtl-Mayer expansion from the measured pressure upstream of the corner, together with the addition of the expansion wake interaction. At $p_i = 1.0$ atm, $x_c \approx 105\,mm$, indicating that the peak of the explosive pressure rise should occur close to the upstream transducer in the combustion duct. As shown, the pressure there oscillates between the values plotted, which is consistent with a local region of steep pressure gradient shifting slightly due to small fluctuations in the flow. The pressure distribution on the thrust surface is very similar to that at the higher pressure, indicating that although the location and magnitude of the explosive pressure rise is different in the two cases, no effective difference exists in the overall degree of mixing and combustion.

At $p_i = 0.5$ atm, $x_c \approx 180\,mm$, and the compression waves giving rise to the pressure peak originate just upstream of the expansion corner. Evidence of these waves, one directly incident on the thrust surface and the other reflected from the upper surface of the duct, can be seen in the pressure distribution at 770 μsec. However, this pressure distribution is very sensitive to the reservoir pressure, as may be seen by plotting a pressure distribution 100 μsec later, when the reservoir pressure has decayed by only 5%. It can be seen that evidence of the compression wave directly incident on the surface has disappeared. The persistence of the reflected one is consistent with the downstream displacement of the corner expansion on the upper side of the wake allowing the compression wave to form there.

The effect of increasing the combustor length at $p_i = 1.0$ atm is seen in fig.9(a) in the results at $M_i = 4.4$. These were performed in the free piston shock tunnel T4, at The University of Queensland, with a thrust divergence angle of 11°. The same combustor configuration was used, but the distance between the injection station and the expansion corner was 490 mm. Fig. 6 indicates that the explosive pressure peak occurs at X_c = 140 mm, and therefore there is adequate provision for further mixing and combustion after the peak. It can be seen in the figure that a significant increase in the incremental specific impulse is recorded at $T_i = 1100\,K$.

The results indicate that, at the temperature of interest, the generation of thrust depends on the value of the parameter, $p_i\,D/U_i$, achieved in the combustor. If this value is sufficient, an explosive pressure rise occurs. The strength and location of the explosive pressure rise has little effect on the thrust produced, indicating that mixing of the fuel and air may occur before or after the pressure peak without significantly affecting the heat release. However, if the value of $p_i\,D/U_i$ is too small, and the heat release associated with the explosive pressure rise does not occur, the thrust falls.

A comment should be made on the effect of combustor skin friction on the thrust. Regarding the combustor as extending from the injection station to the corner expansion, the friction force may be written

$$f = sD\,\rho U^2\,C_F/2$$

where s is the perimeter length of the combustor cross section, ρ is the density, U the velocity and C_F the mean skin friction coefficient. Putting $\rho = p/RT$, this becomes

$$f = \left(sU^2/2RT\right)C_F\,pD \quad .$$

Since the combustor wall is highly cooled, a value of 2.5×10^{-3} might be taken for C_F[9]. Then, at a velocity of 2.3 km s^{-1} and a temperature of 1100 K, this yields

$$f = 3.2 \times 10^{-3}\,pD \text{ Newtons}$$

Thus, to minimise the friction force, the value of pD must be minimised. But the value of pD should be sufficient to allow the explosive pressure peak to

occur in the combustion chamber, and this implies that there is a lower limit for the skin friction force. For example at p_i = 1.0 atm, a minimum combustion chamber length of, say, 150 mm is necessary to realise the specific impulse values shown in fig.9(a), and this leads to a friction force of 48 N. With hydrogen fuel, at an equivalence ratio of unity, this yields a loss in specific impulse of 185 sec, or 10% of the peak value of 1250 sec shown in fig.9(a). This is a significant loss and, moreover, one which will increase with the velocity. However it should be remarked that the combustion chambers used here are very small, and the skin friction loss in specific impulse will reduce as the linear dimensions of the combustion chamber are increased.

6. CONCLUSION

The sharply rising pressure, here called an explosive pressure rise, which appeared in Pulsonetti's work at pre-combustion temperatures around 1100 K, also appeared in the present work at about the same temperature. However, because of the higher pressure levels involved and the dimensions of the combustion chamber, the magnitude of the pressure rise was reduced. Nevertheless, its effect could be observed in measurements of the thrust produced by a simple nozzle. In particular, the thrust was seen to fall off when the combination of pressure and length of the combustion chamber was insufficient to realise the pressure rise.

The experiments indicated that, when the explosive pressure rise did occur in the combustion duct, its strength and location had little effect on the thrust produced, indicating that mixing of the fuel and air may occur before or after the pressure peak without significantly affecting the heat release. However, it should be remembered that only a moderate explosive pressure rise was experienced in these tests, and the situation may be different with a larger explosive pressure rise.

It is worth noting that a thrust nozzle with an area ratio of approximately 4 was used in the experiments. One dimensional theory indicates that this fails to fully realise the thrust potential of the combustion chamber flow. For example, an area ratio of 10 may be expected to increase the thrust by approximately 40%, which would increase the maximum value of incremental specific impulse for the long combustion duct of P_i = 1.0 atm to 1800 sec.

The need to study this effect is given a particular urgency by the fact that it occurs at temperatures where the incremental specific impulse peaks. There are many features yet to be established. The mechanisms which cause the effect, though probably originating in the chemical kinetics of combustion, are not understood. The range of temperature over which it is the preferred mode of combustion needs to be determined, together with the effect of the mixing layer structure. It would be interesting to see if the larger pressure rise recorded in Pulsonetti's work would lead to a larger incremental specific impulse, and whether some degree of pre-mixing of fuel and air upstream of the combustor would have the same effect. The relationship, if any, between this effect and a detonation wave needs to be explored. These, and other aspects of the effect need to be understood before it can be successfully incorporated into scramjet design.

Acknowledgments

The authors would like to thank the Australian National University for making the shock tunnel T3 available. Most of the experimental work was conducted under the Australian Research Grants Scheme and NASA grant NAGW-674

REFERENCES

1. Pulsonetti, M.V., "Scaling Laws for Scramjets" Ph.D. thesis, Univ. of Queensland, 1996.
2. Stalker, R.J., "Development of a Hypervelocity Wind Tunnel" Aeronautical J. of the Royal Aero. Soc., Vol 76, 1972, pp374-384.
3. Rogers, R.C. and Schexnayder, C.J. (Jr.) "Chemical Kinetic Analysis of Hydrogen-Air Ignition and Reaction Times" NASA Tech Paper 1856, 1981.
4. Jacobs, P.A., Rogers, R.C., Weidner, E.H. and Bittner, R.D., "Flow Establishment in a Generic Scramjet Combustor" J. Prop. & Power, Vol.8, No.4, 1992, pp890-899.
5. Rogers, R.C. and Weidner, E.H., "Scramjet Fuel-Air Mixing Establishment in a Pulse Facility" J.Prop. & Power, Vol.9, No.1, 1993, pp127-133.
6. White, F.M., "Viscous Fluid Flow" 2nd Ed. McGraw-Hill Inc. New York 1991, pp.470-481.
7. Stalker, R.J. & Morgan, R.G., "Supersonic Hydrogen Combustion with a Short Thrust Nozzle" Combustion & Flame Vol.57, No.1, 1984, pp.55-70.
8. Stalker, R.J., Morgan, R.G, & Netterfield, M.P., "Wave Processes in Scramjet Thrust

Generation" Combustion & Flame, Vol.71, No.1, 1988, pp.63-77.

9. Hopkins,E.J., Inouye, M., "an Evaluation of Theories for Predicting Turbulent Skin Friction & Heat Transfer on Flat Plates at Supersonic and Hypersonic Mach Numbers" AIAA J. Vol.9, No.6, 1971, pp.1003.
10. Wendt, M. & Stalker, R.J., "Transverse and Parallel Injection of Hydrogen with Supersonic Combustion in a Shock tunnel" to be published in Shock Waves Journal.

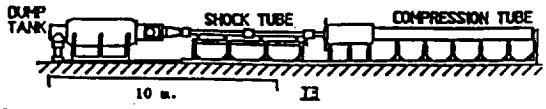

Fig.1. Free Piston Shock Tunnel T3

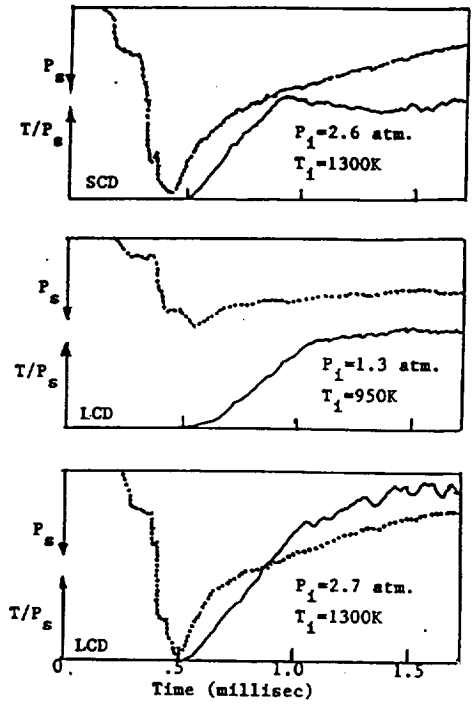

P_s - Reservoir Pressure
T - Thrust
SCD- Short Combustion Duct
LCD- Long Combustion Duct

Fig.3. Normalised Thrust Records

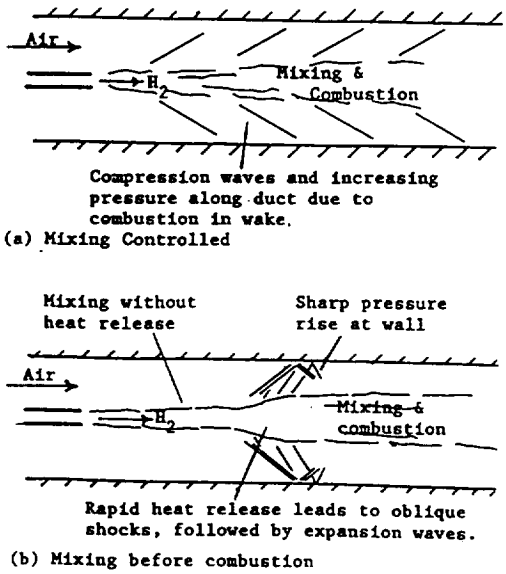

ig.4. Supersonic Duct Combustion

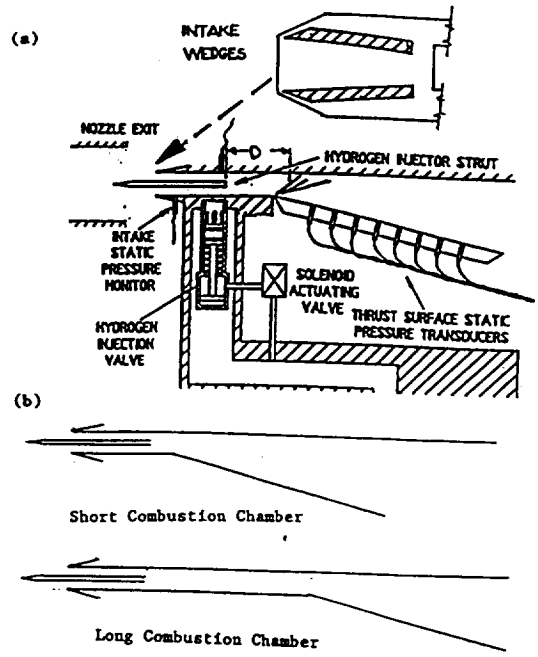

Fig.2. Model Configurations

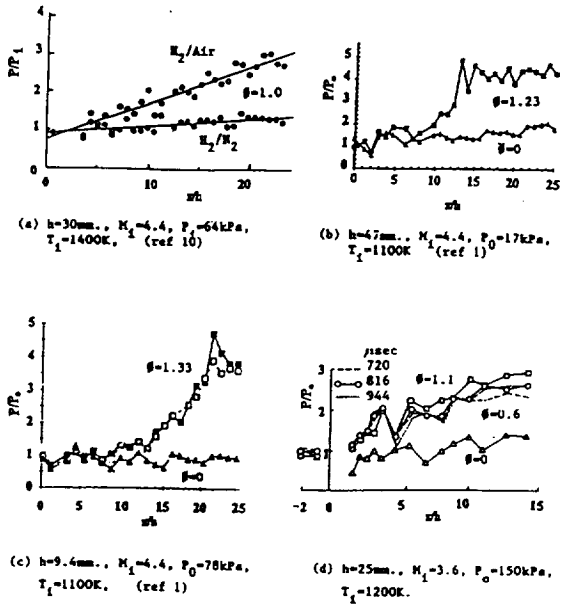

Fig.5. Pressure Distributions along Constant Area Duct

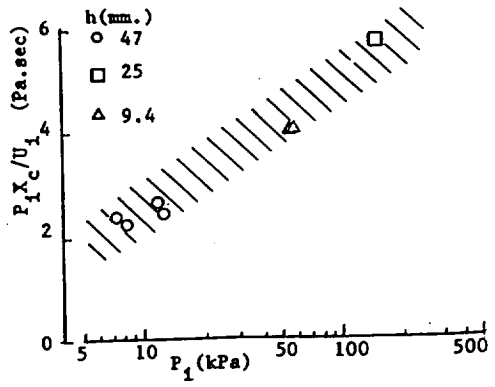

Fig.6. Location of Pressure Peak

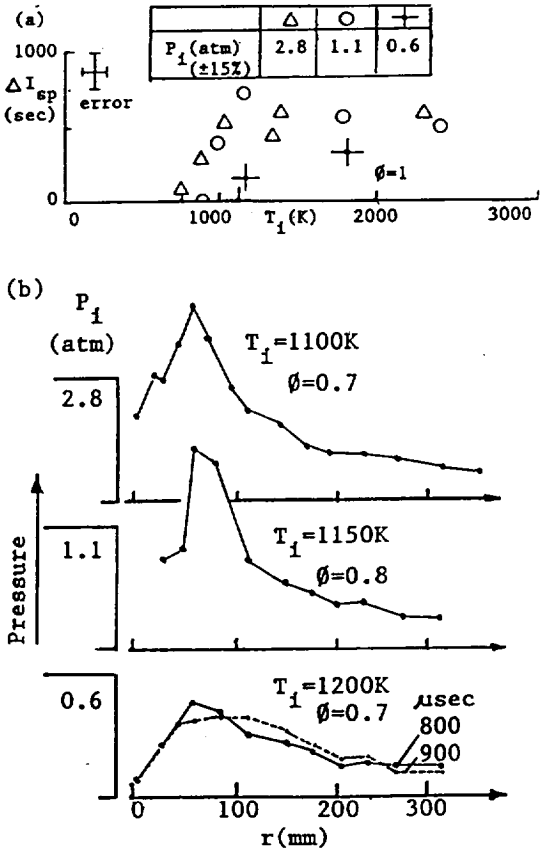

Fig.8. Thrust Measurements - Short Combustion Duct

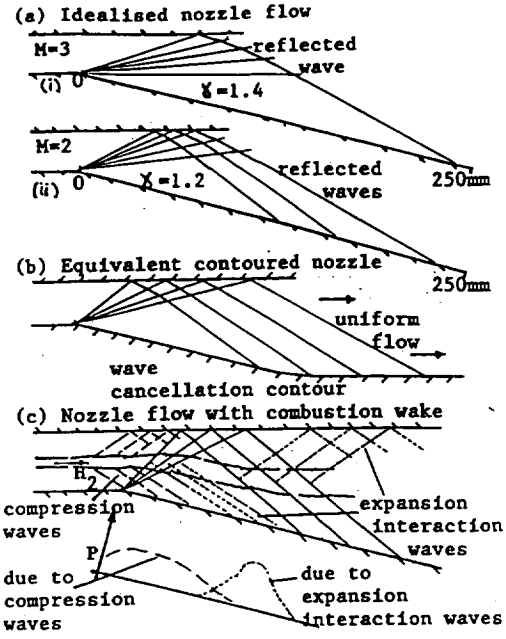

Fig.7. Thrust Nozzle Flows

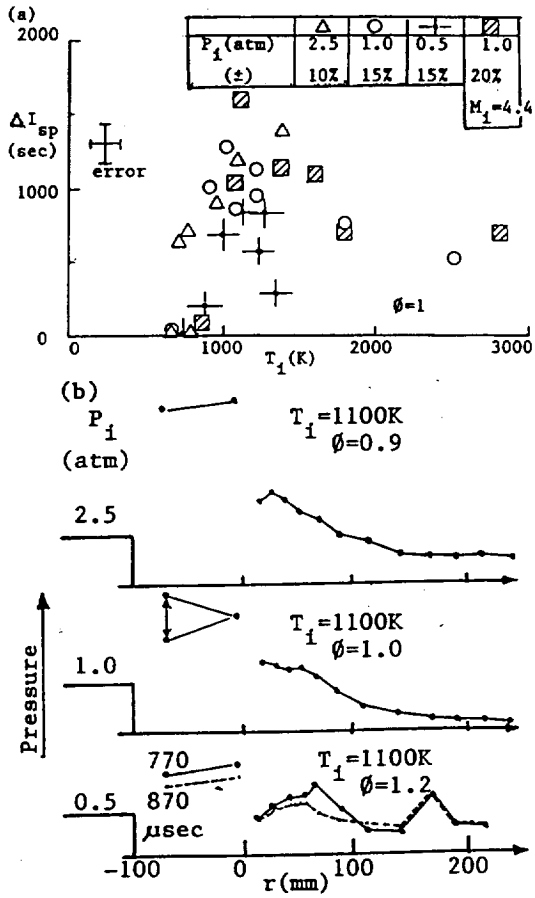

Fig.9. Thrust Measurements - Long Combustion Duct

BLANK

EXPERIMENTS ON CRUISE PROPULSION WITH A HYDROGEN SCRAMJET

R J Stalker and A Paull

Department of Mechanical Engineering, The University of Queensland

ABSTRACT

Measurements of drag have been made, in a shock tunnel, on a simple integrated vehicle-engine combination for hypersonic cruise with hydrogen scramjet propulsion. The test flow Mach number was 6.4, and the velocity was 2.45 km s^{-1}. Zero drag, which is the necessary condition for cruise, was achieved as the equivalence ratio approached one. It was found that an analysis using established aerodynamic concepts was adequate for predicting drag in the case of no combustion. When combustion occurred results of direct connect experiments provided a qualitative guide to the measured levels of drag, and indicated that thrust nozzle combustion was taking place. An heuristic analysis is used to point to the important effect this may have on propulsive lift.

NOMENCLATURE

A	cross section area
A_∞	capture area of intake
C_D	drag coefficient $\left(D / \left(5 \rho_\infty U_\infty^2 A_\infty \right) \right)$
D	drag
G	number of model flow passes
H_s	stagnation enthalpy
I_{sp}	specific impulse
ΔI_{sp}	fuel on increment of specific impulse
L	lift
M	Mach number
P	pressure
P_s	nozzle reservoir pressure
U	velocity
T	temperature
γ	ratio of specific heats (assumed = 1.35)
ρ	density

Subscripts:

∞	freestream
f	combustor entrance
i	pre-combustion

1. INTRODUCTION

The supersonic combustion ramjet, or "scramjet", is theoretically capable of providing propulsion at high hypersonic speeds [1,2], and this type of engine has been the subject of considerable research [3,4]. It is seen as being possible use for boost propulsion (essentially, propulsion of an air breathing satellite launcher) or for cruise at hypersonic speeds. The propulsion requirements for the cruise application are less demanding than for boost in that it is only necessary to provide sufficient thrust to balance the drag, whereas for boost the thrust must not only overcome drag but also accelerate the vehicle.

Hydrogen is the preferred fuel for both these applications [2] because, in addition to the release of large amounts of chemical energy per unit mass when it burns with air, its cooling capacity in the liquid form is greater than any known fuel, and its reaction kinetics are relatively rapid, thus minimising the length of the combustion chamber.

The difficulty and expense of hypersonic flight is such as to strongly encourage preliminary research in ground facilities, particularly with subscale models of engines, and of integrated vehicle-engine combinations. Heated blowdown facilities have generally been favoured for scramjet research, and these have been widely used for experimentation on hydrogen fuelled engines [5,6]. However, the requirement that the static pressure, the stagnation enthalpy and the model scale should all be sufficient to ensure vigorous combustion of hydrogen in air has effectively precluded experiments with vehicle-engine combinations. This is unfortunate, as the engine and the vehicle configurations must be closely integrated for scramjet propulsion.

This paper reports on investigation of a model configuration representative of integrated vehicle-engine combinations for hypersonic cruise. The experiments were performed in a shock tunnel facility which, by producing higher stagnation enthalpies at hypersonic speeds than a blowdown facility, more readily allows vigorous combustion to take place. Previous experiments [7,8] have been done with an axisymmetric configuration and a mixture of hydrogen and silane as the fuel. The silane acted as an ignition promoter, thereby avoiding the difficulties involved in achieving vigorous combustion of hydrogen alone. The present experiments were done with hydrogen alone as the fuel, and involve a model configuration which is potentially able to generate lift. Therefore they represent an early step in experimental study of hypersonic cruise propulsion by hydrogen scramjets.

The paper begins with a description of the model, and goes on to consider analysis of the flow path through the model, both without and with combustion. Then the experiments are described and the results presented, to be followed by a discussion of their implications before concluding.

2. MODEL CONFIGURATION

The model configuration chosen to represent a cruise vehicle is shown in fig 1. It is designed for ease of manufacture and to be amenable to approximate analysis. Attention is also given to high speed performance aspects of a hypersonic cruise vehicle. Thus all of the external surfaces are parallel to the incident stream direction to ensure that they do not generate inviscid drag. This also implies that the intake capture area is equal to the vehicle frontal area, thus maximising the mass flow of combustion air. The skin friction and heat transfer to the combustion chamber walls are higher than any other

part of the vehicle surface, so the drag and heat load from this source is minimised by minimising the combustion chamber perimeter. With a fixed combustor shape, this leads to a single combustion chamber, rather than multiple ones.

Fuel injection takes place via a circular duct, drilled at an angle of 30° to the freestream direction, which exits into the flow through a surface orifice immediately upstream of the combustion chamber entrance. The downstream length of the cowl is sufficient to ensure that the thrust nozzle is not affected by the expansion waves from the cowl trailing edge.

The volume of a vehicle should be sufficient to contain the payload, all the ancillary equipment, and the fuel. The suitability of a configuration from this point of view is determined by the volume coefficient $\tau = Vol/S^{1.5}$ where S is the planform area. The value of τ for the configuration of fig 1 is 0.09 which, by falling in the range 0.06 to 0.10, may be regarded as suitable for a hydrogen fuelled vehicle [9].

The lifting configuration shown in fig 1 could not be tested in the shock tunnel, as the present state of development of the force balance used is such that it can only operate with axial loads. Therefore the experiments were conducted with the test model shown in fig 2. Essentially, this consisted of two of the cruise models shown in fig 1, joined along the plane AA^1. The symmetry of the resulting model eliminated lateral loads, thereby allowing measurement of the propulsive effect of the hydrogen scramjets.

3. THE FLOW PATH - FUEL OFF

When the scramjets are operating, the air captured by the intake and passed through the engines is compressed, heated by combustion, and then expanded to produce a propulsive effect. Initially, the flow path through one scramjet is considered in the absence of combustion.

The air is compressed in the intake by a system of shock waves formed by the intake ramp and the compression corners between the two dimensional intake ramp and the swept sidewalls. The resulting shock pattern is similar in form to that described by Anderson and Nangia [10], and is shown in fig 3. The primary shocks originate at the leading edge of the intake ramp and the swept leading edge of the sidewall, and form triple points where they meet the secondary shocks from the sidewall and from the intake ramp. The triple points are joined by a further primary shock, as shown. The secondary shocks propagate into the uniform flow following the primary shocks, and are of a strength appropriate to plane waves with the flow deflection angles of the sidewall and the intake ramp. The secondary shocks from the sidewalls meet and reflect at the intake centre line, at approximately the same distance from the ramp leading edge as the secondary shocks from the ramp reflects from the cowl.

As the flow passes downstream, it also experiences shock waves originating at the cowl leading edge. This leading edge is swept, with the intention that it may permit operation of the intake in a partially choked condition. It is noted that sweepback weakens the leading edge shock, and the combination of this with the expansion which follows closely downsteam of the shock allows the effect of the shock to be neglected in analysing the intake flow.

The minimum cross sectional area occurs at the entrance to the combustion chamber. The sidewalls of the combustion chamber diverge slightly, so that the increase in area may help to alleviate flow choking at the combustion chamber entrance. At a station 60 mm downsteam of the combustion chamber entrance, the surface is deflected by 9° to form a thrust nozzle.

In the absence of combustion, the air may be taken to be calorically perfect, with a value of γ =1.35. The main features of the flow in the intake can then be analysed by taking into account the primary and secondary shocks, as well as their reflection. This leads to an array of shocks at the entrance to the combustion chamber, with additional complication added by the generation of expansion waves there. Rather than attempting detailed analysis of the flow which follows, it is convenient to assume one dimensional flow in the combustion chamber. The Mach number, M_f, and pressure P_f, at the combustion chamber entrance can then be obtained from the relations for adiabatic flow in a steamtube, ie

$$\frac{A_f}{A_\infty} = \frac{M_\infty}{M_f}\left[\frac{1+M_f^2(\gamma-1)/2}{1+M_\infty^2(\gamma-1)/2}\right]^{(\gamma+1)/2(\gamma-1)} \exp\left(\Delta S/R\right) \qquad 1.$$

and

$$\frac{P_f}{P_\infty} = \frac{A_\infty}{A_f}\,\frac{M_\infty}{M_f}\left[\frac{1+M_\infty^2(\gamma-1)/2}{1+M_f^2(\gamma-1)/2}\right]^{1/2} \qquad 2.$$

where A_∞ is the cross sectional area in the freestream of the steamtube captured by the intake, A_f is the cross sectional area of the combustion chamber entrance, ΔS is the

entropy rise across the intake shocks, and R is the gas constant. From M_f/M_∞ and

P_f/P_∞, T_f/T_∞, U_f/U_∞ and ρ_f/ρ_∞ can also be obtained.

The assumption of one dimensional flow then allows calculation of the flow throughout the combustor, until it reaches the expansion corner. There the air passes through a Prandtl-Meyer expansion and subsequently flows over the surface of the thrust nozzle with a spanwise divergence angle which allows the flow boundaries to match the diverging sidewalls.

By following the flow path outlined, an inviscid drag can be calculated. For the conditions of table 1 below, this calculated inviscid drag coefficient for the model, based on the frontal area, is 0.097.

There is also a substantial skin friction drag to be accounted for. Calculation of the skin friction follows closely the method outlined in ref 8. In regions of laminar boundary layer flow, local values of the skin friction coefficient are given by using the reference enthalpy method [11]. Previous experiments in the shock tunnel [12] have indicated that boundary layer transition occurs at a Reynolds' number, based on distance from the leading edge, of approximately 2×10^6, and when this was applied to the model it was found that only the boundary layer on the external surfaces, and on the intake up to the secondary shocks, could be regarded as laminar. Noting that the pressure rise across the

secondary shocks would tend to induce early transition, it is clear that all of the flow downstream of the secondary shocks, apart from a small region near the leading edge, will be turbulent. This includes the boundary layers in the combustion chamber and the thrust nozzle.

The theory of Spalding and Chi [8] was used to calculate the turbulent boundary layer skin friction. The boundary layer on the intake surfaces downsteam of the secondary shocks was assumed to be all turbulent, with a Reynolds' number corresponding to a streamwise distance of 40 mm from the shock wave. The Reynolds' number at the entrance to the combustion chamber was taken to be the mean value around the cross sectional perimeter, and the boundary layer downstream of that station was assumed to develop uniformly on all surfaces. The boundary layer was assumed to pass through the Prandtl-Meyer expansion at the thrust surface corner without a change in the local skin friction coefficient. With these assumptions, the turbulent skin friction drag could be calculated, and when this was added to the skin friction drag of the laminar regions of flow, a contribution of 0.086 to the drag coefficient of the test model was obtained. Thus the ratio of viscous drag to inviscid drag was 0.89, reaffirming the importance of viscous effects at hypersonic flight speeds.

The calculated value of the total drag coefficient was 0.183, and this is consistent with the measurements reported below. For the cruise model, the skin friction drag on the plan$\overset{\epsilon}{\wedge}$AA^{1} should be added, and this would increase the drag coefficient by 7%. The calculated value of the lift to drag ratio for that model then would be 1.7.

4. THE FLOW PATH - FUEL ON

Consideration of the flow path with combustion begins by noting that, as shown in fig 1, the fuel is injected at an angle of 30° to the freestream direction immediately upstream of the combustion chamber entrance, and therefore the flow in the intake may be assumed to be unaffected by fuel addition. However, as the flow passes downstream of the point of injection, mixing of the hydrogen and air takes place and, for appropriate flow conditions, vigorous combustion ensues.

The appropriate conditions for combustion can be determined approximately by using the results of an experimental investigation [13] of the simple configuration shown schematically in fig 4(a). The combustion chamber was a constant area rectangular duct, 25 mm high and 50 mm wide. A strut spanned the midplane of the duct, and hydrogen fuel was injected from the trailing edge of the duct. At 175 mm downstream of the point of injection, one surface of the duct was deflected 15° to form a thrust nozzle, and this was instrumented for pressure measurement. Two transducers were located in the combustion duct to monitor the combustion pressure, and a further transducer adjacent to the injector monitored the airflow entering the duct from an M=3.6 shock tunnel nozzle. Further details can be found in ref 13. Some previously unreported results from these experiments are used for the present purpose.*

Thus, these were direct connect experiments, and were such that an essentially two dimensional flow was produced. Pressure distributions obtained for fuel on and fuel off conditions are shown in fig 4(b) for a range of pre-combustion temperatures, T_i. When these pressures are integrated over the thrust surface, and account is taken of the thrust

* The assistance of R G Morgan with these experiments is greatly appreciated.

surface angle, a thrust can be obtained. Then, taking the difference between the fuel on thrust and the fuel off thrust, and combining the result with the measured fuel mass flow, the incremental specific impulse can be obtained. It can be seen that, starting from zero at T_i=680 K, the incremental specific impulse rises somewhat at 790 K and reaches its maximum measured value at 950 K. Thus the onset of substantial thrust generation occurs at pre-combustion temperatures between 790 K and 950 K.

It is interesting to observe that the pressure in the combustion chamber rises more slowly than the incremental specific impulse, signifying that at least some of the combustion and heat release must take place in the thrust nozzle as the temperature is increased.

In the range of temperatures of interest, the combustion chamber flows are reaction limited, rather than mixing limited [13]. A correlation of such reaction limited results in combustion chambers geometrically similar to that used in these experiments has been presented in ref 13. At a given temperature, it was found that the combustion pressure rise took place at a streamwise distance from injection which varied approximately inversely as the pre-combustion pressure. Referring to fig 4(b), the pre-combustion pressure was 40 kPa, and as indicated below, the average pressure in the model combustion chamber was 100 kPa. Therefore the estimated distance required for the combustion pressure rise to take place in the model was approximately 70 mm, or the approximate length of the combustion chamber.

It may be noted the fuel injection on the model takes place through a single wall orifice, rather than through a strut spanning the duct, and the combustion chamber flow therefore is not two dimensional. However, experiments have been reported [14] in which the two types of injection were compared under conditions such that the flow was mixing limited, and were found to yield approximately the same combustion pressure rise along the duct. This indicates that mixing is not markedly influenced by the type of injection, and strongly suggests that reaction limited flows will be similarly unaffected. Thus the results of fig 4 may be applied to provide an indication of model pre-combustion temperatures and pressures appropriate to vigorous combustion, and the generation of thrust.

5. EXPERIMENT

(a) The Shock Tunnel

The experiments were performed in the free piston shock tunnel T4 at The University of Queensland. Briefly, this consisted of a compression tube, 27 m long and 228 mm in diameter, in which the temperature and pressure of the driver gas was raised by a free piston compression immediately prior to rupture of the diaphragm at the entrance to the shock tube. The driver gas was a mixer of helium and argon. The shock tube was 10 m long and 76 mm in diameter and, for these experiments, supplied shock heated air to a contoured hypersonic nozzle which expanded from a throat diameter of 25 mm to 263 mm at the test section. Measurements indicated that the Pitot pressure was uniform, to within ±7%, over a test core at least 150 mm in diameter and that, over the range of stagnation enthalpies of interest here, at least three milliseconds of test time elapsed before driver gas appeared in the test section. Further details may be found in ref 8.

(b) The Stress Wave Force Balance

A stress wave force balance was used to measure the axial force on the model. This is described in ref 7, and more fully in ref 8. Briefly, it is a technique which is made necessary because stress waves propagate with a velocity which is of the same order as the flow speed, and therefore the multiple stress wave reflections necessary to bring the model into stress equilibrium do not have time to take place during the short test times available in the shock tunnel. Therefore a quasi-static measurement of axial force, such as that obtained with a conventional strain gauge force balance, is fundamentally impossible. However, if strain gauges are placed on the sting supporting the model, and the time history of stress waves passing into the sting is recorded, then this recording can be deconvoluted to yield the force on the model. If the model is as complex as in the present tests, the deconvolution must be accomplished by use of a computer.

The same stress wave force balance and fuel supply assembly was used for the present measurements as in refs 7 and 8.* The hydrogen fuel tank, together with a quick acting valve, was incorporated in the model assembly, with an aerodynamic shroud surrounding all but the model itself. The hydrogen reservoir was at room temperature and the fuel supply pressure was monitored by a pressure transducer located in the fuel supply duct just before the hydrogen entered the model itself.

* The authors wish to express their appreciation of the part played by D J Mee in performing these measurements.

(c) Choking

The intake area ratio, A_∞ / A_f, was 5.22 in the absence of fuel injection, and the effective intake area ratio became 5.58 when an allowance was made for injection of unmixed fuel at an equivalence ratio of unity. It was found that, although satisfactory flow through the model was established for fuel off test conditions, the injection of fuel at equivalence ratios approaching one before the test flow began caused a violent choking phenomenon to occur, the drag rising by a factor of two or more. This is shown in fig 5. A pitot pressure monitor, which was mounted in the test section to one side of the model, also registered values well in excess of those normally prevailing in the freestream, indicating a major freestream disturbance. A time integrated luminosity photograph of the model in plan view, taken during such a choked test, is shown in fig 5(a), and displays the intense luminosity in the intake which was associated with this condition. By contrast, the fuel off photograph of fig 5(b) shows only faint luminosity in the intake. In the latter case, the pitot pressure monitor recorded normal freestream values.

The choking condition was avoided by delaying injection so that the fuel pressure, and therefore the equivalence ratio, increased during a test. Unfortunately, this meant that the fuel mass flow varied during a test, but as this variation was less than 5% during the time taken for the flow to pass one model length, it was possible to regard instantaneous measurements of the fuel mass flow during the test time as quasi-steady values. During such tests, luminosity photographs showed the same faint intake luminosity as fig 5(b), indicating that the model flow was free of choking.

It is clear that the intake was very susceptible to choking, and that its performance could probably be improved by better design. However, it was adequate for the purpose of these experiments.

(d) Test Conditions

The shock tunnel was operated to produce a nozzle reservoir pressure of 38 ±2.5 MPa throughout the tests. An initial test series was done in which the stagnation enthalpy was varied from 3.0 MJ kg^{-1} to 4.6 MJ kg^{-1} and the results are shown in fig 6 as a drag coefficient. The combustor entrance temperature, calculated through equations (1) and (2), for an inlet area ratio of 5.58 is also shown on the figure. It should be noted that only an approximate mean temperature over the combustion chamber cross section is calculated in this manner.

There may be local zones of higher or lower temperature due to the persistence of shock or expansion waves in the combustion chamber. For example, the fuel was injected a few millimetres downstream of the point at which the secondary shocks from the intake sidewalls meet and reflect, so the fuel was injected into a region with a temperature 15% higher than the calculated value at the combustion chamber entrance. This may have the effect of initially accelerating the combustion reactions, but it is anticipated that this acceleration will persist for only a short flow distance before expansions in the flow will tend to retard the reactions. Thus the mean temperature is the most useful for characterising the combustion process. The results in fig 6 show a minimum in the fuel

on drag at 3.5 MJ kg^{-1}, and so this condition was chosen for further investigation. The associated test conditions are presented in table 1. Conditions in the test section were calculated using a one dimensional non-equilibrium computer program for expansion of air in a hypersonic nozzle, and were partially checked by pitot pressure measurements.

Table 1. Maximum Thrust Conditions

Stagnation enthalpy	3.5 ±0.1 MJ kg^{-1}		
Nozzle Reservoir Pressure	37 ± 2.5 MPa		
Test section:	Velocity 2450 ms^{-1}, Temperature 390 K		
	Density 0.095 kg m^{-2}, Pressure 10.1 kPa		
	Mach number 6.4		
Combustion Chamber:	With fuel injection at ϕ=1 and no combustion		
Entrance:	Pressure 130 kPa	Exit:	Pressure 74 kPa
	Temperature 830 K		Temperature 720 K
	Mach number 4.0		Mach number 4.4
(Exit at thrust nozzle expansion corner)			

6. RESULTS AND DISCUSSION

Drag records obtained as the equivalence ratio was varied are shown in fig 7(a). The reduction in drag as the equivalence ratio increases is evident. Drag results are plotted in fig 8, and are also plotted with a correction for the drag of the sting mount included.

The sting mount is shown in fig 7(b), together with the properties of the flow approaching the mount, estimated by the methods of section 3. The inviscid drag on the mount was calculated by assuming newtonian pressure on the 10° bevel and, when this was added to the viscous drag, an effective sting drag of 14 N was produced. Assuming that the combustion of fuel affects the pressures on the thrust surface, without substantially influencing the density or velocity there, this value of sting drag was applied as a correction to both fuel off and fuel on results.

It can be seen in fig 8 that the fuel off drag is close to the value predicted theoretically in sect 3, establishing confidence in the approximate analysis used for these predictions. When fuel is added, the drag is reduced and, taking the drag of the sting into account, zero drag is produced as ϕ approaches unity. This is the necessary condition for cruise. Referring to the combustion chamber temperatures in table 1, it can be seen that the cruise condition was achieved in the range of temperatures for which the incremental specific impulse increased with temperature in the experiments of fig 4. Taking the difference between the fuel off thrust and the fuel on thrust at the cruise condition, consideration of the measured mass flow of hydrogen then yielded a specific impulse increment of 835 sec. This includes a contribution of 100 sec due to the thrust generated as a reaction to the injection of hydrogen of sonic speed. It also includes any changes to the skin friction due to combustion, but since these are difficult to calculate, and are expected to alter the drag by less than 10%, they are ignored. It will be noted that an incremental specific impulse value of 735 sec would be associated with thrust nozzle combustion in fig 4, suggesting that the same phenomenon may have occurred in the present experiments.

It is interesting to speculate on the possible effect of thrust nozzle combustion on the lift. In the absence of thrust nozzle combustion, burning in the combustion chamber may be represented by sudden heat release at the combustor entrance and, if the analysis of sect 3 is followed, the lift due to combustion can be calculated from the measured thrust produced, after first subtracting the fuel injection thrust, and allowing for the thrust generated at the sidewalls. When this propulsive lift is added to the fuel off lift, then the lift to drag ratio is increased from 1.8 to 2.5. However, when thrust nozzle combustion occurs, it is evident from fig 4 that the pressure rise in the combustion chamber is limited and, noting the combustion chamber divergence of the model, the modest amount of heat release which occurs in the combustion chamber can be approximately accounted for by assuming that the pressure is constant at the entrance value. Then, remembering that a portion of the measured thrust is produced at the sidewalls, and taking this portion in the thrust nozzle to depend on the ratio of the respective areas of the sidewalls and the thrust surface, the part of the thrust produced by the thrust surface can be estimated. This can then be used to calculate the propulsive lift and, when this is added to the fuel off lift, the lift to drag ratio increases from 1.8 to 4.9.

This result for thrust nozzle combustion can only be tentative, as it is based on qualitative interpretation of the direct connect tests of fig 4. Nevertheless, it is worthwhile exploring a consequence of the effect on flight performance. The Breguet equation [9] for the range of a cruise vehicle is $R = I_{sp} U_\infty \left(L/D\right) \ell n(1-\sigma)^{-1}$ where R is the range, I_{sp} is the fuel specific impulse and σ the fuel fraction at start of cruise. Taking σ =0.5, U_∞ =2.45 km s^{-1} and I_{sp} =835 sec allows this equation to be applied to

the cruise configuration under the conditions of the experiments. An L/D ratio of 2.5 then yields a range of 3550 km, while an L/D ratio of 4.9 yields a range of 6950 km. Clearly, propulsive lift is important and, if possible, should be incorporated into measurements of models for hypersonic flight. An extension of the stress wave force balance technique [15] may prove effective in this role.

The Mach number of the test flow was 6.4, but it should be noted that the test section velocity corresponded to a somewhat higher flight Mach number. For example, at an altitude of 30 km, the mach number would be 7.9.

7. CONCLUSION

Drag measurements in a shock tunnel have demonstrated that the cruise condition, of zero drag, can be produced at hypersonic speeds by using hydrogen scramjet propulsion. The test configuration used was a combination of a lifting, cruise, model with its mirror image, thereby generating a non-lifting configuration. The cruise model was designed for ease of manufacture, and to be amenable to approximate analysis. The experiments were conducted at a Mach number of 6.4 but the flow velocity corresponded to a somewhat higher Mach number.

It was found that the fuel off drag could be satisfactorily predicted by the analysis, but not the fuel on performance. In the latter case, it was necessary to rely on some previous direct connect experiments, and these could only assist a qualitative interpretation of the results.

The fuel on condition yielded zero drag at a test section stagnation enthalpy of 3.5 MJ kg^{-1} and this was found to be qualitatively consistent with the results of the direct connect experiments. It was observed that thrust nozzle combustion occurred during these direct connect tests, under conditions which approximated those in the model. An heuristic analysis indicated that thrust nozzle combustion could almost double the lift of the cruise model, and thereby drew attention to the important role that propulsive lift could play in hypersonic cruise.

Acknowledgments

The authors would like to express their appreciation of the support received from the Australian Research Council, and through NASA grant NAGW-674.

REFERENCES

1. Ferri, A. *Review of Problems in Application of Supersonic Combustion.* J. Royal Aero. Soc. 1964, Vol. 68, No. 645 pp575-597.

2. Swithenbank, J. *Hypersonic Air-Breathing Propulsion.* Pergamon Press, Oxford, Progress in the Aerospace Sciences (ed D. Küchemann), 1967, Vol. 8, pp229-294.

3. Billig, F.S. *Research on Supersonic Combustion.* Journ. Propulsion and Power, 1993, Vol. 9, No. 4, pp449-514.

4. Curran, E.T. and Heiser, W.H. *Fluid Phenomena in Scramjet Combustion Systems.* Annual Reviews, Calif., Ann. Rev. Fluid Mech, 1996, Vol. 28, pp323-360.

5. Guy, R.W. and Mackley, E.A. *Initial Wind Tunnel Tests at Mach 4 and 7 of a Hydrogen-Burning, Airframe-Integrated Scramjet.* Presented at 4th Int. Symp. on Air Breathing Engines, Lake Beuna Vista, Florida, April 1-6, 1979.

6. Andrews, E.H. and Mackley, E.A. *NASA's Hypersonic Research Engine Project - A Review.* NASA Tech. Memo 107759, Oct. 1994.

7. Paull, A., Stalker, R.J. and Mee, D.J. *Scramjet Thrust Measurement in a Shock Tunnel.* Aero. J. of Roy. Aero. Soc., 1995, Vol. 99, No. 984, pp161-163.

8. Paull, A., Stalker, R.J. and Mee, D.J. *Experiments on Supersonic Combustion Ramjet Propulsion in a Shock Tunnel.* J. Fluid. Mech. 1995, Vol. 296, pp159-183.

9. Küchemann, D. and Weber, J. *An Analysis of Some Performance Aspects of Various Types of Aircraft Designed to Fly Over Different Ranges at Different Speeds*. Pergamon Press, Oxford, Progress in Aeronautical Sciences, 1968, Vol. 9, pp329-456.

10. Anderson, D.A. and Nangia, R.K. *Comparison of Numerical and Experimental "Conical" Flowfields in Supersonic Corners with Compression and/or Expansion*. Aero. Quart, 1977, Vol. 28, Pt. 4, pp293-306.

11. Hayes, W.D. and Probstein, R. *Hypersonic Flow Theory*. Academic Press, New York, 1959, p296.

12. He, Y. and Morgan, R.G. *Transition of Compressible High Enthalpy Boundary Layer Flow over a Flat Plate*. Aero. J. of Roy. Aero. Soc., 1994, Vol. 98, No. 972, pp25-34.

13. Stalker, R.J., Morgan, R.G. and Paull, A. *A Shock Tunnel Investigation of Scramjet Performance with Partially Premixed Combustion*. AIAA paper no. 96-4534. Presented at AIAA 7th Int. Space Planes & Hypersonic Sys. & Tech. Conf. Nov. 18-22, Norfolk, VA 1996.

14. Wendt, M.N. and Stalker, R.J. *Transverse and Parallel Injection of Hydrogen with Supersonic Combustion in a Shock Tunnel.* Shock Waves J. 1996, Vol. 6, pp 53-59.

15. Mee.J., Daniel, W.J.T. and Simmons, J.M. *Three-Component Force Balance for Flows of Millsecond Duration*. AIAA Journ., 1996. Vol. 34, No. 3, pp590-595.

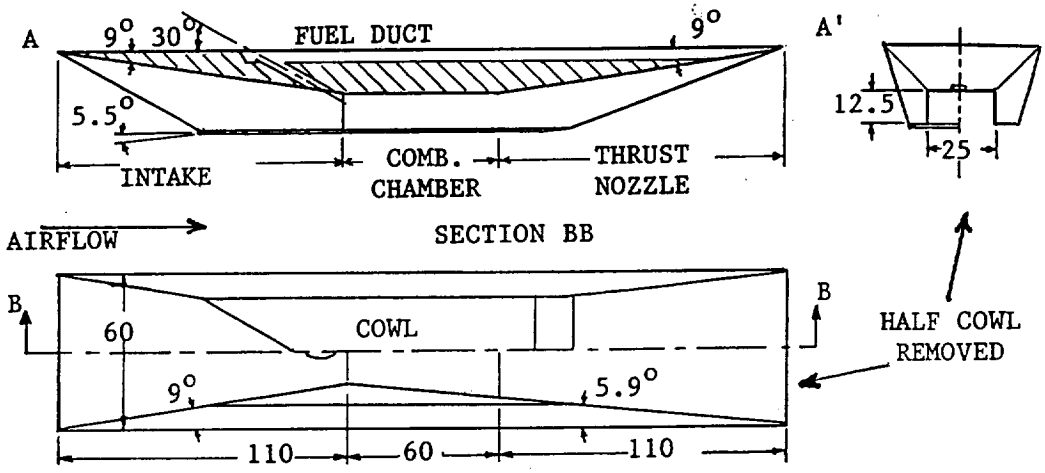

Fig.1. Cruise Model Configuration (Dimensions in mm.)

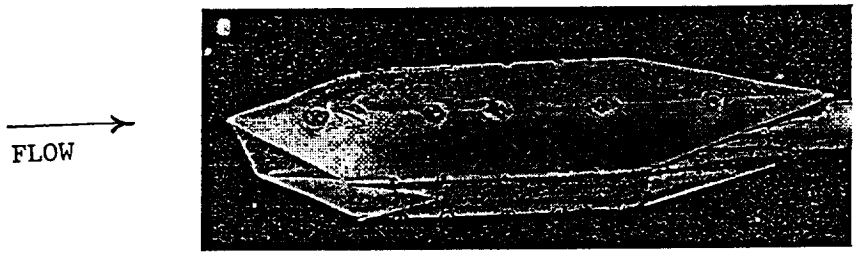

Fig. 2. Test Model

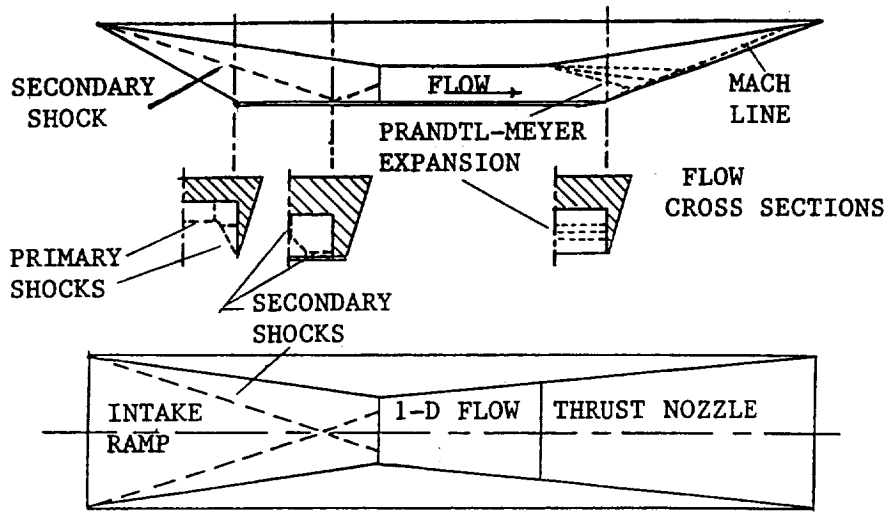

Fig.3. Flow Path - Fuel Off

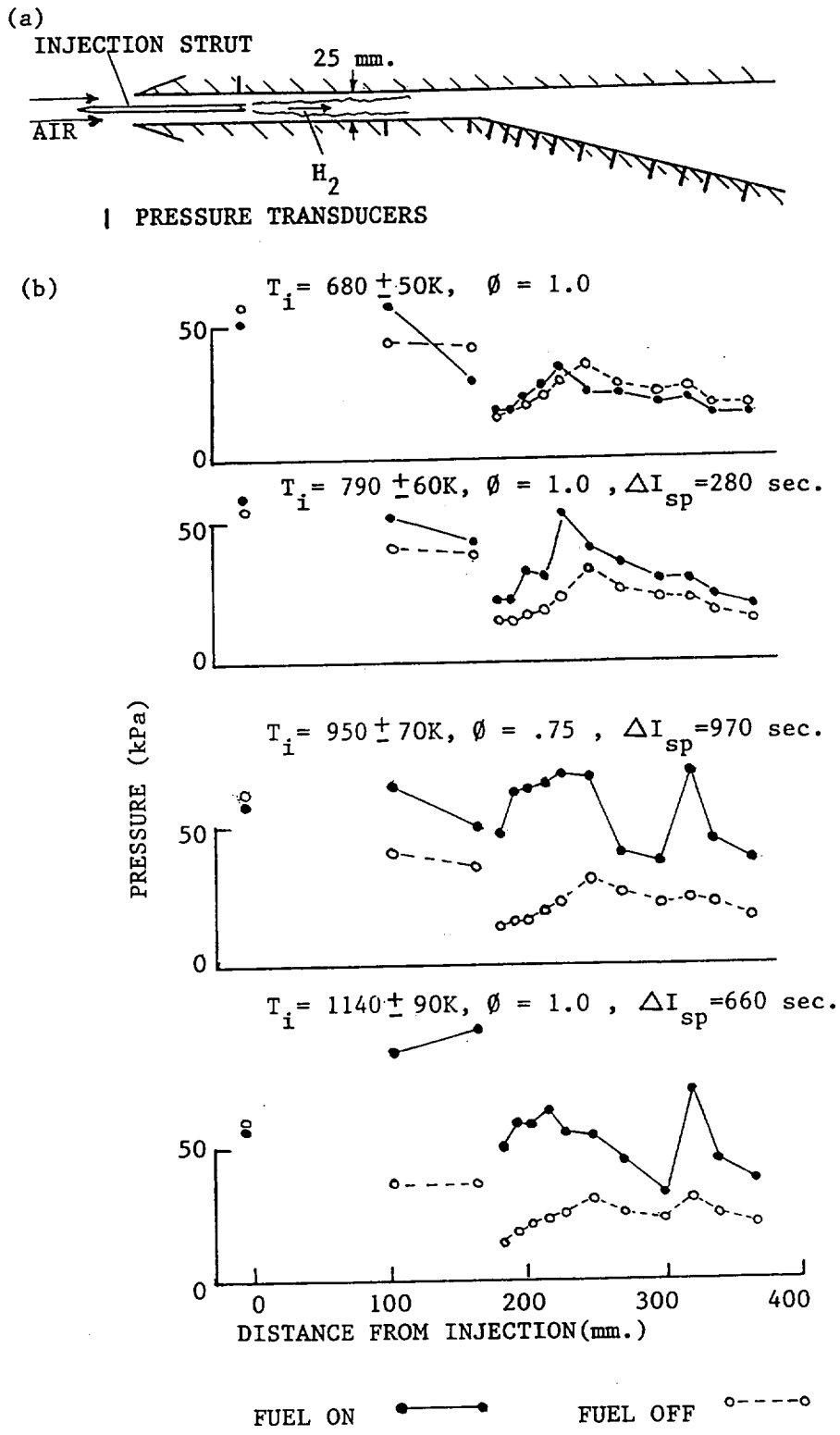

Fig. 4. Direct Connect Experiments (T_i= precombustion air temperature, Ø= equivalence ratio , ΔI_{sp}= incremental specific impulse.)

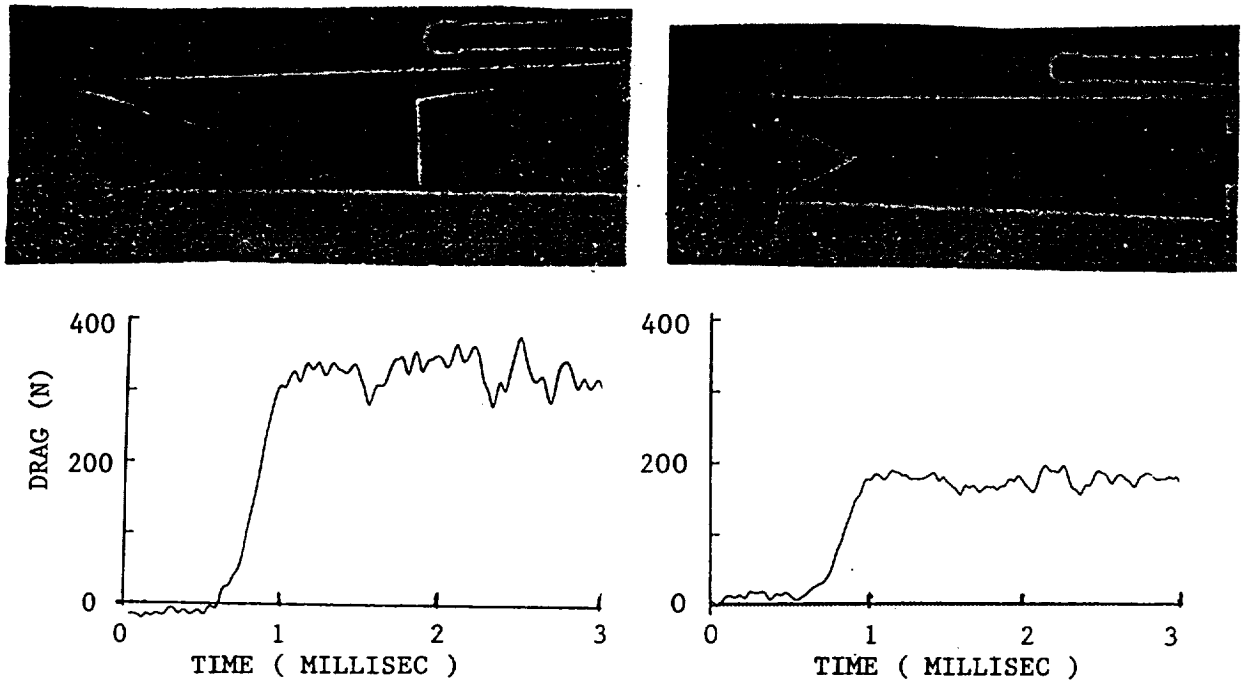

(a) FUEL ON

(b) FUEL OFF

Fig. 5. Model Flow Choking (H_s = 4.0 MJ.kg.$^{-1}$, Photographs at f90, Film Polaroid 667, ASA 3000.)

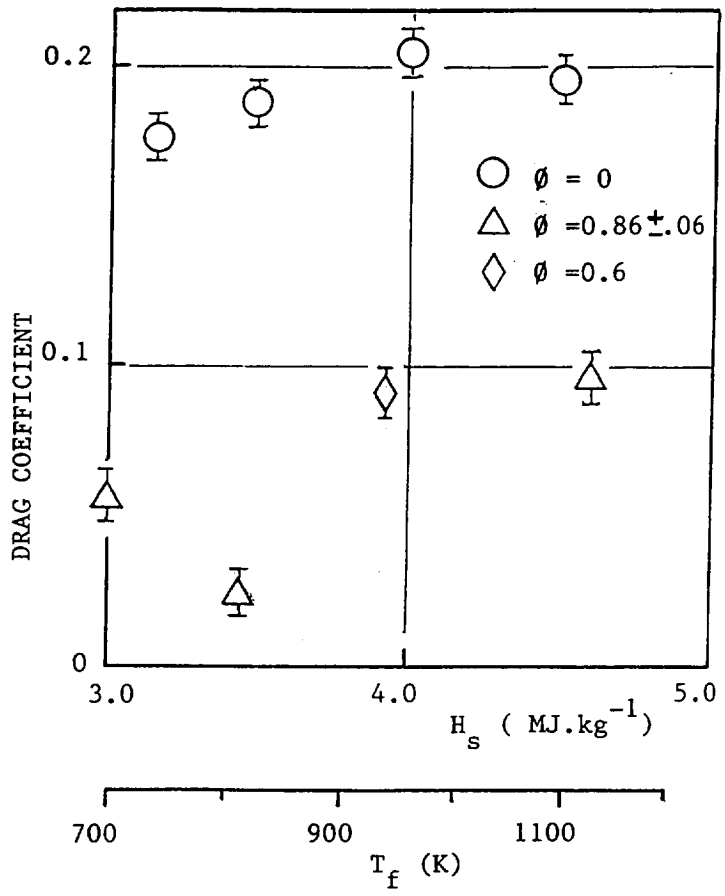

Fig. 6. Combustion Chamber Entrance Temperature Effect
(T_f= combustion chamber entrance temperature,
H_s= stagnation enthalpy, Ø= equivalence ratio.)

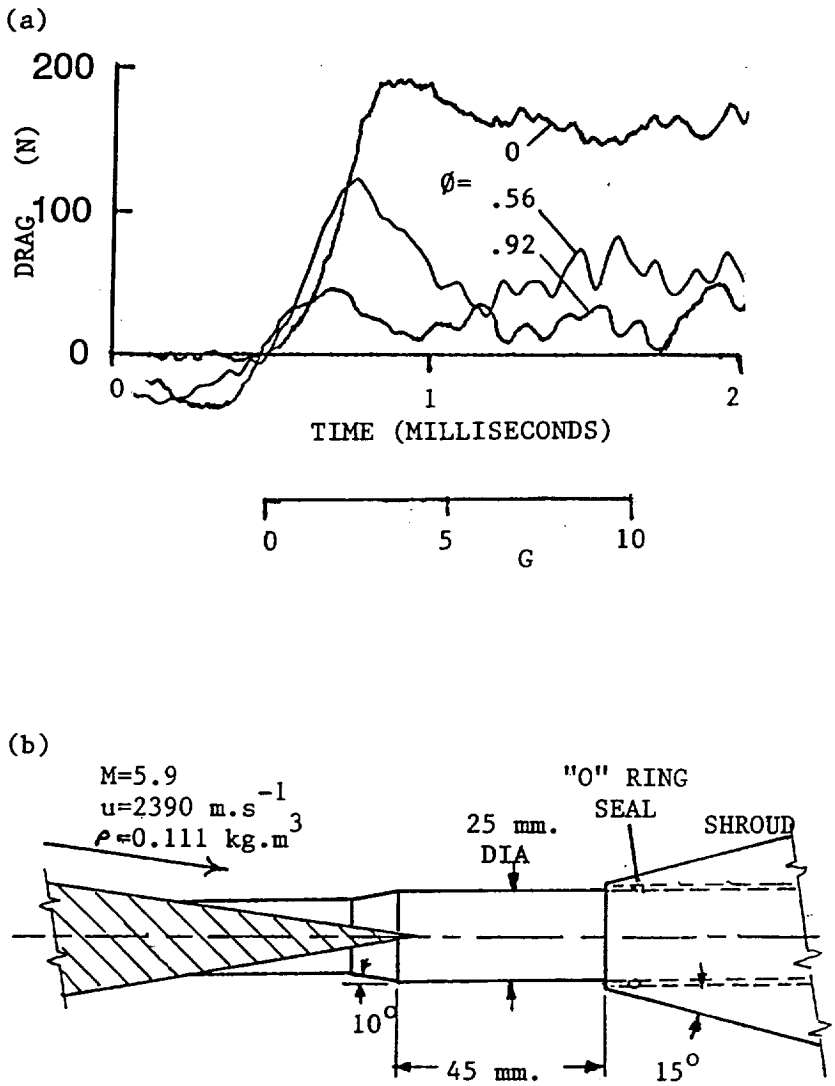

Fig. 7. Test Records and Sting Detail (H_s= 3.5 MJ.kg^{-1},
G = number of model lengths traversed by freestream,
M = Mach number, u = flow velocity, ρ = density)

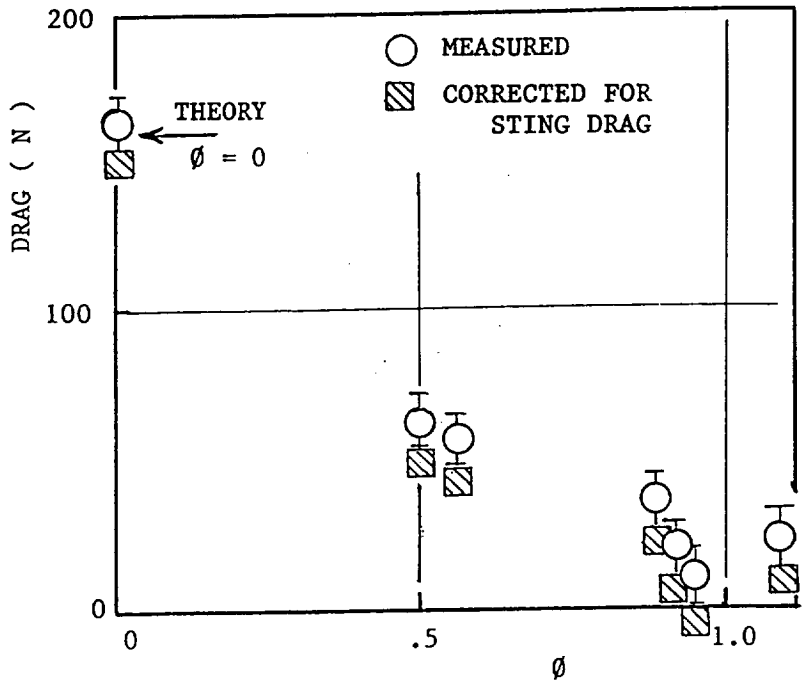

Fig. 8. Drag of Test Model (H_s= 3.5 MJ.kg^{-1}, P_s= 37 MPa., M = 6.4 ; Ø = equivalence ratio)

BLANK

DRAG MEASUREMENTS IN CARBON DIOXIDE TEST FLOWS USING A HYPERVELOCITY EXPANSION TUBE

A.L. Smith and D.J. Mee

Department of Mechanical Engineering
The University of Queensland
Brisbane QLD 4072, AUSTRALIA

October 1995

Abstract

A technique is described for the measurement of aerodynamic drag in a hypervelocity expansion tube in which the test flow period may be as short as 50 μs. The technique is an extension of the stress wave force balance first proposed by Sanderson [1]. The tests were conducted in a Carbon Dioxide test flow where the flow speed was in excess of 7 kms^{-1}. The validity of the technique is first demonstrated by comparing the forces measured on a range of sharp cones with those expected theoretically. Agreement to within 10% is achieved. Two re-entry type heat shield geometries were then tested with the experimental drag forces being compared with a Modified-Newtonian prediction. In both cases agreement to within 11% was obtained.

Key words: Drag measurement, Carbon Dioxide, Expansion tubes, Deconvolution, Hypervelocity, Re-entry vehicles

1 Introduction

Since the early 1960's experiments in hypervelocity flows have been conducted using shock tunnels. Shock tunnels are useful for conducting experiments for aerodynamics and propulsion purposes, at speeds up to Earth orbital velocities. However shock tunnels are limited in the range of stagnation enthalpies and test velocities that may be produced.

Free piston driven expansion tubes offer a wider range of stagnation enthalpies and test flow velocities and are therefore particularly useful in producing flows that are representative of re-entry at near orbital velocities.

The impulsive nature of both shock tunnels and expansion tube facilities restricts the steady test flow period that is produced. These may be as short as 1 ms for shock tunnels and 50 μs for expansion tubes. Consequently, tradition force measurement techniques cannot be employed as there is insufficient time for the model and its support to reach static equilibrium.

Although a number of techniques have been proposed for the measurement of aerodynamic forces in short duration test flows the most successful has been the stress wave force balance. This technique has been developed over the last five years to allow force measurements to be obtained on a variety of models in the T4 free piston shock tunnel, where the test time is around 1 ms.

This paper addresses an extension of this experimental technique to the measurement of drag force in hypervelocity expansion tube, where the test time is approximately 50 μs. It is envisaged that this measurement technique will be useful in the study of aerobraking and aerocapture manoeuvres within a Martian atmosphere.

2 Experimental Facility

The experiments were conducted in the X1 facility located at The University of Queensland (Neely *et al.* [2]). This facilty was originally designed as a reflected shock tunnel but has been adapted to investigate the mating of a free piston driver with an expansion tube. The X1 facility is shown schematically in Figure 1.

The free piston driver uses a 3.4 kg piston which is contained within the compression tube. The compression tube has an internal diameter of 100 mm and is 2.3 m in length. Both the shock and acceleration tubes have internal diameters of 37 mm and are 2.08 m and 2.94 m in length, respectively.

The facilty was operated as a free piston driven expansion tube using Carbon Dioxide as the test gas. The test condition produced approximately 50 μs of steady test flow. The typical filling pressures and test flow conditions, along with their respective uncertainties, are listed in Table 1.

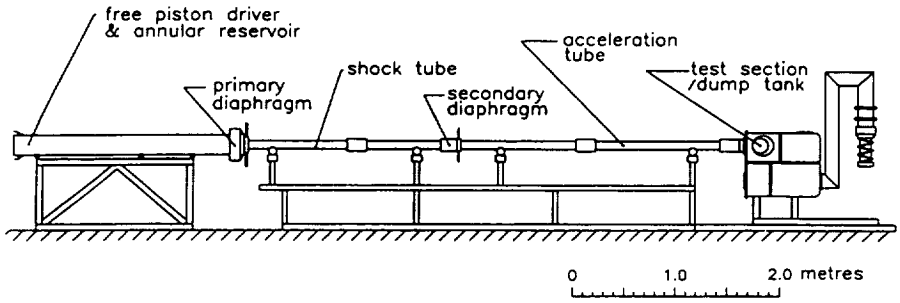

Figure 1: Layout of the X1 facility.

The facilty is instrumented with ionisation gauges and piezoelectric pressure transducers mounted along the walls of both the shock and acceleration tubes. These allow measurement of the shock speed and static wall pressure in both the shock and acceleration tubes. A piezoelectric pressure transducer was also used for measurements of the centreline Pitot pressure.

Table 1: Typical fill pressures and test conditions for the X1 facility.

Operating Mode	Expansion Tube	
Driver gas	80% He	20% Ar
Test gas	CO_2	
Acceleration gas	He	
Fill Pressures		
Compression tube (kPa)	78 kPa He	17 kPa Ar
Shock Tube (kPa)	5 kPa	
Acceleration tube (Pa)	100 kPa	
Test Flow		
Shock velocity (ms^{-1})	7200	±2.0%
Test velocity (ms^{-1})	7200[1]	±2.0%
Static pressure (kPa)	15.6	±2.0%
Temperature (K)	2987[1]	±1.9%
Density (kgm^{-3})	0.0194[1]	±10.0%
Total Enthaply ($MJkg^{-1}$)	30.13[1]	±2.6%
Specific heat ratio	1.253[1]	±0.2%
Pitot pressure (kPa)	1232	±5.0%
Mach number	7.43[1]	±4.3%

[1] Quantity obtained from equilibrium chemistry solver.

3 Force Measurement Technique

The force measurement technique presented here is based upon a scaled down version of a prototype stress wave force balance originally designed by Sanderson [1]. The stress wave force balance design has since been extended by Tuttle et al [3] and Porter et al [4] such that the technique is capable of resolving forces on a variety of model configurations, even those producing thrust, Paull et al [5]. All these experiments were conducted in the T4 free piston shock tunnel, located at the University of Queensland. The most significant difference between the original stress wave force balance and the design presented here is that the time in which forces are able to be resolved.

The stress wave force balance involves connecting the model to an elastic stress bar and suspending the arrangement in the test flow so that there is no restriction to movement in the flow direction (see Figure 2). With the sudden arrival of the test flow a drag force is exerted on the model causing stress waves to propagate and reflect within the model and the stress bar. These stress waves are measured and recorded using strain gauges mounted on the stress bar. The dynamic behaviour of the system can be modelled as a linear system described by the convolution integral,

$$y(t) = \int_0^t g(t-\tau)u(\tau)d\tau \tag{1}$$

where $u(t)$ is the input to the system (the drag force time history), $y(t)$ is the resulting output (the strain in the stress bar) and $g(t)$ is the unit inpulse response function. In experiments, the unknown drag on the model

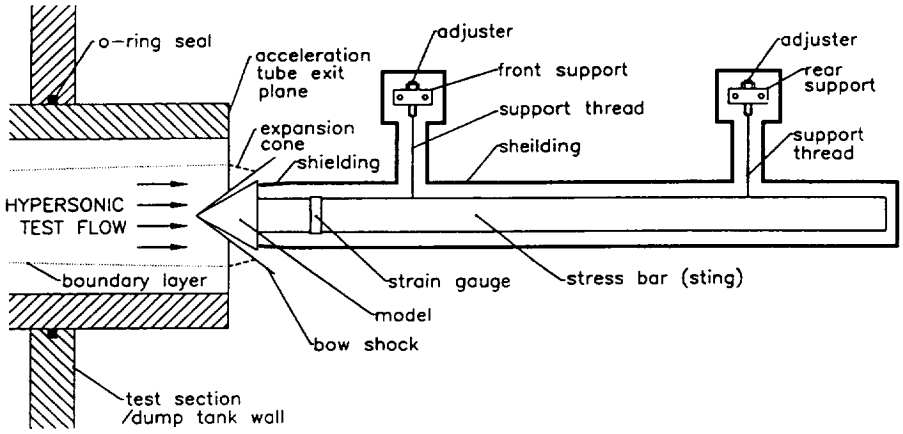

Figure 2: A schematic representation of the X1 force balance.

is determined from the measured output strain signal and the impulse response function. Thus, the problem is an inverse one and the drag may be found using a numerical deconvolution procedure.

The application of the stress wave force balance presented in this paper scales directly from previous work conducted in T4 in that the number of reflections of waves within the models during the test times are similar and the impeadance matching between the models and stress bars are similar. The performance of the proposed design was tested using dynamic finite element modelling of the arrangement to calculate the response of the balance to expected tunnel drag time histories. Deconvolution of this output with the impulse responses (also calculated using dynamic finite element modelling) indicated that the applied load could be recovered.

4 Force Balance Development

The force balance was designed to mount within the test section of the X1 facility and to support a small model within the test flow. Predictions of the test core, based upon the development of the boundary layer in the acceleration tube, indicated that the maximum model size was approximately 20 mm in diameter. The expansion cone produced by the expanding test gas (refer to Figure 2) constrained the model geometry such that oblique bow shock reflections from the expansion cone would not impinge on the model. This was a particular concern for conical models.

Based on the above geometrical constraints, three different models were manufactured: a series of sharp cones ranging in angle from 20° to 45° in increments of 5°, an Apollo heat shield [7] and a Viking heat shield [8] (refer to Figure 3). All of the models were made from 4140 Steel which was sufficiently robust to withstand the serverity of the test conditions. The models were threaded into the stress bar.

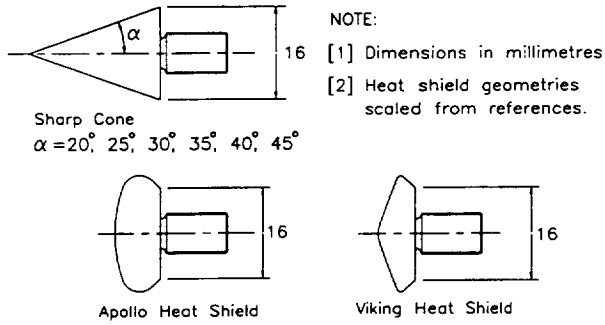

Figure 3: The model geometries used in the X1 facility.

The brass stress bar of 8 mm outside diameter, 7 mm inside diameter and 550 mm length, was instrumented with Kulite ULP 120-160 semi-conductor strain gauges. The strain gauges were mounted in a half bridge (bending compensation arrangement), approximately 60 mm remote from the threaded conection to the model. This formed the basis of the force balance onto which all the different models could be attached. Brass was chosen as the stress bar material because it has a relatively low elastic wave speed (3560 ms^{-1}). This serves to increase the period before stress waves reflected from the downstream end return to the gauge location. The instrumented stress bar was then suspended in a rigid shielding and aligned so that a small gap remained between the model and the shielding (refer to Figure 2).

Note that the arrangement of the stress bar and shielding at the base of the model will influence the base pressure. The balance geometry has been designed to minimize the pressure acting on the base of the models by minimizing the gap between the model abd the shielding. A finite gap is necessary in order to allow the model to be free to move under the influence of the aerodynamic drag. For the present models it is estimated that this gap needs to be 0.03 mm (but is generally set to 0.5 mm) to ensure that the model does not come into contact with the buffer during the test time. An estimate of the pressure acting in the base region can be made by assuming that the pressure in that region starts from the inital test section pressure and rises with time as gas leaks through the gap.

The dynamic responses of the eight different model/stress bar arrangments were analysed using the finite element package MSC/NASTRAN. This enabled unit step responses to be obtained for a uniformly distributed pressure loading on the models. The unit step responses were then used to obtain the unit impulse response functions which were latter used in the deconvolution of the measured strain time histories.

5 Experimental Results

Experiments were conducted in two stages. The first stage involved verifying the response of the force balance to short duration tests flows. The second stage involved conducting a series of experiments to obtain drag force measurements on re-entry vehicle models.

5.1 Verification Of Force Balance

At the chosen test condition the X1 facility produced a steady test flow for a period of approximately 50 μs. This is illustrated in Figure 4 by a typical centre-line Pitot presure time history. The Pitot pressure time history is characterised by the initial rise in pressure due to the acceration gas, followed by the arrival of the test gas after which expansion waves propagate downstream from the driver indicating the arrival of the driver gas.

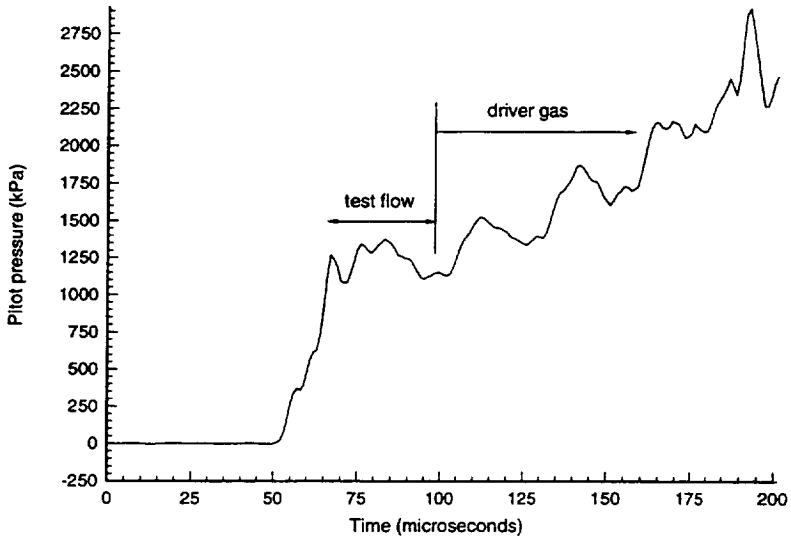

Figure 4: A typical Pitot pressure time history measured in the X1 facility.

Drag measurements were obtained for the conical models through deconvolution of the measured strain time histories, as described in section 3. The deconvolved drag measurements were then compared directly to a theoretical drag prediction. The prediction was based upon the inviscid Taylor-Maccoll [6] theory for an attached conical shock in a perfect gas. The validity of this prediction was verified by calculations of the combined effect of skin friction and base drag on the model. For all cases the bow shock produced was fully attached which meant that conditions behind the shock could be used to estimate the effect of skin friction. The effect of base drag was estimated by modelling the rise in pressure in the base region as the isentropic flow (from the conditions behind the shock) into the evacuated shielding. The results from these calaculations indicated that the combined effect of skin friction on the model and pressure acting in the base region (for the geometrical arrangement shown in Figure 2.) was less than 2% of the net drag on the model during the period of the test flow.

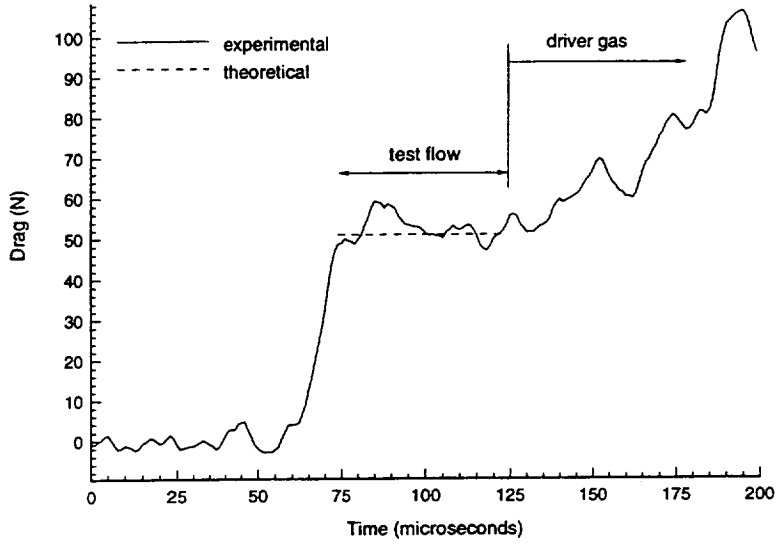

Figure 5: A comparison between the measured and predicted drag force on the 30° cone model [CO_2 at M=7.4].

A typical deconvolved drag signal obtained from the 30° cone model, along with the predicted drag force, appears in Figure 5.

Figures 4 and 5 indicate that the deconvolved drag has a similar time history to the measured Pitot pressure, in that a steady drag level is measured during the period of the test flow. Note that size restrictions in the test section prevented Pitot pressure and drag measurements being obtained simultaneously. Thus zero on the time scale is arbitary.

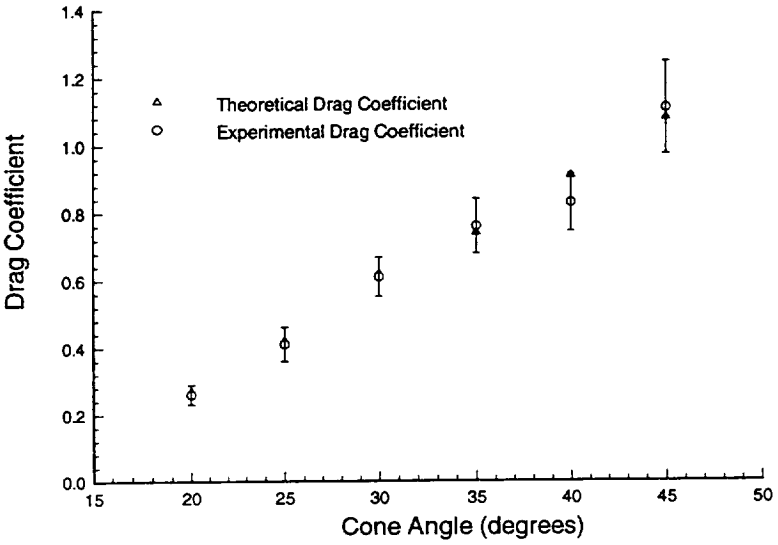

Figure 6: A comparison of the experimental and theoretical drag coefficients on increasing cone angles [CO_2 at M=7.4].

Agreement between predicted and experimental drag levels was found to be within 10% for repeated tests on all the conical models. The difference was attributed primarly to uncertaincies in the test flow conditions which corresponded to a 12% uncertainty in the measured drag coefficient. The comparison between experimental and theoretical drag coefficients for the range of cones tested is presented Figure 6. The error bars corespond to the uncertainty in the experimental results. The results from these experiments indicate that the force balance can be used to measure forces in short duration test flows.

5.2 Drag Force Measurements On Re-entry Heat Shields

The force balance was then used to obtain drag measurements on the Apollo and Viking heat shield models, as depicted in Figure 2. Theoretical predictions for the drag on these models were made using the finite element meshes of the models described in Section 4 and a Modified-Newtonian flow solver. An example of the finite element meshes for the Apollo heat shield used is presented in Figure 7.

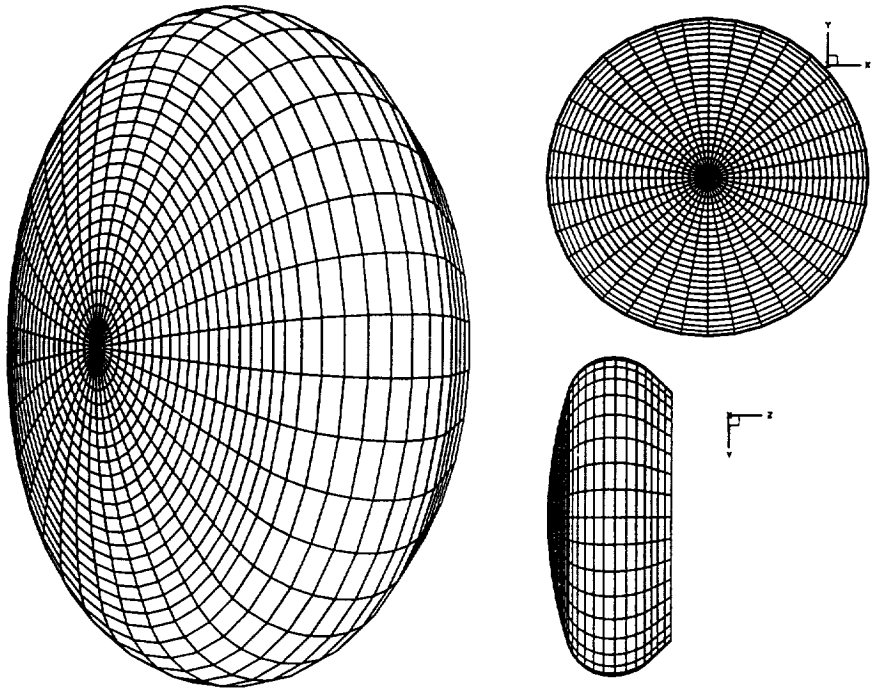

Figure 7: The finite element mesh of the Apollo heat shield used in conjuction with the Modified-Newtonian flow solver.

Figures 8 and 9 illustrate typical deconvolved drag measurements along with theoretical predictions for the Apollo and Viking heat shield models respectively, plotted for the duration of the test flow. Inital overshoot in the measured drag time history has been attributed to the time associated with the formation of the bow shock over the blunt model. This result was also observed in the drag time histories of the conical models. In general, increasing cone angle caused a larger initial overshoot in the drag. The formation of the bow shock wave, resulting in an overshoot in the pressure/force time history, is reported by Davies [10].

Figures 8 and 9 again indicate that the deconvolved drag history follows the Pitot pressure time history. Repeat shots on both models were used to obtain drag coefficients specific to the measured test conditions. This showed that agreement between experimental and predicted drag levels was to within 11%. This is also consistent with the uncertainty of test conditions produced by the X1 facility and the inherrent inadequacies of the Modified-Newtonian flow solver. The effect of skin friction and pressure in the base region was less signicant for the re-entry models than the conical models. This is due to the bluntness of the models. Therefore this did not represent a significant uncertainty in obtaining drag force predictions. The measured and predicted drag levels results for all tests were averaged and appear in Table 2.

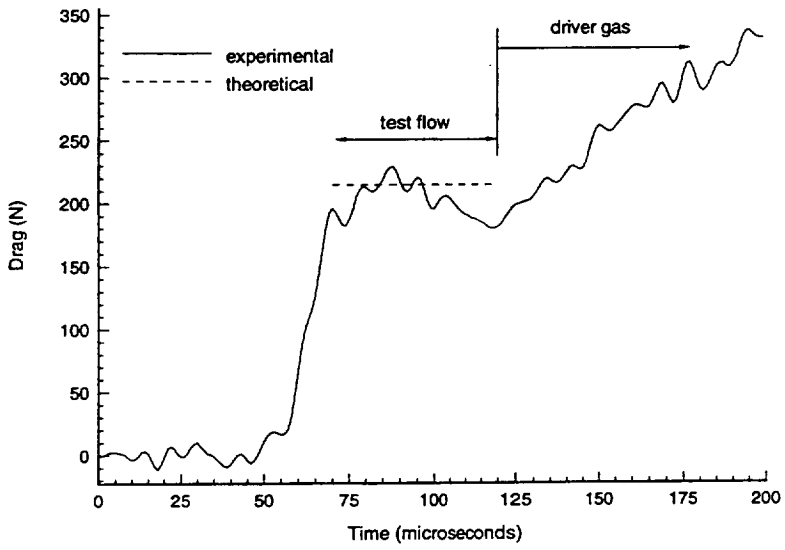

Figure 8: The measured and predicted drag force on the Apollo heat shield model [CO_2 at M=7.4].

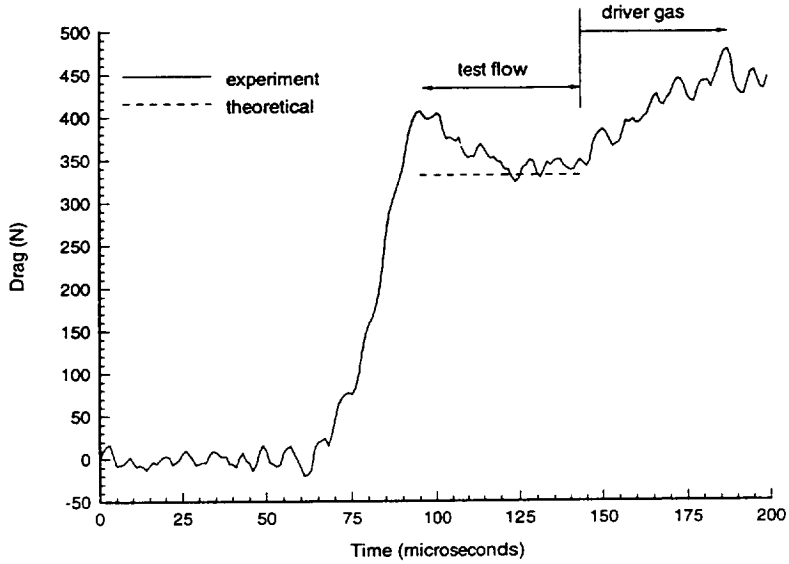

Figure 9: The measured and predicted drag force on the Viking heat shield model [CO_2 at M=7.4].

Table 2: Average measured and predicted drag coefficients for typical re-entry heat shields [CO_2 at M=7.4]

Model	$C_{D(measured)}$	$C_{D(predicted)}$
Apollo Heat Shield	1.56	1.60
Viking Heat Shield	1.81	1.65

6 Conclusion

An extension of the force measurement technique has been developed for use in a free piston driven expansion tube. Preliminary tests were used to verify the response of the force balance to the short duration test flows that are typical of expansion tubes. The force balance was then used to obtain drag measurements on two re-entry type vehicles shapes, in Carbon Dioxide test flows. In general, agreement between experimental and predicted drag levels was found to be within 11%.

The sucessful measurement of drag forces in the X1 facility extends the usefulness of short duration hypervelocity facilities, especially in the area of aerobraking and aerocapture studies. This is envisaged to be important for the development of interplanetary flight vehicles.

7 Acknowledgements

The authors gratefully acknowledge the financial support of the Australian Research Council under grant A8941305 and the use of the Modified-Newtonian flow solver developed by K. Austin at the University of Queensland, Department of Mechanical Engineering.

8 References

[1] Sanderson S.R. and Simmons J.M. *Drag balance for hypervelocity impulse facilities*, AIAA Journal, 29(12):2185-2191, 1991.

[2] Neely A.J., Stalker R.J. and Paull A. *High enthalpy, hypervelocity flows of air and argon in an expansion tube*, The Aeronautical Journal, 175-186, June/July 1991.

[3] Tuttle S.L., Mee D.J. and Simmons J.M., *Drag measurements at Mach 5 using a stress wave force balance.*, Experiments in Fluids, 19(5):336-341, 1995.

[4] Porter L.M., Paull A., Mee D.J. and Simmons J.M., *Shock tunnel measurements of hypervelocity blunted cone drag.*, AIAA, 32(12):2476-2477, 1994.

[5] Paull A., Stalker R.J. and Mee D.J., *Scramjet thrust measurement in a shock tunnel.*, The Aeronautical Jounal, 161-163, May 1995.

[6] Mee D.J., Daniel W.J., Tuttle S.L. and Simmons J.M., *Balances for the measurement of multiple components of force in flows of a millisecond duration*, 19th International Symposium on Shock Waves, 26-30 July 1993 Marseille, France.

[7] Park C., *Nonequlibrium Hypersonic aerothermodynamics*, John Wiley and Sons, Brisbane 1990.

[8] Miller C.G., *Shock shapes on blunt bodies in hypersonic-hypervelocity helium, air and CO2 flows, and calibration results in Langley 6-inch expansion tube.*, NASA TN D-7800, 1975.

[9] Taylor G.I. and Maccoll J.W., *The air pressure on a cone moving at high speed*, Proc. Royal Society (London), Series A, 139:278-297, 1932.

[10] Davies L., *Bow-shock establishment and stagnation-point pressure measurements for a blunt-nosed body at supersonic speeds*, NPL Aero Report 1098, 1964

AIAA 96-0854

A Two-Stage Free-Piston Driver for Expansion Tubes

C. J. Doolan and R. G. Morgan
Department of Mechanical Engineering
The University of Queensland
Brisbane, Australia

AIAA 34th Aerospace Sciences
Meeting & Exhibit
January 15-18, 1996
Reno, Nevada

A Two Stage Free-Piston Driver for Expansion Tubes

C. J. Doolan* and R.G. Morgan†
The University of Queensland
Brisbane, QLD, 4072, Australia

Abstract

A new free-piston driven expansion tube facility has been designed and constructed at the University of Queensland. This paper presents some results from the commissioning of the driver unit. The driver is a unique two stage free-piston device employing a compound piston consisting of two separate parts. Experimental results outline the performance of the two stage machine and show its feasibility for driving an expansion tube facility.

1 Introduction

There is currently considerable interest in the use of potential aerobraking spacecraft used for interplanetary missions[1-3]. These missions require very large Earth re-entry velocities (13-16 kms^{-1}). The flowfields surrounding such craft involve a complex mix of dissociation, ionisation and radiation making accurate calculations difficult. Computational fluid dynamics (CFD) codes require experimental data for validation purposes, however to date there are limited experimental facilities which can produce these high enthalpy flows.

One method of producing high enthalpy (80-130 $MJkg^{-1}$) flows in air is the super-orbital expansion tube[4]. Here, we define super-orbital as a velocity in excess of low Earth orbital velocity (7.9 kms^{-1}). This facility type uses a free-piston compressor and an array of three shock tubes, as shown in fig. 1. Here, the enthalpy multiplication effect of expansion tubes is used to produce the high velocities required for super-orbital simulation. In order to produce the necessary high shock speed through the air filled shock tube, the free-piston driver performance is enhanced by the addition of an upstream, helium filled shock tube, the secondary driver tube. By operating the secondary driver tube in an overtailored mode, a higher effective driver temperature can be obtained[5].

Useful test-flows have been obtained in a small scale pilot facility[4] (38 mm test jet) and it is planned to build facilities with increased test section cross-sectional areas. To build these facilities within the limits of a typical university budget, a different free-piston driver design is required. Conventional, single bore free-piston drivers make use of a large area change at the diaphragm station. This is done so an increased shock speed can be achieved for a given burst pressure. Also, by maintaining piston speed after rupture, the driver gas pressure can be sustained thus preventing unsteady expansion waves disrupting the test flow. However, for a large scale facility (200 mm shock tube bore) capable of 200 MPa burst pressures, this area change becomes expensive in terms of materials and fabrication. Even though a higher burst pressure is required, the overall facility cost can be reduced by using a driver whose bore is approximately the same as the driven shock tubes. In addition to this, numerical simulations by Jacobs[6] reinforce the suspicion that any area change at the end of the compression tube can provide a mechanism for waves which are detrimental to shock tube flows.

A constant-area driver requires an adequate volume of gas behind the diaphragm prior to rupture in order to delay the reflected unsteady expansions from distrubing the test flow. In a single bore free-piston driver, ths would equate to unfeasibly long compression tubes (approximately 100 metres in length). To reduce the compression tube length, a two stage driver has been developed. Basically the driver works using a principle similar to two stage reciprocating compressors[7].

*Graduate Student, Member AIAA.
†Associate Professor, Member AIAA.

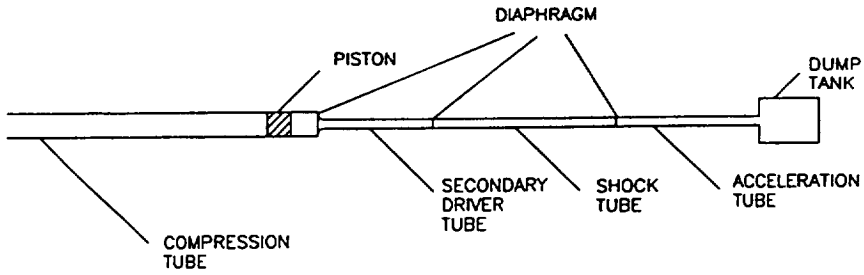

Figure 1: Free-piston driven super-orbital expansion tube

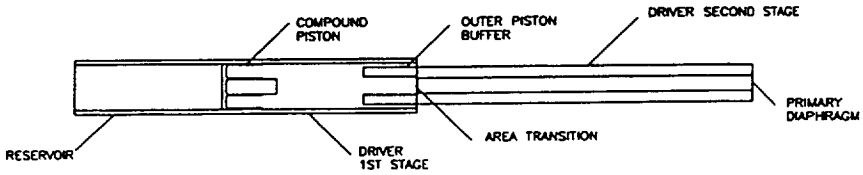

Figure 2: Two Stage Free-Piston Driver Concept

A schematic of the concept is shown in figure 2.

The adiabatic compression process is characterized by an initial low pressure rise with a large swept volume followed by a rapid pressure rise during the final stages of compression. By using a large bore first stage compression tube, the required volumetric compression can be achieved in a reduced overall length. The low pressures in the first stage allow a light wall tube to be used, further reducing facility cost.Two concentric pistons, a light aluminium outer and a heavy stainless steel inner, perform the bulk of the volume compression in the first stage at low pressure. The pistons then separate at a location where approximately 85% of the available reservoir work is converted to piston kinetic energy. The light outer piston is stopped and the heavy inner piston, which contains the majority of the energy, is used to compress the driver gas to its final conditions in the second stage. In order to study the operational characteristics of the two-stage free-piston driver, the medium sized expansion tube facilty, X-2 has been constructed. This paper will present some of the results from the commissioning of the driver section.

2 Basic Theory

Preliminary operating performance and benefits of two-stage free piston drivers over conventional single stage machines can be seen by considering some simple gas dynamic theory. Perhaps the two most important criteria for assessing the two-stage driver are size (length) of the final gas slug and its temperature before diaphragm burst. The temperature can be achieved by using a sufficiently high compression ratio, while the final gas slug length depends upon the geomtery of the facility. The designer must be careful in selecting the geometry of the driver as it influences safety as well as operational issues.

Theory assuming ideal gas behaviour outlined by Morgan[6] can be used to provide an estimate of facility performance with respect to a particular chosen geometry. Here, the geometry of X-2 will be used. Figure 3 shows the increase in slug length available over single stage machines for various area ratios (A_R) and stage one compression ratios (λ_1). Figure 4 shows the variation of the compound piston pressure ratio (P_d/P_r) with λ_1 and compression ratio (λ). If the pressure ratio of the driver gas to the reservoir gas (P_d/P_r) becomes greater than unity before the second stage, a potentially dangerous situation exists. The more massive inner piston possesses a higher inertia than the aluminium outer therefore if an acceleration reversal occurs, the pistons may separate prematurely, causing damage to the facility. The geometry and operating conditions can be chosen so as to minimise this risk.

These results illustrate that in order to keep P_d/P_r below unity over a large range of compression ratios, λ_1 must be kept below 6. Also, by limiting the area ratio to 9 (to keep the first stage bore a practical size) 3 to 4 times the slug length of compressed gas generated in a single stage machine can be used if λ_1 is kept between 4 and 6.

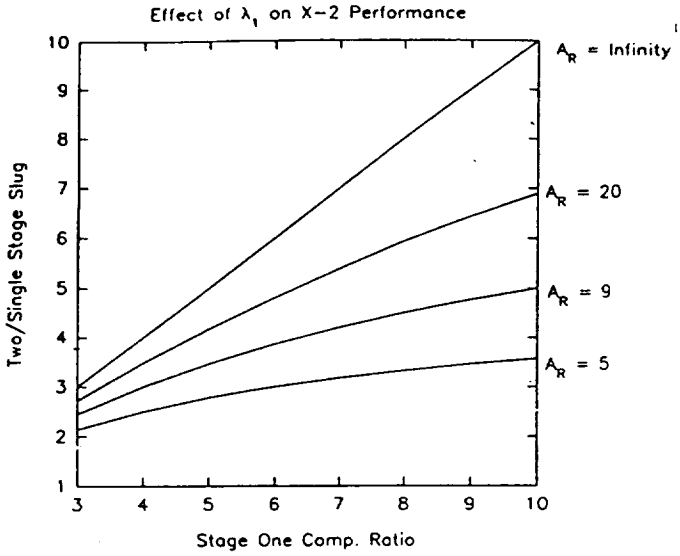

Figure 3: Increase in slug length of two/single stage free piston drivers

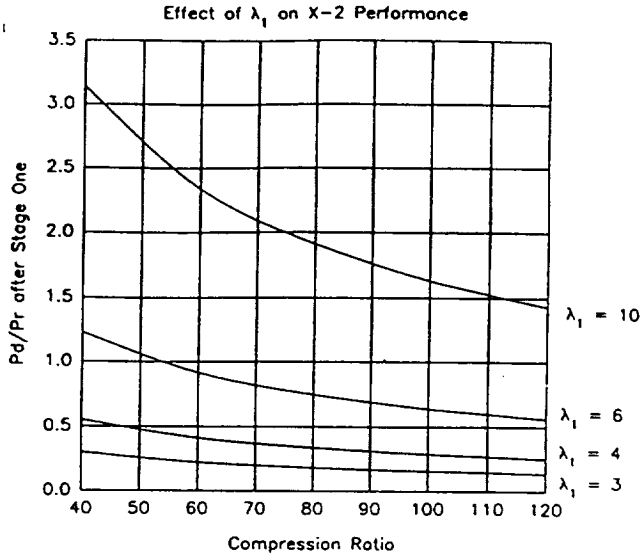

Figure 4: Pressure ratio across compound piston after stage one

Alternatively, this ratio can be thought of as the decrease in length a two stage driver offers over conventional drivers for the same amount of driver gas, at the same condtions before diaphragm rupture.

This analysis allows a convenient way of sizing the components for X-2 and for showing the benefits of the two-stage free piston driver for a constant area diaphragm station facility.

3 The X-2 Facility

The X-2 facility layout is shown in figure 5. The driver uses a large reservoir to accelerate the piston. The reservoir volume is 0.23 m^3 and is approximately three times the volume of the compression tube.

The compound piston is required to be accelerated to a high speed (50-100 m/s) within the first stage (1.1 metres of compression allowed) and because the first stage has a large bore (273 millimetres), a piston launch mechanism is required which provides little flow resistance to the reservoir gas. For this reason a double diaphragm arrangement is used to launch the piston. The diaphragms are clamped in a pre-deformed groove around their periphery which allows only a small clamping area with respect to the bore (25%). The diaphragms used for the results shown in this paper were unscored 0.6 mm thick aluminium. Using these diaphragms the reservoir pressure can be varied from 800 kPa to 1.6 MPa, for the results shown here the reservoir pressure was varied between 1.1 MPa and 1.25 MPa.

A sketch of the compound piston arrangement is shown in figure 6. The large outer piston is used as a sabot or carrier piston for the much heavier inner piston. The outer piston is made from a structural grade aluminium and weighs 8 kg. Bearing surfaces for the outer piston consist of a molybdenum sulphide and carbon/graphite doped teflon material (Lussint 332). The piston is sealed with an o-ring supported in a special dove-tail groove at the rear of the piston.

The heavy inner piston is constructed from AISI 316 stainless steel and has a mass of 16 kg. The piston uses a high pressure chevron seal at its front which is of a similar design to that used on the T4 and T5 pistons. Two sets of brakes are fitted to the inner piston. These are required to prevent the inner piston from destroying the outer piston in the event of the diaphragm not bursting, or in a "blanked off" test. The brakes rest on conical seats and are split into four shoes per seat (see figure 7). The shoes consist of an aluminium base with an automotive friction material bonded to the top surface. A pressure sensitive teflon tape is fixed to the conical surface of the shoes which minimises the friction between the shoes and the piston. When the piston undergoes a large acceleration reversal, such as when the pressure reaches its peak during the compression process, the brake shoes deploy, sliding up the conical surface and engaging the friction material with the bore of the compression tube. The taper angle is chosen such that there is minimal

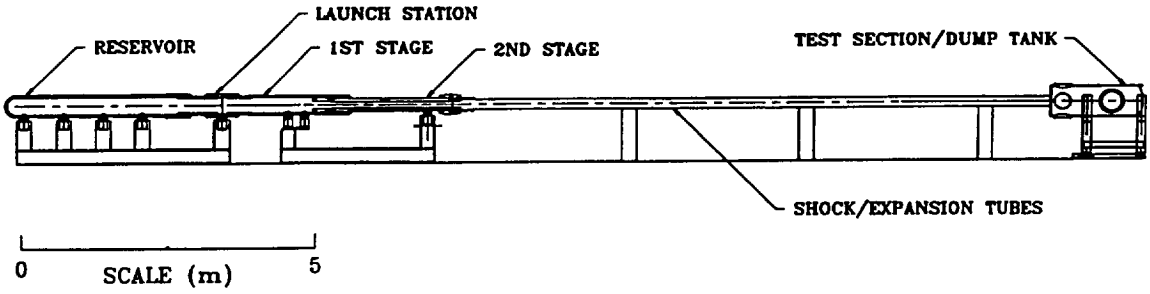

Figure 5: X-2 Facility Layout

slippage after the brakes are engaged. In practice it is noticed that there is between 100 and 375 mm of slippage during a blanked off test. An o-ring is used on each set of brakes to keep them secure during piston handling and inner piston transfer to the second stage.

The first stage compresson tube provides the bulk of the compression process, which is done at low pressure (up to 2% of burst pressure). The outer piston is stopped at the end of the first stage by the use of a cylindrical, composite polyurethane buffer (fig. 8), bonded to a mounting plate attached to the end wall of the second stage. By sandwiching stainless steel plates between polurethane pads, tensile stresses are set up in the free surfaces of the pads , effectively increasing the stiffness of the overall composite. By varying the length of the pads and the number of plates[8], the stiffness of the buffer can be tailored to suit a certian range of impact energies. An elastomer material such as polyurethane has a distinct advantage over a gas dynamic buffer. In this case, the piston is required to be stoppped in a short distance (90 mm), an elastomer provides a high retardation force over the duration of the deceleration. A gas dynamic buffer has an expotential increase in retardation force, which equates to very high pressures (100 MPa) if the piston is to be stopped in a short distance. Initially, stress waves in the elastomer supplies a high stopping force. Towards the end of the stroke, the natural spring characteristics of the elastomer allow a stopping force of the same order as the initial stress wave.

The current buffer has been designed to withstand a 17 KJ impact which equates to a 8 kg piston travelling at 65 m/s. The size of the buffer also affects the first stage compression ratio (λ_1). As mentioned previously, the overall performance is sensitive to this ratio and must be kept large enough for an adequate volume of compressed driver gas. The current buffer allows $\lambda_1 = 4.3$.

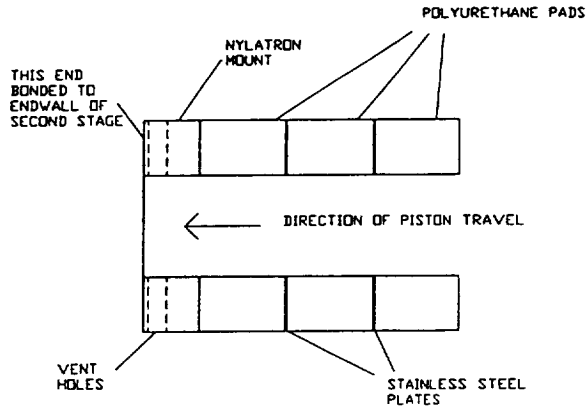

Figure 8: Composite Polyurethane Buffer, Sectioned View

An array of 24 holes is drilled around the rear mount (nylatron). These holes are required to vent any gas trapped in the front cavity of the outer piston to the second stage. Any driver gas not compressed into the second stage results in reductions in facility performance. Also, these holes provide a safety feature. In the event of a buffer failure, the plastic flow area around the vent holes limits the force transmitted to the facility to a safe value.

After the pistons separate, the inner piston travels down the second stage compression tube, where it compresses the driver gas to its final conditions and brings itself to rest before diaphragm burst. The second stage is of a multi-wall design, with an 18 mm thick sleeve interference fitted via liquid nitrogen cooling along the bore. The inner bore is 91 mm and the outer diameter is 225 mm. In order to compensate for any misallignment of the first and second stages, a tapered nylon conical entrance is provided for the second stage, allowing the inner piston some protection as it traverses the area transition.

At the end of the second stage is a diaphragm

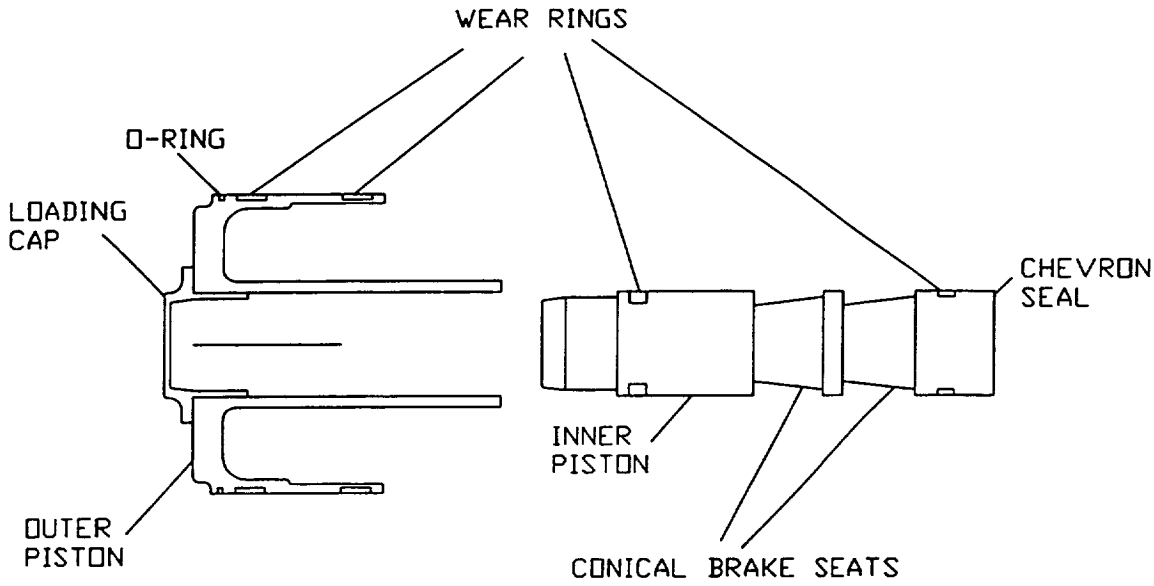

Figure 6: Sketch of X-2 Compound Piston Arrangement

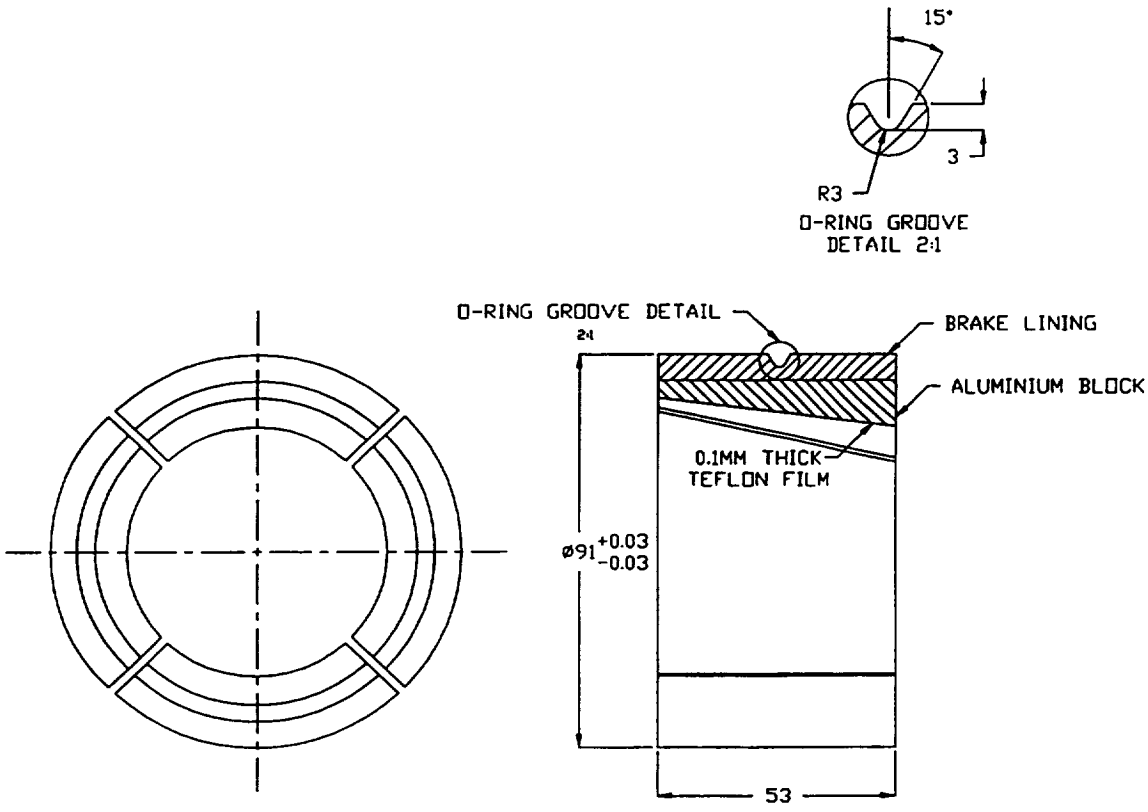

Figure 7: X-2 Inner Piston Brakes, Dimensions in Millimetres

station which can accomodate up to a 5 mm stainless steel diaphragm and is designed to withstand a 100 MPa impulsive load. The pressure loading occurs over a very short time frame (40-60 ms) with the highest pressure rise occuring typically over the last 5 ms. This induces stress waves in the driver and shock tubes which are not normally present in a static pressure vessel. The transient stress loading is accounted for in the design stage. The diaphragm is held in place with the use of a free-piston clamp. This clamp transmits an initial pre-load to the diaphragm from the tourque developed by tightening the capstan nut. As the pressure increases in front of the piston during operation, a small space allows this pressure to work on a large area of the free-piston clamp, making the axial load on the diaphragm directly proportional to the burst pressure. This ensures a large clamping load on the diaphragm, preventing slippage during operation.

The two-stage driver will be used to generate flow in 10 metres of shock tubes with an eighty-five millimetre nominal bore. These tubes are machined into seven lengths varying in length from 2.5 metres to 500 millimetres. The tubes have been constructed from ex-World War 2 17 pound anti-tank gunbarrels.

The test section/dump tank has been constructed from the reservoir of an ex-submarine torpedo launcher. It has dimensions of 500 mm bore and is 1500 mm long. In order to achieve the very low pressures rquired for super-orbital testing (fill pressures 1-20 Pa), a 13 inch Edwards oil diffusion pump has been fitted to a large flange welded to the dump tank wall. Four access ports 90 degrees apart are provided at the test section end for instrumentation and optical access.

4 Experimental Results

Results from the commissioning the X-2 two-stage driver section will be presented here. In order to test the energy absorbing capacity of a rubber buffer first used for stopping the outer piston, a dummy 17.5 kg steel piston was constructed. This piston is essentially the same design as the aluminium outer piston shown in figure 6, however the inner piston holder has been removed. The dummy piston is loaded into the first stage only (no inner piston) and conditions are selected so the piston strikes the buffer with a predetermined amount of energy. These tests are also useful for studying the unsteady flow past the area transition into the second stage. If a heavier driver gas is used, such as nitrogen or argon, calculations show the Mach number at the area transition can approach unity. This increased Mach number sets up a non-uniform pressure distribution within the compression tube affecting the piston dynamics. As heavier driver gases will be required to be used in the two-stage driver for sub-orbital expansion tube operation it is benificial to understand this process.

Figure 9 compares the experimental results obtained during a dummy piston run with a numerical simulation. Numerical results are obtained by using a quasi-one-dimensional Langrangian code[6]. Breifly, this code uses engineering correlations for viscous effects and point mass dynamics for piston motion. The initial gas volumes are split into a number of cells and are allowed to interact using an approximate Riemann solver which computes cell interface pressures and velocities. The results shown here use an initial air reservoir pressure of 1.1 MPa and a 200 kPa nitrogen driver gas. Pressure was measured 30 mm upstream of the primary diaphragm station using a piezo-electric ceramic pressure transducer. The driver was "blanked off" using a steel plate at the diaphragm station. Good agreement between experiment and simulation is observed. Peak pressures match within 6%. Figure 10 displays the Mach number at the area transition as calculated by the numerical code. This result demonstrates that the flow past the area transition can be adequately modeled for a heavy driver gas.

Dual piston experiments were also performed. For these tests, a helium driver gas was used. The driver was again "blanked off" for the results presented below. A number of experimental runs were performed, examining the peak pressures obtained and comparing them to theory based on ideal gas theory. It was found that during the dual piston expriments, the natural rubber buffer was filling all of its available volume during outer piston impact. This was causing slight deformation of the outer piston each shot and the buffer was exchanged to the polyurethane/stainless steel plate design discussed in the previous section. Both the rubber and polyurethane buffers showed excellent impact properties with no measurable changes in dimensions from run to run. The buffer strain was kept below 30% in all cases.

Figure 11 is an example of a typical pressure trace record (measured 30 mm upstream of the diaphragm station) of a dual piston run. The trace shows an early pressure rise which suddenly changes slope with some oscillations super-

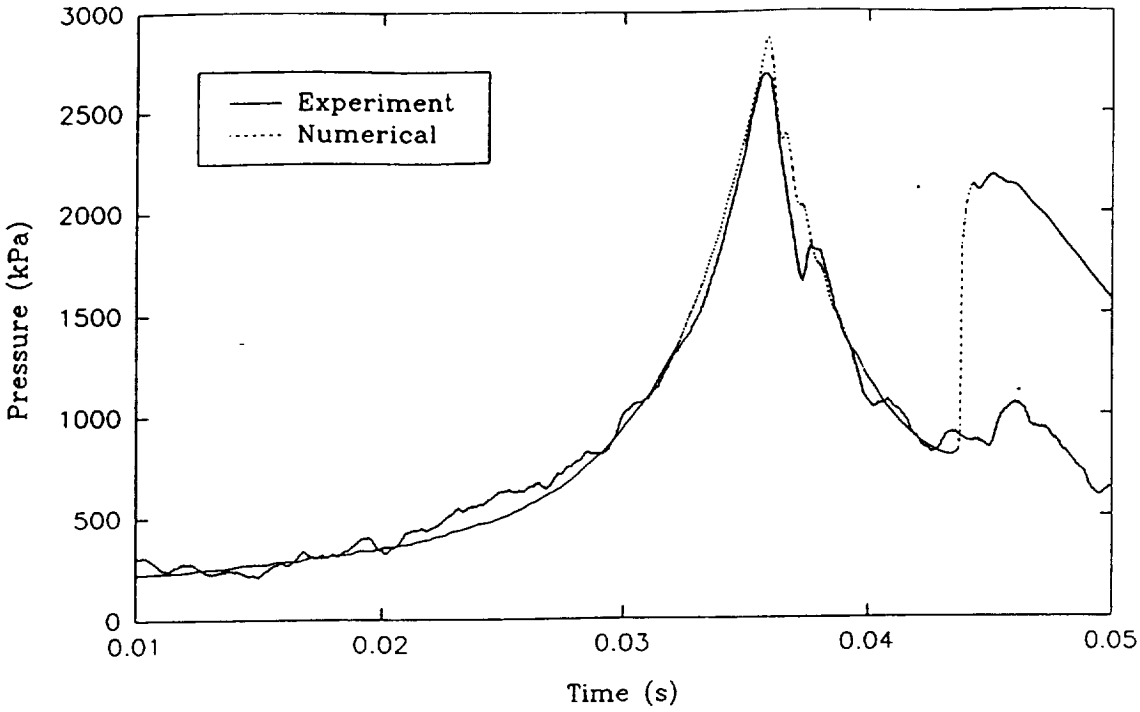

Figure 9: Comparison between Experiment and Numerical Simulation for the Nitrogen Driver Gas, Dummy Piston Test

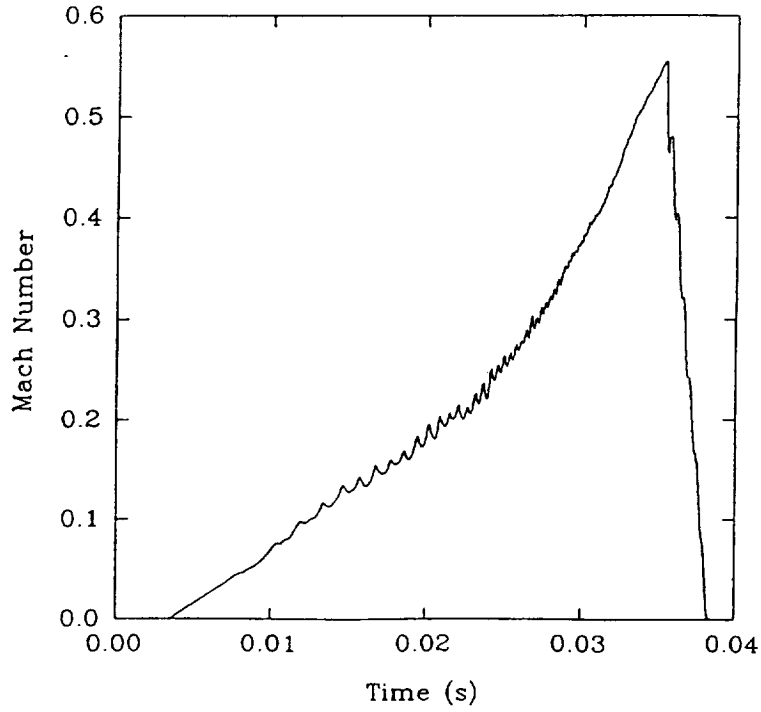

Figure 10: Numerical Mach Number History at the Area Transition for the Nitrogen Driver Gas, Dummy Piston Test

imposed upon it. The change in slope corresponds to the point where the inner piston is transferred into the second stage. The change in slope occurs due to both the instantaneous change in piston acceleration (as both the mass drops and the reservoir pressure is removed at piston transfer) and the change in rate of volumetric compression at the area change.. The slight oscillations can be explained as weak expansion waves generated by the acceleration change. These oscillations are quickly damped out as the inertia of the inner piston compresses the gas to its peak pressure. At this point, the brakes on the piston should be deployed against the wall of the compression tube. The piston rebounds as the brakes bind bringing the piston to rest with between 3 and 5 MPa residual pressure in front of the piston.

Figure 12 is a graph of initial reservoir pressure (P_{r*}) normalized by the initial driver gas fill pressure (P_{d1}) versus the peak driver gas pressure (P_{df}) normalized by the initial reservoir pressure. Compared against the exerimental data are theory lines, calculated using ideal gas theory (section 2). It can be seen that for the case with no losses an approximate 1.5 times higher burst pressure is expected. If a 15% inner piston kinetic energy loss term is included, a more reasonable agreement exists. This loss term is included by reducing the expected kinetic energy of the inner piston at the start of the second stage by 15%. There are a number of factors which may cause this loss in piston energy:

- Non-ideal expansion of reservoir gas. This is unlikely due to the good agreement of the dummy piston tests with numerical results.
- Excessive friction during piston transfer. A small misallignment might cause some excess friction against the conical nylon lead-in insert to the second stage.
- Premature brake deployment. The inner piston is under constant deceleration along the length of the second stage, this might partially deploy the brakes causing slight rubbing against the tube wall.

These results show that the two stage driver performs in a similar manner to conventional free-piston machines and in accordance with simple gas dynamic theory. This suggests the two stage free-piston concept is a feasable driver design for an expansion tube facility.

5 Conclusions

A two stage free-piston driven expansion tube facility has been constructed at the University of Queensland. The facility uses a unique free-piston design which allows a constant area between the driver and driven tubes. A compound piston is employed in two stages which drastically reduces the overall length of the free-piston unit.

The driver section has been tested with a steel dummy piston and dual aluminium and stainless steel pistons. The steel dummy piston tests showed the effect of the increased Mach number at the area change when using a heavy driver gas. The dual piston tests showed the performance of the device to be similar to conventional free-piston machines. The experimental data was described well by ideal gas theory if a 15% mechanical loss term was included. This suggests the two stage free-piston concept is a feasible driver design for an expansion tube facility.

Future work for the X-2 is the determination of a bulk driver temperature by shock speed measurements. A super-orbital test condition will then be found, bringing the facility to full operational status.

6 Acknowledgements

The author gratefully acknowledge the financial support given by NASA grant NAGW-674 and the Australian Research Council. The military hardware was most generously supplied by the Australian Defence Science and Technology Organisation and Sydney University, Australia.

7 References

[1]Walberg, G., "How Shall We Go to Mars? A Review of Mission Scenarios," *Journal of Spacecraft and Rockets*, Vol. 30, No. 2, 1993, pp. 129-139.
[2]Braun, R.D., Powell, R.W. and Lyne, J.E., "Earth Aerobraking Strategies for Manned Return from Mars," *Journal of Spacecraft and Rockets*, Vol. 29, No. 3, 1992, pp. 297-304.
[3]Mitcheltree, R.A. and Gnoffo, P.A., "Thermochemical Nonequilibrium Issues for Earth Re-Entry of Mars Mission Vehicles," *Journal of Spacecraft and Rockets*, Vol. 28, No. 5, 1991, pp. 552-559.
[4]Neely, A.J. and Morgan, R.G., "The Super-orbital Expansion Tube Concept, Experiment and Analysis," *The Aeronautical Journal*, March,

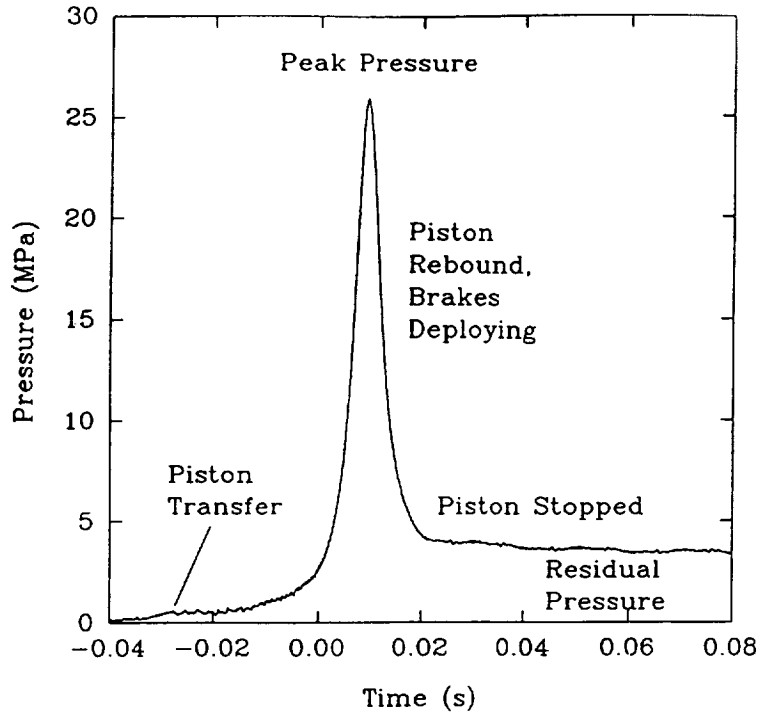

Figure 11: Pressure History Measured 30 mm Upstream from Diaphragm Station;Initial Reservoir Pressure 1.21 MPa and Initial Driver Gas Pressure 32.5 kPa

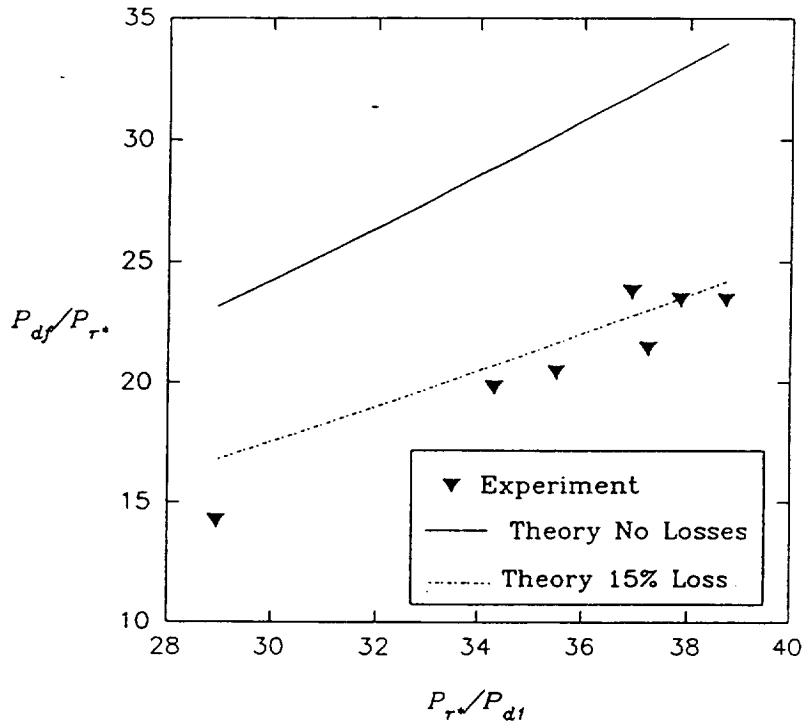

Figure 12: X-2 Driver Performance

1994, pp.97-105.
[5]Morgan, R.G. and Stalker, R.J., "Double diaphragm driven free piston expansion tube," *Proc. 18th Int. Symp. Shock Tubes and Waves,* Springer-Verlag, 1991.
[6]Jacobs P.A. "Quasi-one-dimensional modeling of a free-piston shock tunnel," *AIAA Journal,* Vol 32, No. 1, 1994, pp.137-145.
[7]Morgan, R.G., " compound isentropic free-piston driver for expansion tunnels," *Proc. 11th Australian Fluid Mechanics Conference,* Hobart Australia, 1992.
[8]Brydson, J.A., "Rubbery Materials and their Compounds," Elsevier Applied Sciences, 1988, pp.23-24.

BLANK

Mass spectrometer measurements of the freestream flow in the T4 free piston shock tunnel

R. R. Boyce, M. Takahashi*, R. J. Stalker

*** Present address : Kakuda Research Center, National Aerospace Laboratory, Japan**

Background

The design of the next generation of space vehicles is heavily dependent on both ground testing facilities and on Computational Fluid Dynamics (CFD). As well, CFD technology is heavily dependent on ground testing facilities for validation. Ground testing facilities that can simulate the real gas effects encountered in reentry are thus extremely important.

One aspect of ground testing that is very important and has been a source of difficulty in the past is the issue of the knowledge of the test flows produced. Accurate knowledge of the values of the freestream parameters is essential for : (i) undertaking fundamental fluid/chemical phenomena studies; (ii) relating different ground tests to each other; (iii) scaling ground test results to full scale flight; and (iv) providing the necessary input data for CFD codes, in the context of CFD validation or for using CFD to aid in the interpretation of experimental results.

The freestream temperature and composition in high enthalpy wind tunnels such as free piston shock tunnels (Stalker, 1972) are usually not measured directly, but are inferred from nozzle flow calculations which use knowledge of the nozzle reservoir conditions and assumptions concerning the fluid dynamic and thermochemical processes in the nozzle expansion flow. There is evidence, both theoretical (Park, 1990) and experimental (MacDermott & Dix, 1972 and Skinner & Stalker, 1996), that indicates that the flow solvers used to compute nozzle expansions of highly dissociated air do not correctly model the nonequilibrium rate processes in the expanding flow. The flow solvers most widely used in impulse facilities are steady state quasi-one-dimensional inviscid nonequilibrium chemistry codes such as NENZF (Lordi, Mates & Moselle, 1965), and steady state two-dimensional/axisymmetric inviscid nonequilibrium chemistry codes such as SURF (Rein, 1989). NENZF constrains vibration to be either frozen at the nozzle reservoir temperature or in local equilibrium with the translational temperature throughout the flow. SURF uses the sudden-freeze approximation for the vibrational relaxation for a user-specified freeze temperature. These assumptions lead to incorrect values for the freestream parameters, particularly the freestream composition which deviates from that of atmospheric air due to the high enthalpy levels associated with shock tunnel flows.

The behaviour of vibrational and chemical rate processes in compressing flows, for example flows after strong shock waves, is modelled well, particularly when using two-temperature models (Park, 1990). On the other hand, the process of vibrational relaxation in expanding flows is not completely understood, and is usually modelled with the Landau-Teller formula derived empirically from data from shock wave flows. The empirical constants in the formula are not necessarily valid for expanding flows (see for example Blom et al, 1970) since high vibrational levels tend to be overpopulated relative to equilibrium distributions in expanding flows, resulting in a stronger contribution from anharmonicity than for shock

wave flows. Furthermore, if the nozzle flow is dissociated, as it is for shock tunnels, atomic recombination is affected by the high vibrational state overpopulation. Recombination occurs preferentially into these levels, particularly oxygen recombination, which is the rate limiting process in the chemical relaxation. Chemical reaction rates are typically not derived from expanding flow experiments, and will not accurately account for the above effect when used in nozzle flow codes. Thus the flow solvers that are generally in use today are based on chemistry and vibration relaxation assumptions that are not necessarily applicable to expanding flows.

The freestream composition is a sensitive indicator of the correctness of the modelling of the relaxation in the nozzle flow, and to date there has only been limited experimental measurements of the composition for high enthalpy facilities. Direct simultaneous measurements of species concentrations have consisted to date of time-of-flight mass spectrometer measurements in the AEDC arc-heated wind tunnel (MacDermott & Dix, 1972) and more recently in the T4 free piston shock tunnel (Skinner & Stalker, 1996). The results from the two tunnels are qualitatively in agreeance. In both cases, a deviation was observed from predictions using standard nozzle flow solvers (such as NENZF) of the measured relative species concentrations in the test gas. In particular, the relative concentration of NO was found to be higher, and the extent of oxygen dissociation an order of magnitude lower, than predicted over a broad range of stagnation enthalpies. These experimental results suggest that the suspicions of the flow solvers are well founded. However, the spectral resolution obtained by Skinner (in particular that of the NO spectral peak) was low, and electrical noise was significant throughout his data. Solutions to these problems, and more extensive experimental measurements of freestream species concentrations, are needed to improve the quality of results derived from high enthalpy ground based facility research.

The work presented here consists of an extensive series of experiments in which an improved version of the time-of-flight mass spectrometer of Skinner & Stalker (1994) has been employed to measure the freestream composition of the T4 free piston shock tunnel.

Improvements to the mass spectrometer

The key features of the mass spectrometer are : (i) a system of hollow conical skimmers that sample and expand the test gas, forming a molecular beam; (ii) a pulsed electron beam that ionises species in the molecular beam; (iii) a series of cylindrical electrodes that deflect and accelerate the ions into the drift tube; and (iv) an electron multiplier that detects the arrival of the ions (separated according to their mass) at the end of the drift tube.

An evaluation of the problem areas of the mass spectrometer was made, the main ones being

(i) the charge-to-voltage amplifier possessed large baseline noise characteristics

(ii) oil contamination of the electron multiplier detector due to its location immediately above the oil diffusion pump

(iii) poor ducting after the ionisation/deflection region, leading to a buildup of background molecules which scatter the ions and limit the spectra resolution

(iv) the mass spectrometer was housed in a large flexible rig, which renders it susceptible to stress and cracking when exposed to the shock tunnel environment and during installation into the tunnel, leading to poor vacuum

These problems were addressed in the following manner. A new charge-to-voltage amplifier was designed and manufactured in-house. A very strong, inflexible frame was designed and manufactured, along with a rail system that enables the mass spectrometer in its frame to be easily installed/removed from the tunnel, and easily traversed across the test section. The new frame ensures that the mass spectrometer is not allowed to flex under stress, and therefore helps to ensure the vacuum integrity of the instrument. A new interface wall section for the test section was designed and manufactured that allows the various tubing to the mass spectrometer to be easily connected/disconnected. This aids in maintenance/repair which is occasionally required while the instrument is in T4. Improvements were made to certain flanges/joints to improve the ability of the instrument to attain high vacuum. The main diffusion pump was moved downstream away from the electron multiplier cavity to prevent oil mist contamination of the electron multiplier. A new cavity was designed and manufactured, and a new high vacuum stainless steel connecting section between the diffusion pump and the cavity was designed and manufactured. A modified ioniser/deflector was designed and built to improve the alignment of the ion beam with the drift tube. Finally, a new faster cathode ray oscilloscope was purchased for data acquisition.

Current experiments

With the improved mass spectrometer, an extensive series of experiments were performed in which the centre-line freestream composition produced by a nominal Mach 5 contoured nozzle was measured. The stagnation enthalpy was varied from 2.5 to 17 MJ/kg, and the nozzle supply pressure varied from 12 to 40 MPa (by means of varying the primary diaphragm thickness from 2 to 5 mm mild steel). The relative peak area in any mass spectrum produced by the time-of-flight mass spectrometer does not directly correspond to the freestream composition - effects such as mass separation in the skimmer system (see, for example, Knuth (1995)), different ionisation efficiencies, dissociative ionisation, and different ion collection efficiencies, lead to the relative amounts of each species reaching the detector being different to that of the freestream. Apart from the ionisation effects (which are documented for most species of interest in the literature), the effects are primarily mass dependent, and so a large number of calibration experiments were performed. These calibration shots consisted of measurements of test gases containing known mixtures (N_2/Ar, N_2/He, O_2/He, N_2/H_2), to determine relative peak area calibration factors on the basis of relative mass. The lowest enthalpy air shots (for which dissociation should be negligible) were also used for this purpose.

Finally, an investigation into a possible mechanism for early driver gas arrival in the test section was conducted. A 22 mm thick plate covered in a honeycomb of 12 mm orifices was placed between the compression and shock tubes to break up vortices produced by compression tube wall boundary layer gas being scooped up and jetted forwards by the piston motion.

Complete mass spectra were obtained every 53 μs throughout the flow duration, and were averaged in groups of five to improve the signal-to-noise ratio. Figure 1 shows a comparison

between typical raw data (unaveraged) produced by the original mass spectrometer (the Mark 1a) and the current improved version (the Mark 1b), as well as a typical complete mass spectrum from the current instrument. The improvement in peak resolution with the current version is evident, aided mainly by the improved amplifier and relocation of the diffusion pump.

Results

The results of the experiments are presented below in three parts : the freestream test gas composition (components of air); driver gas arrival times; and the early driver gas arrival mechanism investigation.

Figures 2 to 5 present measured and theoretical peak areas for N, O, O_2 and NO, relative to the N_2 peak area, as a function of the stagnation enthalpy for the 2 mm primary diaphragm case. The other diaphragm cases produced identical trends. The solid theoretical curve represents nonequilibrium chemistry / equilibrium vibration freestream calculations made with NENZF. The short-dashed curves represent relative peak areas for room temperature air. The non-zero levels for N and O indicates the degree of dissociative ionisation of N_2 and O_2 produced by the mass spectrometer (and which is accounted for in the calibration factors taken from the calibration and low enthalpy air shots). The long-dashed curves represent freestream compositions frozen at the nozzle reservoir levels. The irregularities in the theoretical curves are because calculations were only done at the experimental conditions (for which different pressure sometimes occur for a given enthalpy) and joined by straight lines in the figure.

The results suggest that the mass spectrometer is detecting no monatomic nitrogen or oxygen (to within experimental uncertainty) other than that produced by dissociative ionisation in the instrument, even at flow conditions where significant freestream dissociation is expected. The level of O_2 detected is greater than predicted with NENZF, while the level of NO agrees with the theoretical predictions. While these results may cast doubt on the validity of the theoretical predictions, they are also consistent with possible catalytic recombination phenomena in the skimmer system (Stoekle, Auweter-Kurtz & Laure, 1996; Caram et al, 1994). Over the range of enthalpies investigated, the level of freestream N is expected to be very small (and this is supported by the current results), and so any NO produced by catalytic recombination would be very small. On the other hand, the amount of O_2 produced is potentially large, as is the amount of O lost, and this is observed and is consistent with Skinner's results. The NO result is not consistent with that of Skinner, probably a result of the improved peak resolution in the current experiments.

Figure 6 presents the arrival time of driver gas (10% of the total mixture) in the test section as a function of stagnation enthalpy. The results extend the previous work of Skinner (1995) to the low enthalpy range covered by the driver gas detector of Paull (1995). Skinner's and Paull's results are also shown in the figure. The current results agree with both Skinner and Paull.

Finally, Figure 7 shows a comparison of driver gas arrival times, as a function of stagnation enthalpy, for experiments with and without the orifice plate described above. It seems from the results that the orifice plate marginally improves the driver gas arrival problem, but the

level of scatter in the current driver gas measurements makes a quantitative conclusion in this case difficult.

Conclusion

In conclusion, a number of important improvements have been made to the time-of-flight mass spectrometer, and these have resulted in an improved peak resolution. Measurements of freestream test gas composition over an extensive range of stagnation enthalpy and nozzle supply pressure have provided results that are consistent with possible catalytic recombination in the skimmer system. Measurements of driver gas arrival in the test section are consistent with previous measurements by Skinner and Paull. Investigations of a possible significant mechanism for early driver gas arrival (that of vortices produced from compression tube wall boundary layer jetting) suggest that this mechanism may contribute to early driver gas arrival, but the extent of this has not been determined due to the scatter of the results. Work planned for the near future consists of investigations of the skimmer system (in particular, experimenting with various skimmer materials and coatings), with the aim of confirming and reducing the effects of catalytic recombination.

References

A. P. Blom, K. N. C. Bray & N. H. Pratt, "Rapid vibrational deexcitation influenced by gasdynamic coupling", Astronautica Acta, Vol. 15, pp. 487-494 (1970).

J. M. Caram, C. B. Madden, J. D. Milhoan, C. D. Scott, G. J. Le Beau, S. Arepalli, S. A. Bouslog & T. J. Urban, "Design of a Mass Spectrometer Probe Tip for the Arc Jet Facility", AIAA 94-0356 (1994).

E. L. Knuth, "Composition distortion in MBMS sampling", Combustion and Flame, Vol. 103, No. 3, pp. 171-180 (1995).

J. A. Lordi, R. E. Mates & J. R. Moselle, "Computer program for the numerical solution of nonequilibrium expansions of reacting gas mixtures", CAL Report No. AD-1689-A-6 (1965).

W. N. MacDermott & R. E. Dix, "Mass spectrometric analysis of nonequilibrium airflows", AIAA Journal, Vol. 10, No. 4, pp. 494-499 (1972).

C. Park, "Nonequilibrium hypersonic aerothermodynamics", John Wiley & Sons, New York (1990).

A. Paull, "A simple shock-tunnel driver-gas detector", Proc. 20th International Symposium on Shock Waves, Caltech (1995).

M. Rein, "SURF : a program for calculating inviscid supersonic reacting flows in nozzles", GALCIT FM 89-1 (1989).

K. A. Skinner, "Mass spectrometry of hypersonic combustion", PhD thesis, University of Queensland (1995).

K. A. Skinner & R. J. Stalker, "A time-of-flight mass spectrometer for impulse facilities", AIAA Journal, Vol. 32, No. 11, pp. 2325-2328 (1994).

K. A. Skinner & R. J. Stalker, "Mass spectrometer measurements of test gas composition in a shock tunnel", AIAA Journal, Vol. 34, No. 1, pp. 203-205 (1996).

R. J. Stalker, "Development of a hypervelocity windtunnel", Aeronautical Journal, Vol. 76, pp 374-384 (1972).

T. Stoekle, M. Auweter-Kurtz & S. Laure, " Material Catalysis in High Enthalpy Air Flows", AIAA 96-1904 (1996).

Figure 1

The raw data

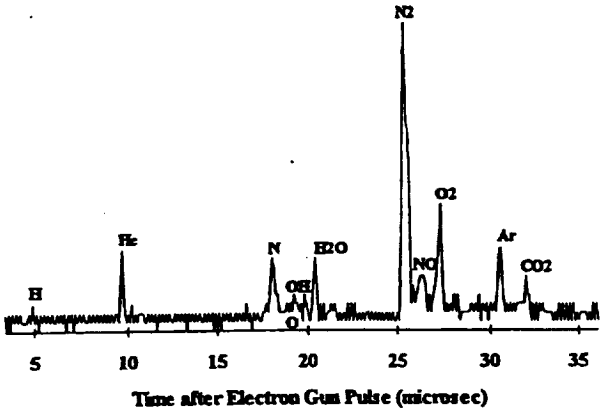

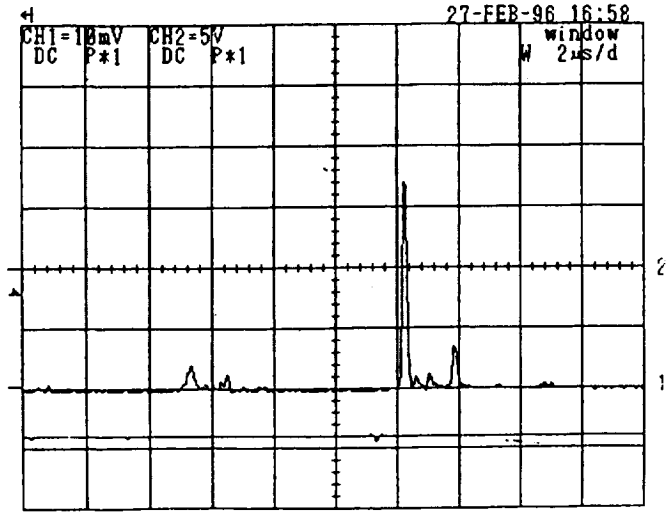

Mark 1a

Mark 1b

Typical mass spectra

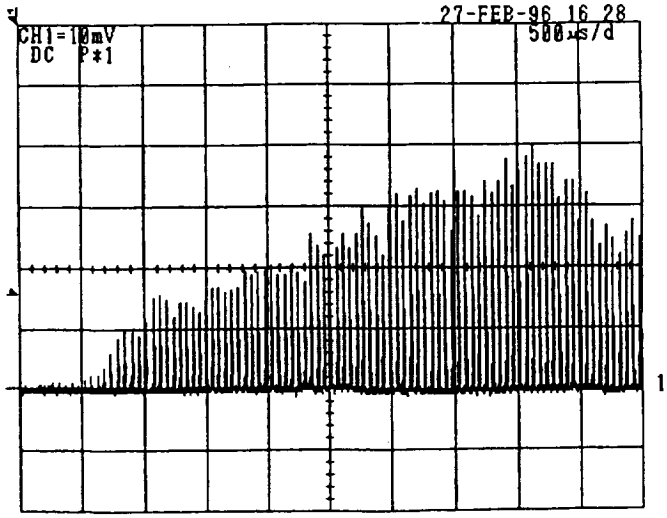

100

Theoretical and experimental peak areas (relative to N_2)

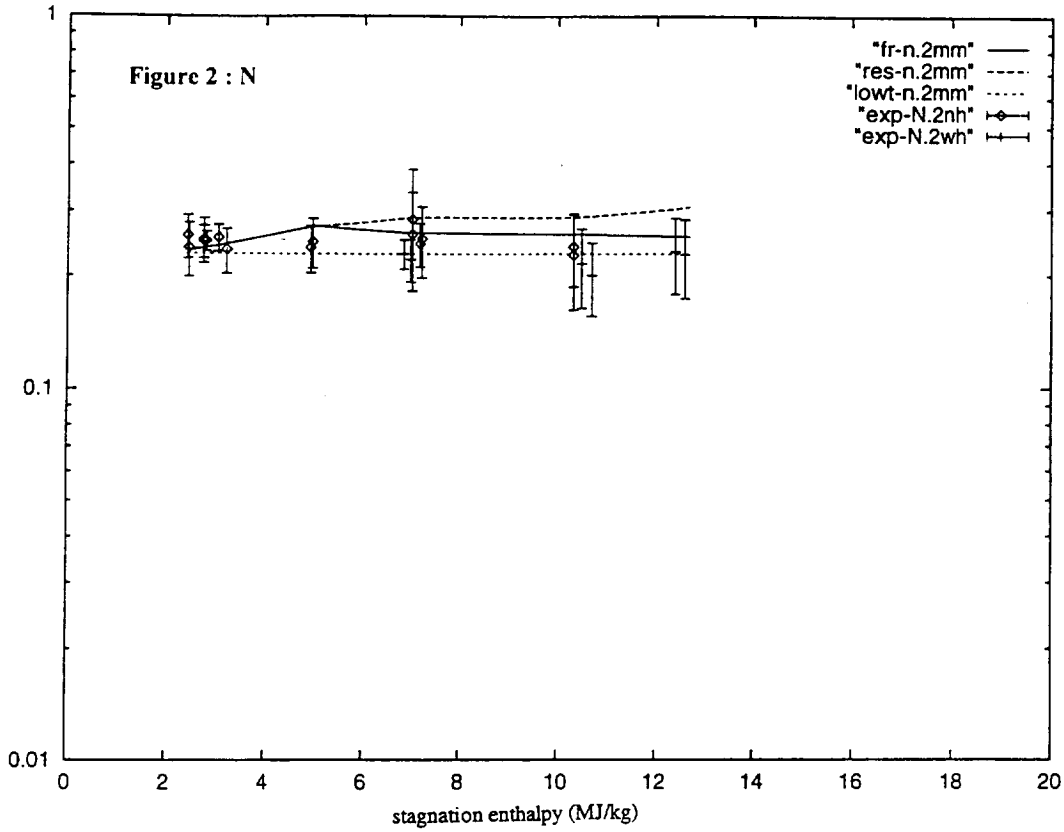

Theoretical and experimental peak areas (relative to N_2)

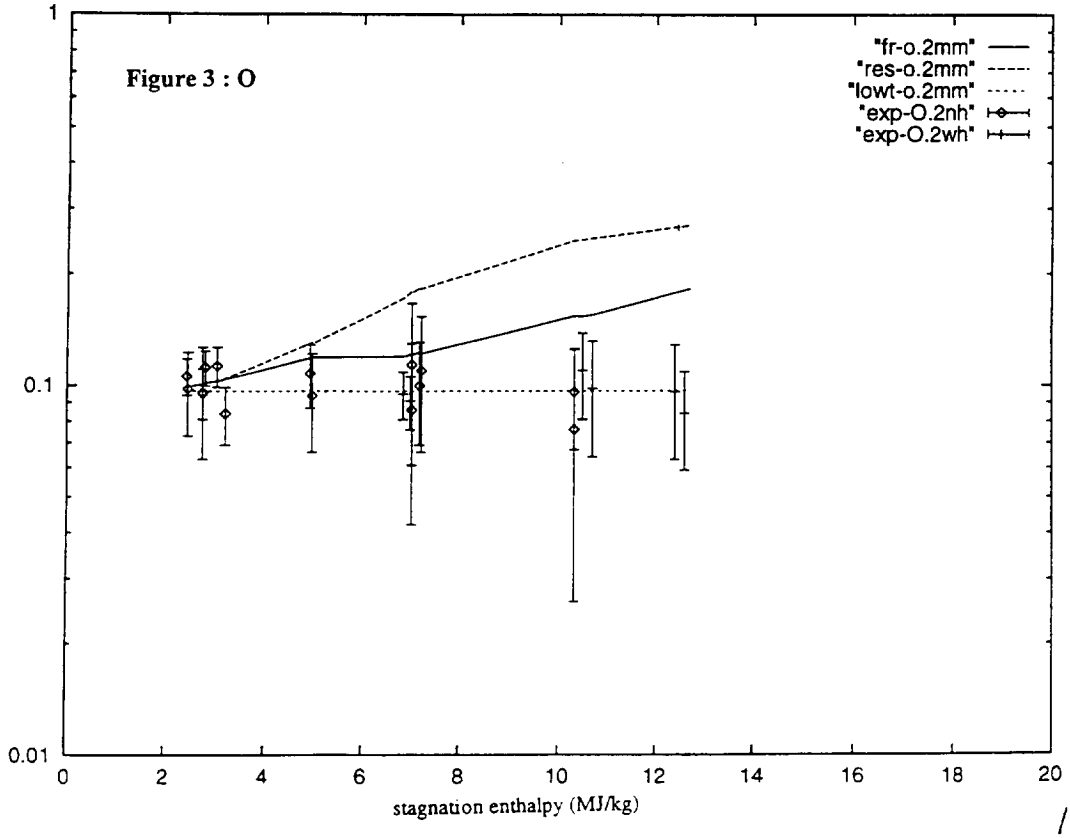

Theoretical and experimental peak areas (relative to N_2)

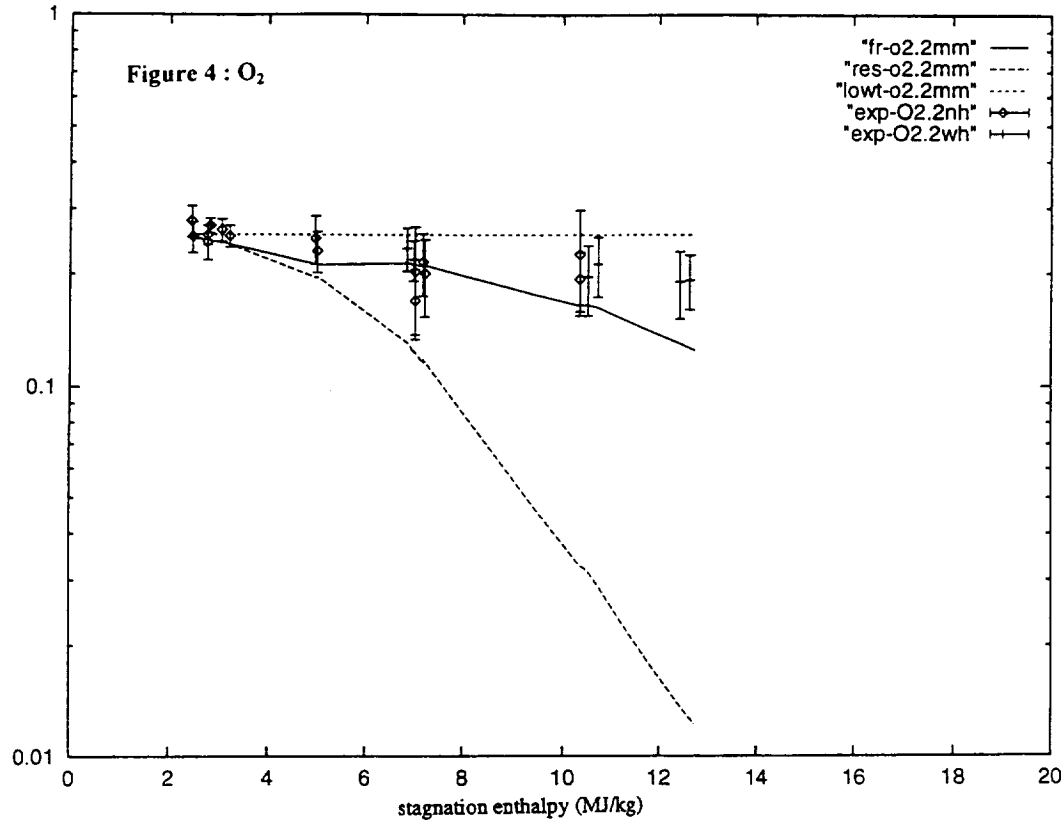

Theoretical and experimental peak areas (relative to N_2)

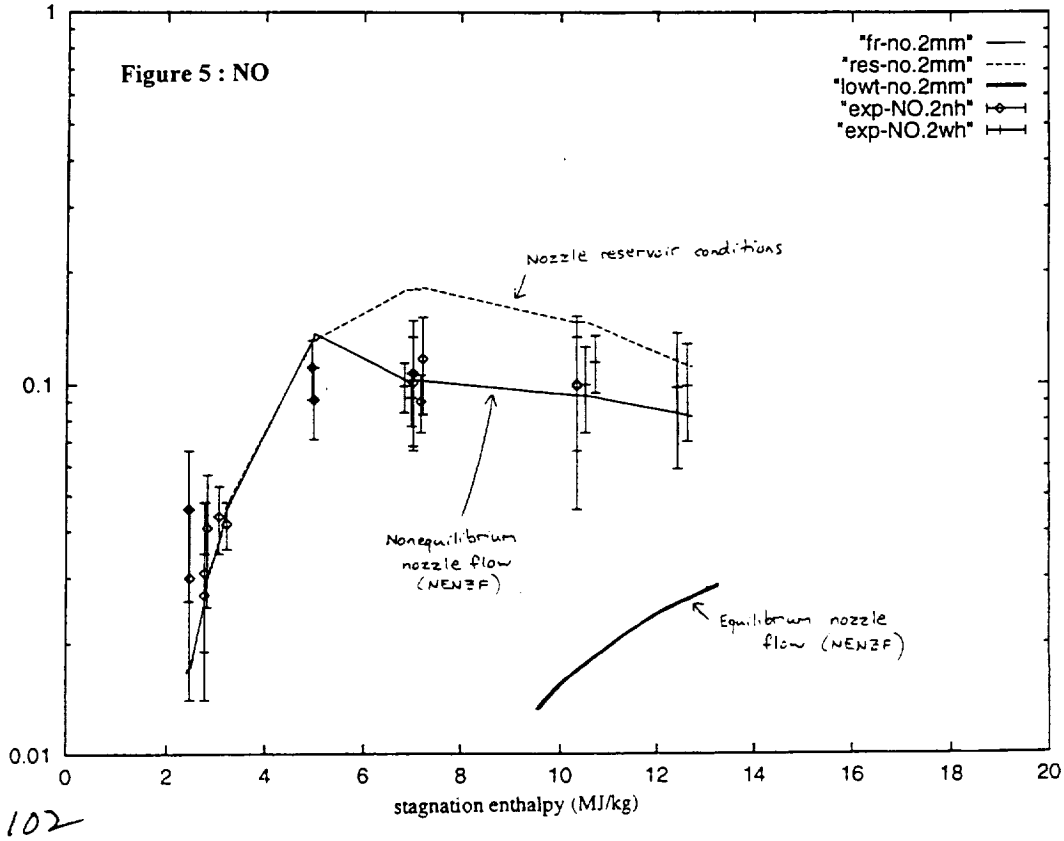

Comparison of Mark 1b with Mark 1a and driver gas detector (Paull)

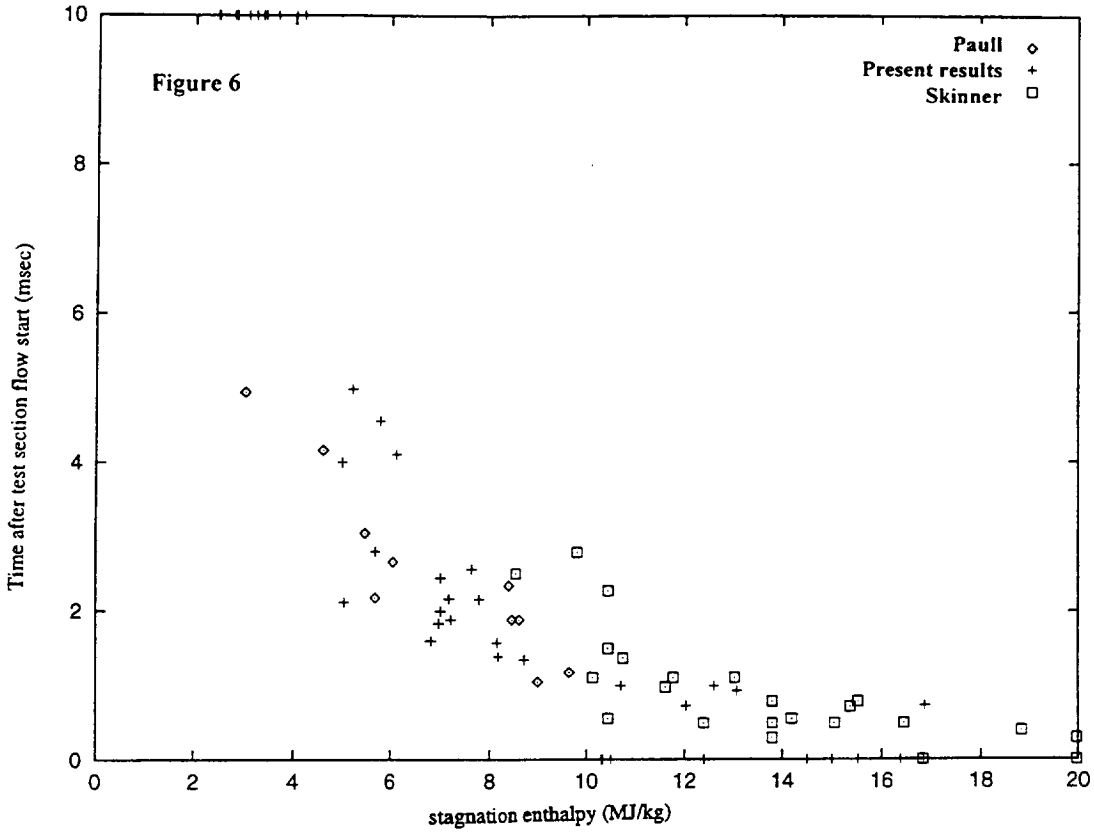

Driver gas arrival time

With and without orifice plate

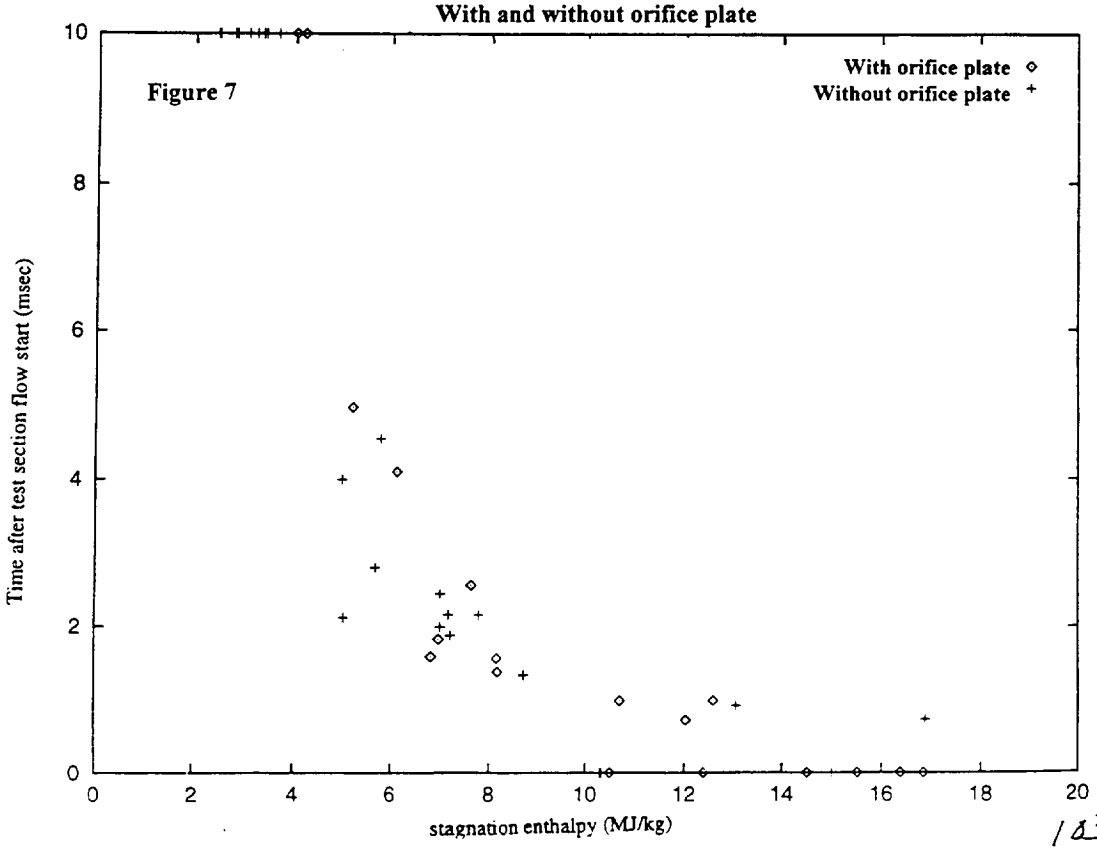

REPORT DOCUMENTATION PAGE

Form Approved
OMB No. 0704-0188

1. AGENCY USE ONLY *(Leave blank)*	2. REPORT DATE	3. REPORT TYPE AND DATES COVERED
	April 1997	Contractor Report

4. TITLE AND SUBTITLE
Shock Tunnel Studies of Scramjet Phenomena 1995
Supplement 13

5. FUNDING NUMBERS
G NAGW-674
WU 522-51-31-10

6. AUTHOR(S)
R. G. Morgan, R. J. Stalker, and A. Paull

7. PERFORMING ORGANIZATION NAME(S) AND ADDRESS(ES)
University of Queensland
St. Lucia
Brisbane, Qld., Australia

8. PERFORMING ORGANIZATION REPORT NUMBER

9. SPONSORING / MONITORING AGENCY NAME(S) AND ADDRESS(ES)
NASA Langley Research Center
Hampton, VA 23681-0001

10. SPONSORING / MONITORING AGENCY REPORT NUMBER
NASA CR-201694

11. SUPPLEMENTARY NOTES
Langley Technical Monitor: R. C. Rogers

12a. DISTRIBUTION / AVAILABILITY STATEMENT
Unclassified/Unlimited
Subject Category 34

12b. DISTRIBUTION CODE

13. ABSTRACT ***(Maximum 200 words)***

Reports by the research staff and graduate students of the Mechanical Engineering Department at the University of Queensland are collected and presented. These reports cover various studies related to the advancement of scramjet technology and the operation of advanced hypervelocity shock-expansion tubes. The report topics include the experimental studies of mixing and combustion in a scramjet flow path, the measurement of integrated thrust and skin friction, and the development of a free-piston-driven expansion tunnel capable delivering a test gas at superorbital velocities. These research summaries constitute supplement 13 of the NASA Grant NAGW-674, for calendar year 1995.

14. SUBJECT TERMS
Scramjets, pulse facility, shock tunnel, expansion tube

15. NUMBER OF PAGES
104

16. PRICE CODE
A06

17. SECURITY CLASSIFICATION OF REPORT	18. SECURITY CLASSIFICATION OF THIS PAGE	19. SECURITY CLASSIFICATION OF ABSTRACT	20. LIMITATION OF ABSTRACT
Unclassified	Unclassified	Unclassified	